Low Temperature Behavior of ZK60 Magnesium Alloy After Thermo-Mechanical Processing

A Thesis

by

SALAR SALAHI

Submitted to the

Graduate School of Sciences and Engineering

In partial fulfillment of the requirements for the degree of

MASTER OF SCIENCE

in the

Department of Mechanical Engineering

Özyegin University

August 2017

Low Temperature Behavior of ZK60 Magnesium Alloy After Thermo-Mechanical Processing

Approved by:

Assoc. Prof. Dr. Güney Güven Yapıcı
Advisor
Department of Mechanical Engineering
Özyeğin University

Assist. Prof. Dr. Mehmet İpekoğlu
Department of Mechanical Engineering
Turkish-German University

Assist. Prof. Dr. Zeynep Başaran Bundur
Department of Civil Engineering
Özyeğin University

ABSTRACT

Low Temperature Behavior of ZK60 Magnesium Alloy After Thermo-Mechanical Processing

Due to its low weight and good combination of mechanical strength and formability, wrought magnesium alloys containing zinc and zirconium are widely used in automotive and aerospace industries. Since mechanical properties of pure magnesium are weak, the addition of alloying elements is used to improve the mechanical response of magnesium alloys. In this study, ZK60 wrought alloy was selected to improve its mechanical properties using thermo-mechanical processes. A systematic combination of heat treatment and warm rolling was applied for this purpose. The solution treated sample was exposed to rolling followed by annealing treatment for enhancing the formability. Static and under stress regimes of aging were performed to form fine precipitates in the Mg matrix.

The low temperature tensile behavior of samples was investigated at temperatures of -60℃, -20℃ and ambient temperature at a quasi-static strain rate of 10^{-3} s^{-1}. The effect of processing parameters including heat treatment, deformation and aging on the microstructure, texture and mechanical behavior of samples were characterized as well.

It was shown that systematic thermo-mechanical processes can significantly refine the microstructure and enhance the mechanical properties of static and stress aged samples. The fine grained structure along with equiaxed and uniform grains were achieved for the stress aged samples, while bimodal structure with coarse grains was observed for the solution treated sample. It was shown that rolling and stress aging can form strong basal texture aligned with the normal direction. It was also observed that in solution treated sample few number of coarse precipitates were formed, while high density of fine precipitates was observed for the static aged sample. The stress aged sample possessed higher density of precipitates relative to the solution treated and static aged samples.

The results obtained from the tensile tests proved that the mechanical properties of both static and stress aged samples were higher than that of the solution treated sample. While the tensile strength and elongation

to failure of solution treated sample was 255 MPa and 11.2% respectively, the tensile response for best condition of static aged sample was improved up to 304 MPa and 25%. The rolling and stress aging processes under the load of 50 MPa for 3 hours improved the tensile strength of samples up to 353 MPa and ductility up to 12.5%. At -60℃, the mechanical response of solution treated sample is limited to strength of 262 MPa and ductility of 2.6%. The mechanical properties of stress aged sample are significantly improved at the same temperature up to strength of 338 MPa and ductility of 9.2%.

ÖZETCE

ZK60 Magnezyum Alaşımının Termo-Mekanik İşleme Sonrası Düşük Sıcaklık Davranışı

Çinko ve zirkonyum içeren işlenik magnezyum alaşımları düşük ağırlığı ve mukavemet-şekillendirilebilirlik kombinasyonu sayesinde otomotiv ve havacılık endüstrisinde yaygın olarak kullanılmaktadır. Saf magnezyumun mekanik özelliklerinin zayıf olmasından dolayı bu özelliklerin ilerletilmesi için ek alaşımlama elementleri kullanılmaktadır. Bu çalışmada ZK60 işlenik alaşımı, mekanik özellikleri termo-mekanik işleme ile geliştirilmek üzere seçilmiştir. Bu amaçla ısıl işlem ve ılık haddelemenin sistematik bir kombinasyonu uygulanmıştır. Çözeltiye alınmış numune haddelemeye tabi tutulmuştur. Şekillendirilebilirliği artırmak amacıyla tavlama işleminden sonra magnezyum matrisinde ince çökeltiler oluşturmak için yüksüz ve yük altında yaşlandırma işlemi yapılmıştır.

Numunelerin düşük sıcaklıktaki çekme davranışı -60℃, -20℃ ve ortam sıcaklığında ve 10^{-3} s^{-1} kuvazi-statik gerinim hızında gözlenmiştir. Isıl işlem, deformasyon ve yaşlandırma da dahil olmak üzere işleme parametrelerinin etkisinin numunelerin mikroyapı, doku ve mekanik davranışı üzerindeki etkisi de karakterize edilmiştir.

Sistematik termo-mekanik işlemenin mikroyapıyı önemli derecede inceltebildiği, yüksüz ve yük altında yaşlandırılmış numunelerin mekanik özelliklerini arttırdığı gözlenmiştir. Yük altında yaşlandırılmış numuneler için eş eksenli ve düzgün taneli ince yapılı yapı elde edilirken, çözeltiye alınmış numuneler için iri taneli bimodal yapı gözlenmiştir. Haddeleme ve yaşlandırma işleminin normal yön ile hizalı, güçlü bazal doku oluşumuna önemli ölçüde yol açtığı gösterilmiştir. Çözeltiye alınmış numunede az sayıda iri çökelti oluştuğu ve yüksüz yaşlandırılmış numunede yüksek yoğunluklu ince çökelti oluştuğu gözlenmektedir. Yük altında yaşlandırılmış numune, çözeltiye alınmış ve yüksüz yaşlandırılmış numunelere göre daha yüksek çökelti yoğunluğuna sahiptir.

Çekme testlerinden elde edilen sonuçlar, yüksüz ve yük altında yaşlandırılmış numunelerin mekanik özelliklerinin çözeltiye alınmış numunelerden daha yüksek olduğunu ortaya koymaktadır. Çözeltiye alınmış numunenin çekme dayanımı ve kopmaya kadar uzaması sırasıyla 225 MPa ve %11.2 iken, yüksüz

yaşlandırılmış numunenin en iyi durumundaki çekme dayanımı ve uzaması 304 MPa ve %25'e kadar yükseltilmiştir. 3 saat süreyle 50 MPa yük altında yapılan hadde ve yük altında yaşlandırma işlemleri, numunelerin çekme mukavemetini 353 MPa'ya kadar artırmıştır. -60°C'de çözeltiye alınmış numune 262 MPa dayanımın yanı sıra %2.6 süneklik göstermiştir. Aynı sıcaklıkta, yük altında yaşlandırma sonrası mekanik özellikler önemli şekilde ilerletilmiş olup, 338 MPa ve %9.2 seviyesi elde edilmiştir.

DEDICATION

This thesis is dedicated to all the people who never stop believing in me, who along with God, have been my ‘footprints in the sand’and who taught me to get up after a fall and start again.

ACKNOWLEDGEMENT

First and foremost, I would like to thank my supervisor, Dr. Güney Güven Yapıcı, for his wonderful guidance throughout the course of my research work. I am indebted to him for his continual encouragement and support to carry out the current study.

On the other hand, I would like to thank my Ph.D. committee members, Assist. Prof. Dr. Mehmet Mehmet İpekoğlu and Assist. Prof. Dr. Zeynep Başaran Bundur for their guidance and attention to this study. I would sincerely thank my colleagues in the MEMFIS group, Seyyedvahid Sajjadifar, Görkem M. Şimşek and Onur Bilgin for the enjoyable time I have passed with them. Special thanks go to my best friend Ali Hosseinzadeh Ghobadlou who has made a valuable contribution to this study. I also would thank my former colleague, Kambiz Shojaei not only for his contribution to this study but also for introducing a new aspect of a positive attitude to me which I will consider throughout my life. I would like to thank Prof. Dr. Hans Maier and his team for their collaboration and their kind hostility during my stay for performing experimental tests in Hannover, Germany.

I highly appreciate my beloved family, especially my parents, Ali and Sariyeh who dedicated their lives to support me throughout my school and university years and deeply thank my dear sister, Aylar for her support and kindness.

The support of Scientific and Technological Research Council of Turkey (TUBITAK), Project No: 214M116 for conducting this research is acknowledged.

TABLE OF CONTENTS

LIST OF TABLES

LIST OF FIGURES

Chapter 1

INTRODUCTION

1.1.Motivation

Compared with steel and copper, magnesium alloys are promising candidates for various structural applications especially for automotive, aerospace and marine industries due to their high elastic modulus and strength to weight ratios [1, 2]. In aerospace and automotive industries, aluminum and steel alloys are widely replaced with magnesium alloy, since it is easier to the machine and due to their excellent castability, formability and weldability [3]. Currently, the aim of automotive industry focuses on decreasing the weight of vehicles. Energy efficiency as a significant concern of heavy industries has made fuel consumption reduction a real challenge which can be attained only by weight reduction of structural parts of the vehicles. The application of magnesium alloys in the vehicle structure can decrease the fuel consumption near to 40% [4].

The first applications of magnesium alloys back to 1960s. However, its high cost forced the manufacturers to substitute it with aluminum [5]. The increase in fuel price and lack of fuel resources once again in late 1990th convinced the automotive industry to make attention to the usage of magnesium alloys in core applications [5, 6]. However, compared to its counterparts such as steel, aluminum, and polymers, magnesium alloys use is still limited.

Magnesium alloys, in general, have good tensile strength and adequate rigidity and because of their low density are lighter compared to iron and aluminum. Magnesium alloys have limited formability at room temperature due to their hexagonal closed packed (HCP) structure [3, 7]. At room temperature, two independent basal slip systems activate for magnesium, and the deformation mechanism is restricted to twinning deformation [8]. At high temperature with activation of non-basal slip systems, the ductility can be enhanced significantly [9]. It is proved that texture in favorable orientation and also grain refinement

can improve the mechanical strength of magnesium due to reduction of the twinning volume fraction. Desired texture can also increase the number of activated basal slip systems and subsequently lead to a better mechanical response [10, 11].

Characterizing the response of materials to deformation processing have always been in the attraction of the researchers. The conventional deformation techniques such as drawing, rolling and extrusion have been used to improve the mechanical properties of the different types of materials [12]. As mentioned, the formability of magnesium at room temperature is limited. The low formability of magnesium alloys is considered to be compensated using hot forming process. At high temperatures near 300°C, the oxidation of magnesium alloys hinders the forming process [13]. Hence, it is important to control the oxidation during hot forming processes. Warm rolling process as a promising method to improve the mechanical strength in the certain direction accompanied with favored texture is previously used for mechanical enhancement of magnesium alloys [14, 15]. During rolling, precipitate nucleation along with an increase in density of dislocations contributes to the mechanical improvement of bulk material [16]. Among all magnesium alloys, rolling efforts have been made especially on alloys containing Zinc elements such as ZK60, AZ31, and AZ91. These efforts prove that rolling can increase the density of dislocation in a wide range and contributes to the nucleation of precipitates containing Zinc element [17]. Deformation processes such as rolling can also influence the grain size of the bulk matrix in magnesium alloys [18, 19]. The grain refinement as an improvement method can enhance the mechanical properties by impeding the movement of dislocation across grain boundaries (GBs). Nano crystalline and fine grained structures have large volume fraction of grain boundaries and exhibit unique mechanical properties compared with coarse grained materials [20, 21].

Mechanical improvement is achieved via precipitate hardening as well. ZK60 alloy containing precipitates of zinc (Zn) and zirconium (Zr) is one the successful methods done to improve the strength using the precipitate hardening method. Microstructural evolution of ZK 60 alloy has been characterized

after precipitate hardening, and a good distribution with fine precipitates has been illustrated for this alloy [22, 23].

A combination of rolling and heat treatment methods can be used for magnesium alloys to increase the mechanical properties. A particular focus on ZK60 alloy demonstrates that the combined use of deformation processing and aging treatments can significantly improve the strength [24, 25]. Thermo-mechanical processing (such as rolling and extrusion) before aging treatments can effectively refine grains and produce a strong texture, which can generate refinement hardening. Recent studies have reported that deformation prior to precipitate hardening processes can improve strength [26]. The high density of dislocations produced by strain hardening methods can accelerate aging kinetics and facilitate the nucleation of precipitates during aging treatments, leading to better aging hardening response. There would be a high competition between slip and twinning deformation on Mg alloys depending on the texture of alloy. It means that at certain directions, high density of dislocations are influenced by pre-strain, profuse twins [27, 28]. The dominant deformation mechanisms need to be investigated for the ZK60 alloy, and the effect of rolling and subsequent aging needs to be characterized.

Stress aging method as a means of precipitate hardening is previously used for aluminum alloys containing copper. During this process, the applied load in a proposed direction can influence the formation of precipitates in a favored direction along with the creation of texture in the microstructure. In addition to the effect of static aging, the effect of stress aging on the mechanical properties of ZK60 alloy is a crucial topic of discussion. In stress aging, a process combining heat treatment with an elastic stress regime is used to enforce stress relaxation or creep-forming during artificial age-hardening of binary alloys. This simultaneous forming and aging technique has been utilized in the manufacturing process of integrally stiffened lightweight structures for aerospace applications [29]. In addition to the effect that plastic deformation prior to aging has on the heterogeneous nucleation of precipitates on dislocations in certain classes of Mg alloys [30], application of an elastic stress during aging can significantly affect the orientation

of precipitates. Depending on the direction of the precipitate habit plane with respect to the stress axis, precipitation may or may not be favored, thus leading to a preferentially oriented precipitate structure [31].

It is noted that a systematic investigation on the effect of combined rolling and aging processes accompanied with specific heat treatment methods is lacking for magnesium alloys containing binary phases of Mg-Zn and Mg-Zr. On the other hand, no efforts have been made to characterize the effect of stress aging on the microstructure, texture and mechanical enhancement of ZK60 alloy. In the current work, warm rolling has been conducted on the solution treated samples of ZK60, and then subsequent aging treatment both in static and dynamic regimes have been examined. The effect of this combined method along with the individual effects of each process on the microstructure, texture and mechanical properties have been investigated and reported.

1.2.Technical Approach

Based on the technological and strategic importance of magnesium alloys and using the motivation outlined in the previous section, ZK60 alloy investigated in this study. The commercial wrought high purity ZK60 alloy slabs were supplied and used in this research. A processing schedule was prepared for this alloy, having a notice on the previous works done on this field. The prepared schedule was ensured to maintain uniform deformation for all the samples during the rolling and heat treatment processes. Controlling the level of oxidation during the rolling and heat treatment process is another factor that can affect the uniformity of the process. The processing schedule was arranged to investigate the sole effect of rolling and subsequent heat treatment process on the mechanical properties and to minimize the adverse side effects of possible crack formation and oxidation.

Based on the light of the motives presented in the previous section, the overall objectives of the current research are stated below. To fulfill these objectives, a set of experimental methods was applied.

1. Performing solution heat treatment on the as-received slabs of ZK60 alloy by minimizing the possible oxidation level to prevent the adverse effect on the mechanical properties.

2. Performing rolling process on the solution treated samples by controlling the process parameters to maintain uniformity of the deformation.

3. Performing aging processes in both static and dynamic regimes by minimizing the effect of oxidation.

4. Investigating the microstructural evolution and texture analysis of treated samples after thermo-mechanical processes and characterizing the trends and contrasts formed in the microstructure and texture.

5. Studying possible deformation mechanisms and describing the effect of operational temperature on the mechanical properties of the treated samples.

6. Characterizing the effect of the microstructure on the mechanical properties of processed samples.

The following goals were set in more details for the specified alloy.

1. Grain refinement and increase in the twinning effects of rolled samples compared to their as-received counterparts.

2. Enhancement of mechanical properties of rolled and static aged samples relative to the as received and rolled samples.

3. Enhancement of mechanical properties of stress aged samples relative to the statically aged samples and the rolled ones via exhibition of finer and more uniformly distributed precipitates.

4. Characterizing the microstructure and texture of the rolled and aged samples and exhibiting microstructural evolution based on the temperature variation.

It is anticipated that a basis will be formed after achieving these goals to understand the microstructure-property relations in the processed ZK60 alloy. The microstructural evolution and mechanical property improvements of the treated samples are characterized and a comparison is made with the solution treated samples. Deformation mechanisms during the post-process thermo-mechanical process and the effect of

temperature during the mechanical tests are then examined to characterize the possible deformation systems in operation for the examined magnesium alloy.

This thesis is divided into five sections. In chapter 2, a brief technical background is presented about the mechanical and microstructural characteristics of the developed alloy. Active deformation mechanism and hardening methods are described for the magnesium alloys. Chapter 3 describes the experimental procedure conducted for this study. In chapter 4, the effect of thermomechanical processes on the microstructure of the developed samples is investigated using the optical, scanning electron and transmission electron microscopy. The effect of rolling and subsequent heat treatments on the mechanical properties at ambient and low temperatures is characterized in chapter 5. Finally, texture evolution is examined for the processed samples and correlation between observed texture and mechanical properties have been made in chapter 6. Conducted experiments and observed results are used to characterize the mechanical response of developed samples at low temperatures.

Chapter 2

TECHNICAL BACKGROUND

2.1.Pure Magnesium Properties

As an alkaline rare earth metal, magnesium has the atomic number of 12. It has a hexagonal close packed structure (hcp) with atomic diameter of 0.32 nm, making it a favorable choice for a solid solution with various types of metals. The arrangement of stacking layers of ABAB in a cell unit is shown in Fig. 2.1. For the mentioned arrangement, lattice parameters are $a = b \neq c$. The low density of 1.738 g cm^{-3} ,nearly 34% lower than that of aluminum makes it one of the lightest structural based metals[32, 33].

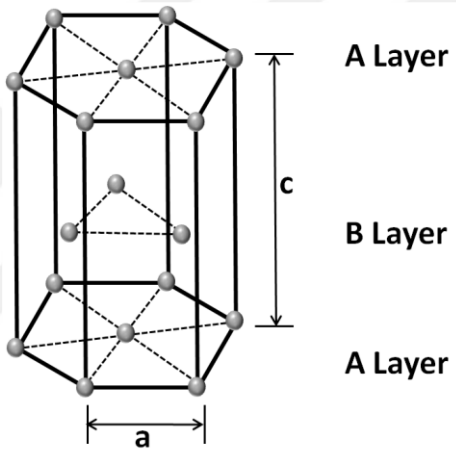

Fig. 2.1. A schematic diagram of a unit cell in magnesium.

Crystal structure of magnesium restricts the number of slip systems and makes its deformation mechanism difficult at ambient temperature. Inherently, mechanical testing results for pure magnesium are considered to be poor. To strengthen the mechanical properties of pure magnesium different methods are applied, and the addition of alloying elements is proposed as a first step. Other strengthening methods such as grain refinement and precipitate hardening can be applied for magnesium [33, 34].

2.2. Magnesium alloy classification

Based on the American Society for Testing Materials (ASTM-E527) [34], the designation of magnesium alloys is made by including letter codes for two major elements at first section and the nominal weight of the composition of the reported elements at the second part. The letter codes and examples of used alloys

are presented in Table 2.1. The letter codes need to follow a descending order and should depend on the amount of alloying elements. A third section may be used for the alloys containing the same amount of elements to address them. In order to illustrate the heat treatment condition, the fourth section is used. F as fabricated, O as annealed, T4 as solution treated and T5 as aged are commonly used temper conditions. An example here can be ZK60E-T6 containing near 6% zinc and 0.5% zirconium, ranked as 5th alloy having a similar composition. T6 is showing the temper condition which is solution treatment followed by aging.

Table 2.1 Major letter codes for magnesium alloys [34]

Letter code	Elements	Examples	Composition (wt%)
A	Alumunium	AZ91	3Al-1Zn
C	copper	ZC63	6Zn-3Cu
E	Rare Earth	EQ21	2.1Di-1.5Ag
K	Zirconium	K1A	0.7Zr
M	Manganese	AM60	6Al-0.13Mn
S	Silicon	AS41	4.3Al-1Si
Z	Zinc	ZK60	6Zn-0.5Zr

Magnesium alloy slabs are prepared both in wrought and as cast forms. Based on the application of the alloy favorable elements are added to strengthen the material. Wrought and cast alloys are described in more details in the upcoming sections.

2.3. Magnesium Cast Alloys

The most usable cast magnesium alloys are aluminum-zinc-manganese (AZ) and aluminum- manganese (AM) or aluminum-silicon series (AS) series. It can be said that most frequently-applied magnesium cast alloys are AZ91 and AM60. AZ Series are widely used where high strength and good castability are required. AZ91D possesses good mechanical strength along with the satisfactory level of resistance to corrosion in salt water [35]. AZ91 containing a lower amount of iron and copper even has higher resistance to corrosion [36]. For the AZ series of magnesium alloys, $Mg_{17}Al_{12}$ particles exists in the as-cast condition. As these series of alloys are heat treated up to 420°C, mentioned phase dissolves in the in solution. Solid

solution strengthening method contributes to the strength of matrix while the presence of this precipitate lowers the ductility of the alloy [36].

For applications requiring a higher level of formability, AM series are used. AM60B alloy having a lower amount of aluminum than the AZ91 shows better formability while the strength is nearly the same with AZ91.The enhancement of ductility in AM series is due to lower volume fraction of the $Mg_{17}Al_{12}$ phase at grain boundaries [35].

The major disadvantage of AZ series is their low resistance to creep. In order to provide satisfactory creep resistance at temperatures ranging from 120℃ to 150℃, AS series are good alternatives. By reducing the volume fraction of $Mg_{17}Al_{12}$ phase and replacing it with the stable phase of Mg_2Si, the creep resistance of AS series is improved at high temperatures [37]. For applications requiring a higher level of creep resistance, at temperatures higher than 200°C, QE and WE series may be used.

2.4. Magnesium wrought alloys

Since most of the industries have shown less attention to the wrought alloys, investigations on the wrought magnesium alloys are more limited. The usage of wrought magnesium alloys only involves 2 percent of total usage of magnesium alloys. The application of sheet alloys of steel and aluminum alloys is widely spread in the structure of automobiles. However, the body weight of the structure constitutes near 25 % of the whole component. Hence the application of magnesium alloy in sheet form can be a good alternative due to their lower weight with comparable mechanical properties [38].

While the castability is the main issue in cast alloys, for wrought alloys it is important to find out the possibility of formability of the processed alloy. Magnesium alloy's intrinsic limitation for plastic deformation arises from its crystallographic structure as it will be discussed in the upcoming section. Lack of interest in wrought alloys has led to the development of few wrought alloys of magnesium having a lower fraction of element and variety of cast alloys. At high temperatures, it is found that alloying elements

forming the intermetallic initiate hot cracking during thermomechanical treatments. The main reason for restriction in adding aluminum to the AZ series is intermetallic compounds [39].

Commercial wrought alloys of magnesium mostly contain aluminum, zinc, manganese, and zirconium. The two wrought alloys widely used are AZ and ZK. ZK series have high strength among all magnesium alloys, though their ductility is limited at room temperature [40]. It is proved that addition of zirconium to magnesium alloy leads to grain refinement and increase of the strength. For instance, ZK 60 alloy has outstanding strength compared with its AZ series counterparts.

Table 2.2 shows the tensile properties of known magnesium wrought alloys. In order to produce a suitable wrought alloy, a reasonable trade off between strength and formability of the alloy is needed to be handled. Plastic deformation can be performed at high temperatures in order to obtain high strength along with favorable formability termed as superplasticity. Commercial AZ31. AZ91 and ZK60 alloys are highly investigated to characterize their superplastic behavior [41].

Table 2.2. Tensile properties of conventional wrought alloys at ambient temperature [41]

Alloy	Tensile strength (MPa)	Elongation to failure (%)
AZ31	240	11
AZ61	265	9
ZK60	277	8
MA210	210	30

2.5. Effect of addition of alloying elements to the magnesium alloy

Due to having a proper atomic diameter matching with aluminum and zinc, magnesium could be easily solid solution strengthened. For aluminum, atomic mismatch with magnesium is nearly 13% and for zinc, it is less than 9%. The current study concentrates on ZK series. Hence the effect of zinc and zirconium

element in magnesium is described. Additionally, the effect of aluminum as the most common alloying element is discussed.

2.5.1. Aluminum

As shown in Fig. 2.2, the solubility of aluminum is 12.7 wt% at maximum level in magnesium. The addition of aluminum improves the castability due to increase in the fluid flow of the melt [36]. On the other hand, further addition of aluminum increases the risk of shrinkage during casting. The solubility of aluminum at room temperature decreases to 2 wt%. Hence brittle $Mg_{17}Al_{12}$ precipitates will form reducing the mechanical strength. This precipitate type locates on the basal plane and has not any effect on blocking the movement of basal dislocations. During age hardening, it forms in long lath shaped particles which also deteriorate the mechanical strength [42].

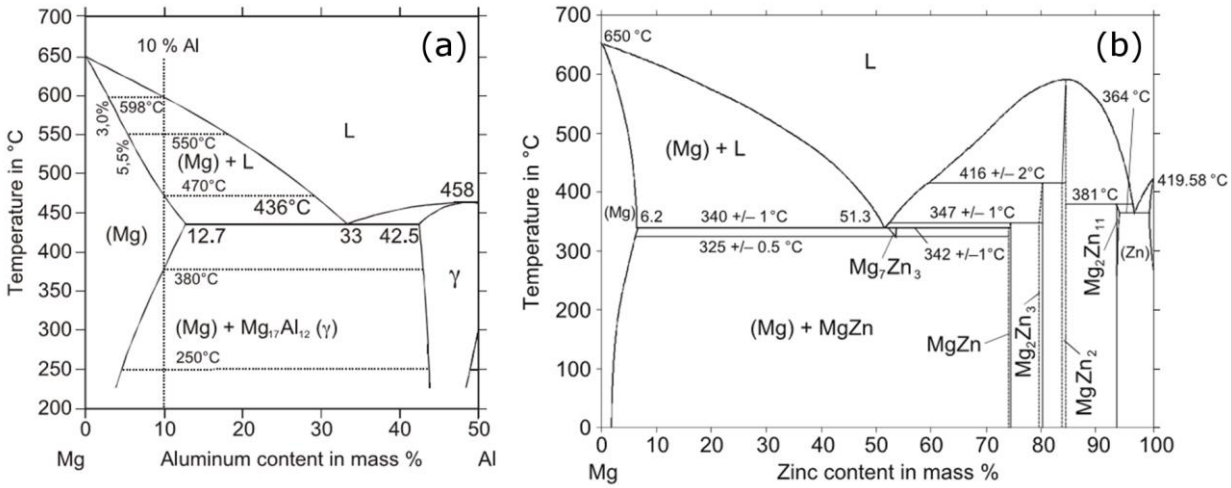

Fig. 2.2. Binary phase diagrams of (a) Mg-Al and (b) Mg-Zn [37]

2.5.2. Zinc

Zinc is the most significant alloying element in ZK alloys. Owning solubility of 6.2 wt% in magnesium, it also contributes to the melt fluidity. The strengthening method of the solid solution increases the critical resolved shear stress (CRSS) on basal planes. Although CRSS value is increased for basal slip, further addition of zinc decreases the CRSS value on prismatic slip leading to improved ductility [43]. The limitation inhibiting more addition of zinc is hot cracking during casting and warm rolling. The addition of

1 to 2 wt% is suggested for AZ alloys while age hardening mechanism will not be operative at this level of addition [44].

2.5.3. Zirconium

Zirconium is known as the most efficient addition for grain refinement in magnesium alloys. It is reported that addition of 0.6 to 0.9 wt% of zirconium into magnesium melt can reduce the grain size significantly and contribute to the formation of more uniform and equiaxed structure [45, 46]. It is not possible to use the zirconium as a refining factor if a principal amount of aluminum (more than 2%) is added to the magnesium matrix. In magnesium-aluminum alloys, a stable compound of Al-Zr is formed inhibiting the grain refinement of structure [46].

2.6. Deformation systems in magnesium alloys

Due to its hcp structure, deformation of the magnesium alloy is restricted at room temperature. Unlike cubic metals, for hcp structures, slip systems are limited, and ductility is low at ambient temperature. Whenever additional slip systems would be activated, high ductility can be achieved especially at high temperatures [47]. In order to understand the mechanical properties of magnesium alloy, it is essential to characterize the deformation mechanisms. Deformation of the magnesium alloy is mainly controlled by slip at room temperature. However, twinning can act as a contributing factor while slip systems are limited. At higher temperatures, grain boundary sliding (GBS) has the primary role in deformation [48].

2.6.1. Slip

Movement of blocks of crystals along the favorably oriented planes of crystals is called slip. Dislocation movement typically occurs along the closed-packed crystallographic orientation known as slip direction with a plane having the highest atomic density (slip direction). Slip systems are termed for a combination of these slip directions and slip planes [49]. The highest atomic density in a magnesium matrix is for (0001) plane (basal plane), and the closed packed direction is $[11\bar{2}0]$. Hence, the most common slip occurs on the basal plane along the $[11\bar{2}0]$ direction. The factor involving in the extension of slip systems are crystal

geometry and orientation of moving plane and the amount of shear stress generated by the applied stress. There is a minimum value for slip. The minimum amount of shear stress at which slip initiates is called the critical resolved shear stress (CRSS). Slip systems for an hcp crystal of magnesium is shown in Fig. 2.3.

Based on the Von Mises criterion, in order to generate a homogeneous shape change in a crystal, five slip systems leading to five independent deformation mechanisms are required. In other words, to consider no volume change during the plastic deformation, five independent components of a strain tensor are needed. Activation of any single slip systems generates a single component of strain tensor. Hence, in order to complete all five components of a strain tensor, activation of five slip systems is necessary [50].Two deformation modes are generated by a basal slip in a magnesium matrix. As mentioned before, the basal slip is the dominant mode at room temperature. Basal slip alone can not provide criteria for uniform deformation at room temperature, and this is the main reason for poor ductility of magnesium at ambient temperature. To provide five independent strain components of the tensor, activations of prismatic and first order pyramidal slip systems are necessary. However, it is reported that poor formability can be observed along certain directions for magnesium even with the activation of mentioned systems [50]. The slip in basal, prismatic and first order pyramidal systems do not contain the <c> component and activation of second order pyramidal slip and twinning is required for accommodating strain in this direction.

The CRSS values for different slip systems are shown in Fig. 2.4. It is observed that basal slip is nearly independent of temperature while the CRSS value for other slip systems decrease significantly at high temperatures.

Dislocations are mainly named as their corresponding Burgers vectors. Dislocations with Burgers vector of 1/3 $[11\bar{2}0]$ are named as <a> dislocations. <a> dislocations are mainly activated in a direction parallel to the basal plane since they can not provide deformation out of basal plane.

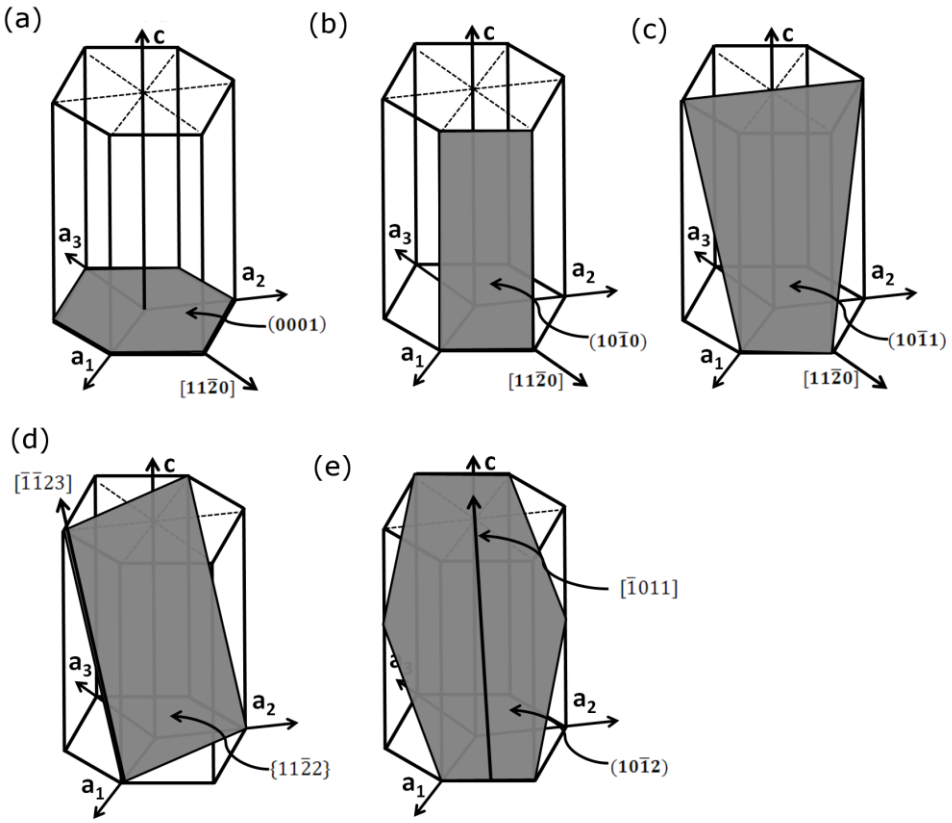

Fig. 2.3. Slip and twinning systems in a magnesium crystal (a) basal (0001) [11$\bar{2}$0] (b) prismatic (10$\bar{1}$0) [11$\bar{2}$0] (c) first order pyramidal (10$\bar{1}$0) [11$\bar{2}$0] (d) second order pyramidal (11$\bar{2}$2) [1123] slip systems (e) tension twinning (10$\bar{1}$2) [10$\bar{1}$0] [50]

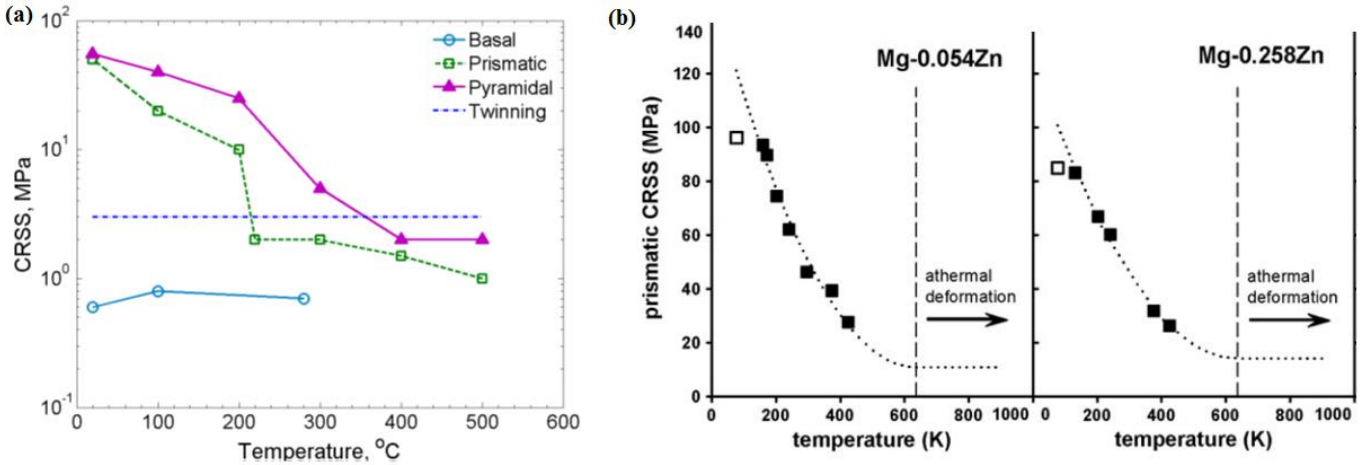

Fig. 2.4. Variation of Critical resolved shear stress (CRSS) values with temperature for different slip systems [51, 52]

In order to initiate deformation in c axis, activation of dislocation in this direction is needed. Dislocations designated as <c+a> have the burger vector of 1/3 [11-23] and their deformation is activated along the c-axis. Second order pyramidal slip is an example in which stress is applied along the c axis, during the

compression [53]. As shown in Fig. 2.4, the CRSS value for activation of <c+a> slip is the highest. It is reported that enhancement of ductility in magnesium alloys is highly dependent on the activation of <c+a> slip [54, 55]. A shown in Fig. 2.4b, the CRSS value for the prismatic slip of magnesium alloys is increasing by decreasing the temperature. This is the main reason for higher strength of magnesium alloys at low temperatures [52].

2.6.2. Twinning

The symmetric orientation of blocks of undeformed crystals generated by the deformation of a portion of deformed crystals is called twinning [49]. A shear displacement caused by deformation enforces the arrangement of atoms in a way that mirror-image effect is formed in the twinned part of the lattice relative to the untwined section. Total strain generated by the twinning is limited, and it mainly depends on the twin shear orientation. It is also reported that twinning can invoke some slip activity by reorientation of lattice and can promote plasticity [56]. Schematic view of a twinning deformation and a comparison with slip mechanism is shown in Fig. 2.5.

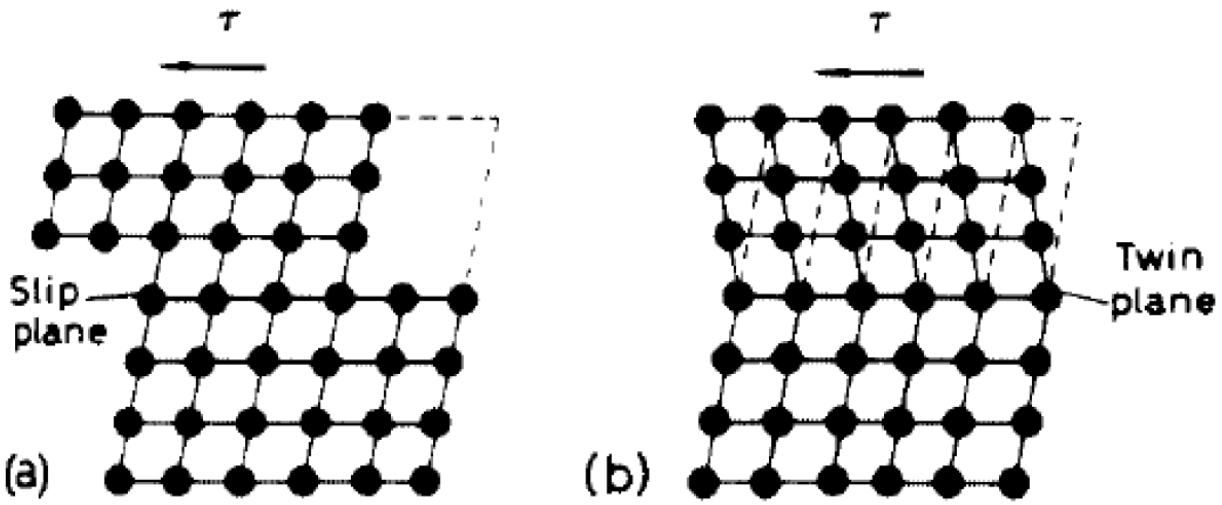

Fig. 2.5. Slip and twinning in a crystal [57]

As mentioned before, there is a critical lack of slip systems at room temperature for magnesium. Hence, the activation of twinning deformation mode is considered to be essential for improving plasticity at room temperature. In case that <a> basal slip cannot accommodate the deformation or where applied stress

parallel to the c-axis is required, activation of twinning becomes necessary. It is reported that under the condition of c-axis extension, (10-12) <10-11> twins are observed [10]. Extension along the c-axis means that the stress is applied parallel to the c-axis in a crystal under tensile extension. Twining along the (10-12) plane is the most easily activated twinning mode in hcp materials.

The effect of grain size in twinning is investigated in previous literature as well. Ecob and Ralph [58] showed that as the grain size microstructure increases, the contribution of twinning to deformation increases linearly. Barnett et al. suggested that by decreasing grain size or increasing temperature, a transition can occur from twin dominated deformation to the slip dominated one [59].

The relative CRSS values for slip and twinning systems at ambient temperature are summarized in Table 2.3 for pure magnesium, AZ31, and ZK60.

Table 2.3. Relative CRSS for various magneium alloys [59]

Material	$\tau_{twin/}\ \tau_{basal}$	$T_{prismatic(a)\ /}\ \tau_{basal}$
Mg	2.5-4.4	48-87
AZ31	3	5.5
ZK60	-	1.5-2

2.7. Texture

Each single grain has certain crystallographic orientation in a unit of structure. In deformation process such as rolling a preferential orientation (texture) in grains is developed and individual planes orient with respect to the axis of principal strain [49]. It is expected for a group of grains to develop a crystallographic texture, since the deformation mechanisms such as slip and twinning occur in the most preferred orientation. For the rolling process, texture is described using planes parallel to the surface of rolling and direction, in which rolling plane is parallel to the rolling direction (RD). A set of pole figures is used to characterize the texture. Pole figures are two-dimensional projections used to illustrate the orientation of a pole for a single crystallographic plane [50].

During rolling of magnesium alloys, a strong basal texture is formed meaning that basal planes of grains are oriented mostly parallel to the rolling direction [60]. It is also worth noting that for rolled samples with basal texture, <c> axis of grains is parallel to the normal direction of rolling (ND). In Fig. 2.6, pole figures for AZ31 rolled sheet are illustrated in different planes.

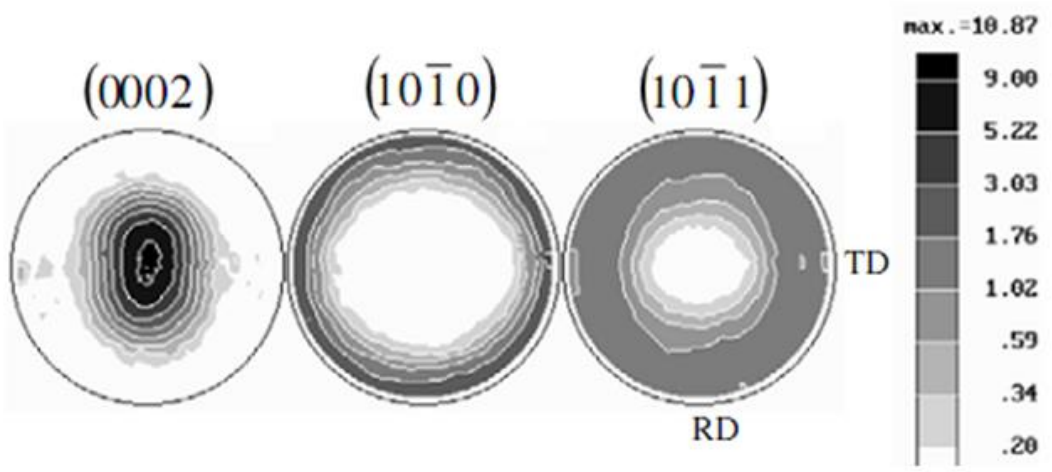

Fig. 2.6. Illustration of basal texture for hot rolled sheets of AZ31 [61]

Basal texture is formed by basal slip system and tension twinning along the c-axis. The rolling process reorients the <c> axis in a way that it becomes parallel to the normal direction of rolling leading to the alignments of basal planes parallel to the rolling direction [62, 63].

Mechanical properties of rolled sheets significantly depend on the orientation of applied stress relative to the sheet's texture. For instance, during compression, if the applied stress is parallel to the basal planes, activation of non-basal slip systems or twinning is required for the initiation of deformation [64].

2.8. Recrystallization in magnesium alloys

One of the important factors for mechanical enhancement of is grain refinement. It is known that during thermo-mechanical processes such as rolling, recrystallization of grains can lead to grain refinement. Recrystallization phenomena in magnesium alloys is briefly described below.

Annihilation and rearrangement of dislocations are two standard methods for reducing stored energy of material during deformation. This process is called as dynamic recovery in which strain-free grains can be

formed typically accompanied by material softening [65]. Recrystallization phenomena that occur during deformation is referred to as dynamic recrystallization (DRX).

A DRX mechanism is suggested for AZ31 magnesium alloys by Ion et al. based on the lattice rotation and dynamic recovery of grains [63]. The proposed mechanism is illustrated in Fig. 2.7. It is supposed that during deformation, tensile twinning is activated and basal planes are rearranged perpendicular to the stress direction. While basal slip is restricted to the grain boundaries, the orientation of lattice initiates the dynamic recovery and lead to the formation of subgrains. Migration of sub-grains along the grain boundaries leads to coalesce of grains and formation of high angle boundaries [66].

DRX can result in the formation of nuclei which can favorably orient during basal or non-basal slip. Depending on the size of newly-developed grains, there might be a chance of sliding. However, previous works suggest that low misorientation angles and strong basal texture are not consistent and intense dislocation movement is dominant [63]. The mechanism discussed above is related to gradual changes in the misorientations of sub-grains from low angle sub-grains to high angle ones and is termed as continuous DRX [67].

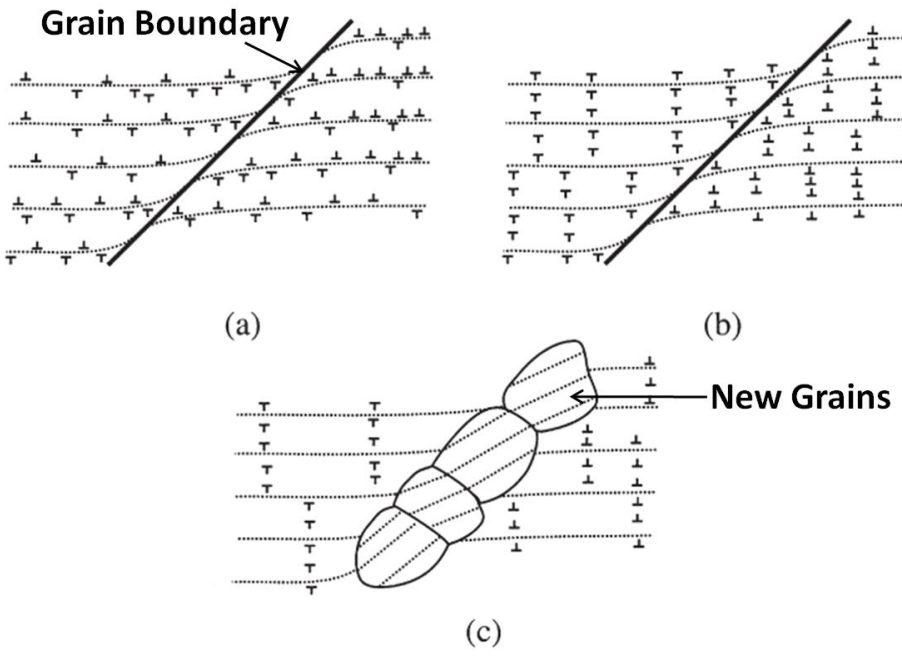

Fig. 2.7. Suggested DRX mechanism in magnesium alloys [67]

2.9. Thermo-mechanical treatment of magnesium alloys

Various deformation processes are designed and applied to reduce the grain size of the metal microstructures. It is well known that grain refinement leads to mechanical improvement in magnesium alloys [68]. A process such as cold and hot rolling, equal channel angular pressing (ECAP), accumulative roll bonding (ARB) and high-pressure torsion (HPT) are used to refine the grains of coarse grained materials. Due to a large amount of strain and intense deformation, mentioned processes are termed as severe plastic deformation (SPD) processes.

It is shown that hot rolling of magnesium alloys can reduce the grain size significantly. Chen et al.[69] investigated the effect of rolling and multi-pass rolling on the microstructure of ZK60 alloy. Formation of fully refined and equiaxed microstructure along with high density of shear bands was reported for hot rolling process [69]. Multi-pass rolling as an efficient method can be used for further grain refinement where grain boundary recrystallization can occur effectively [70, 71]. To obtain a homogenous structure during rolling, it is suggested to perform rolling in temperatures between 300℃ to 400℃, though there is no optimum temperature for rolling.

ECAP process can generate a refined structure by introducing high shear stress. ECAP is typically used to create a microstructure in micro-scale. During the process, a bar or rod is passed along a die which is limited by a channel. Grain refinement was reported for ZK60, and excellent mechanical properties of developed materials were published elsewhere [72-75].

Another method of grain refinement, high-pressure torsion has received significant attention in recent years. The circularly shaped material is pressed and simultaneously a torsion is exposed to the material using two anvils. Further information of HPT can be found in the previous literature [76, 77]. The final microstructure is generally in nano-scale. The average grain size of 0.7 μm is reported for the ZK60 alloy [78, 79].

2.10. Rolling principles

As a thermo-mechanical treatment, a warm rolling was applied in the current study to enhance the mechanical strength of the examined magnesium alloy. Hence, it is necessary to understand the basics of rolling for precise investigation of its effects. In a traditional rolling process, a sheet of metal is contracted between two rolls made of high strength materials while they are rotating in opposite sides [79]. Rolling is highly utilized in the automotive sector for developing high strength sheet metals. A traditional rolling mill apparatus stand is shown in Fig. 2.8. The mechanism of the flat rolling process is illustrated in Fig. 2.9.

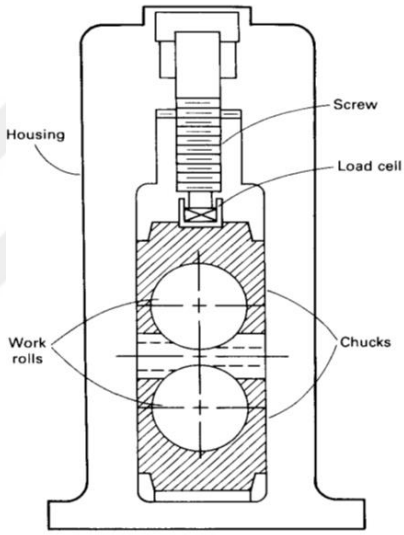

Fig.2.8. Schematic view of a rolling mill [79]

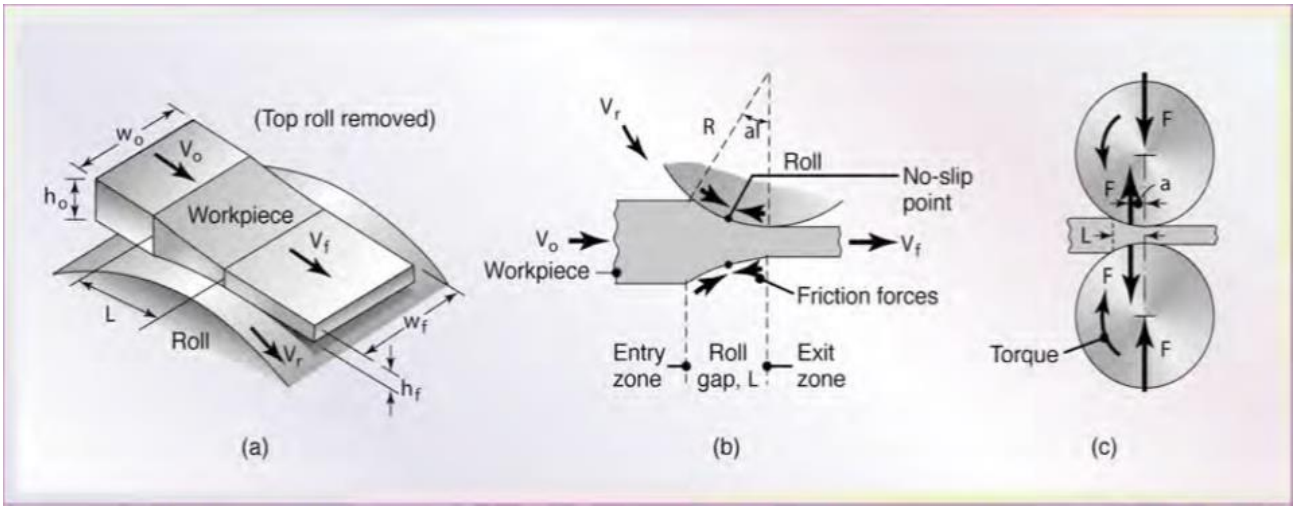

Fig. 2.9. Flat rolling process [79]

2.11. Precipitation Hardening

It is evident that in binary systems, excessive concentration of alloying elements leads to the formation of second phases. The thermo-mechanical process can also accelerate the formation of second phases [80]. These second phases may impede the motion of dislocations by acting as pinning point just as in solutes. Interaction of the second phase precipitates with dislocations is categorized in two ways. If the precipitate size is small, dislocations can cut through them (particle cutting), while for particles with a size larger than a critical value dislocation will circumnavigate around precipitates (particle looping) [57]. Two mechanisms of interaction between dislocations and particles are illustrated in fig. 2.10.

The yield stress for sheared particles is given by [81]:

$$\sigma_{yp} = Z_p M G K_P^{\frac{3}{2}} \left(\frac{fR}{b}\right)^{1/2} \quad (5)$$

where R and f are the average radius of precipitates and volume fraction of precipitates, respectively

The yield stress needed for precipitate lopping is given as:

$$\sigma_{y_0} = 2MGb/L_p \quad (6)$$

where L_P is the average inter-particle spacing in the glide plane and is called as the Orowan stress.

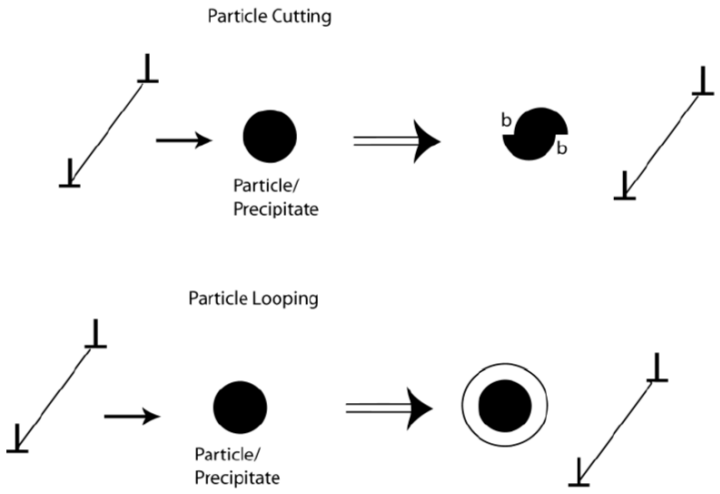

Fig. 2.10. Dislocations interaction with precipitates [57]

To establish a stable precipitation hardening, systematic arrangement of solutionizing, quenching, and aging treatments is required. In solutionizing, alloy is heated up to the mono-phase region, and it is kept for a long time to dissolve pre-existent precipitates. Then, it is quenched to avoid the formation of precipitates during cooling. Finally, at a temperature lower than the mono-phase region, the solid will be heated up to form fine precipitates [80].

2.12. Hall-Petch Strengthening

Grain refinement, as disused previously, is one of the effective methods for strengthening of materials. Grain boundaries act as physical obstacles against the motion of dislocations [49]. Grains have various crystallography orientations that change from grain to the next one. As this misorientation between grains increases, high angle grain boundaries play a role of barrier against the movement of dislocations. The effect of grain size on the mechanical strength of metals is expressed using the Hall-Petch relation [82]. The relationship proposed by Hall and Petch can be seen as follows:

$$\sigma_0 = \sigma_i + kD^{-1/2} \tag{10}$$

where, σ_0 and σ_i are the initial friction stress and the yield stress, respectively. K is the locking parameter and D is the grain diameter. It is inferred form this relation that reduction of grain size leads to higher yield strength which is termed as grain refinement strengthening.

2.13. Low temperature mechanical behavior of magnesium alloys

Low temperature behavior of magnesium alloys is investigated in literature. Mechanical properties of AZ91 magnesium alloy is investigated at temperature of -20℃ by Ahmad et al. [83]. It is said that AZ 91 alloy is deformed by the slip. However, at low temperature it is observed that twinning can be activated. At -30℃, Ahmad et al. observed severe damage in β-phase leading to more brittle fracture causing a reduction in the ductility. twins were observed at low temperature of -30℃. Both slip and twinning are activated at low temperature based on the observations of microstructure.

Plastic deformation of AZ31 was investigated at low temperatures by Wang et al.[84]. It was observed that by decreasing temperature, the tensile strength of samples was increased while the elongation to failure was decreased. Deformation mechanism was described by the dislocation-based theory. The dislocation motion mechanism was proposed to change by decreasing deformation temperature. At temperatures higher than 173K, the interaction between dislocations with forest dislocations was observed while at temperatures below 173K dislocation motion is under control of dislocation interaction with local lattice friction.

Chapter 3

EXPERIMENTAL METHODS

3.1. Initial material's characterization and processing details

The as received material used in this study was a zink-zirconium magnesium alloy commercially termed as ZK60. A wrought slab of ZK60 was received with dimensions of 400×300×25mm. The chemical composition of the as-received material is summarized in Table 3.1.

Table 3.1. Chemical composition of as-received slab of ZK60

Alloy	Mg (wt.%)	Zn(wt.%)	Zr(wt.%)	others(wt.%)
ZK60	92.34	6.32	0.93	≤0.5

The as-received material was exposed to solution treatment and then were warm rolled to develop a fine grained structure. Annealing treatment was performed on the rolled samples to restore the formability. Development of fine and uniform precipitates in processed samples was conducted by two methods of artificial static aging and stress aging. The details of processing procedure will be described thoroughly in the upcoming sections.

3.2. Alloy processing

Prior to the conduction of aging, it is necessary to remove the history of heat treatment for the as-received slab and to refine the structure as well. Hence, solution treatment and rolling are performed on the samples, respectively. Further heat treatments are performed to improve the mechanical response.

3.2.1. Solution treatment

Using electron discharge machine (EDM), samples with dimensions of 50×40×4 mm were cut and prepared for solution treatment. Solution treatment was conducted at 500℃ for 2 hours inside a vacuum furnace to avoid the adverse effects of oxidation. After insertion of samples into the furnace , argon gas was used inside the chamber and pressure was decreased to 10^{-3} mbar using the vacuum apparatus. Fig. 3.1. Indicates the vacuum furnace used for solution treatment procedure. Samples were removed from the

chamber after 2 hours and were quenched in water to preserve the attained structure. After solution treatment process, it is expected that a uniform microstructure is obtained.

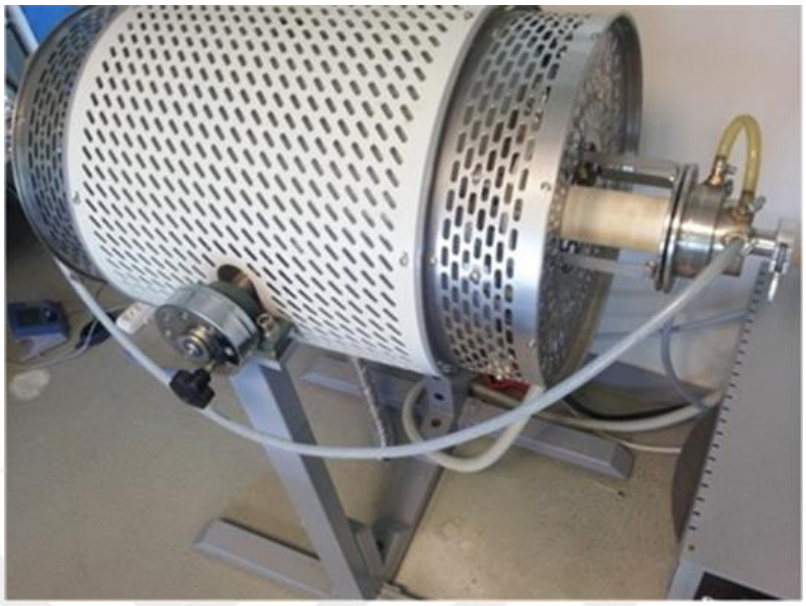

Fig. 3.1. Vaccum furnace used for heat treatment process

3.2.2. Warm rolling

Thermo-mechanical process is conducted to develop a stable structure with fine grains. A systematic rolling schedule is developed for the samples. The rolling was performed at 300℃. The samples for rolling were heated inside a furnace for 10 minutes and then were rolled. The samples were quenched in the water to preserve the obtained structure. The same procedure was repeated at every pass of rolling. The initial slabs of rolling had the thickness of 4 mm while the final rolled sample's thickness was 2 mm. In every pass, 5 percent total reduction in thickness was achieved. More reduction was not possible to perform due to the formation of edge cracks in later stages of rolling as shown in Fig. 3.2.

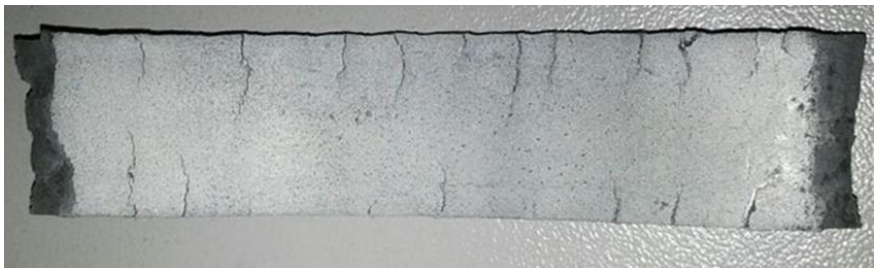

Fig. 3.2. Formation of edge crack in later stages of rolling

The material was deformed by unidirectional rolling in all passes. Total reduction in thickness of 50% was achieved for the rolled samples. As the rollers were not heated, preheating of samples at every pass was necessary. Rolling was conducted with speed of 0.17 ms^{-1} with rollers made of hardened as shown in Fig. 3.3. Sample gathering was done for investigation of microstructural evolution after rolling as shown in Fig. 3.4.

3.2.3. Annealing treatment

As it will be reported in the upcoming sections, the rolled samples exhibited high strength while their ductility was decreased to 2%. In order to restore the formability of samples after rolling, annealing heat treatment was applied. Annealing was performed in the vacuum furnace at a temperature of 350℃ for 2 hours. The samples were then quenched with water. The ductility of annealed samples was enhanced due to the formation of more equiaxed grain in the structure. This was in good agreement with the finding of previous literature [85, 86].

Fig. 3.3. Rolling mill used in this study

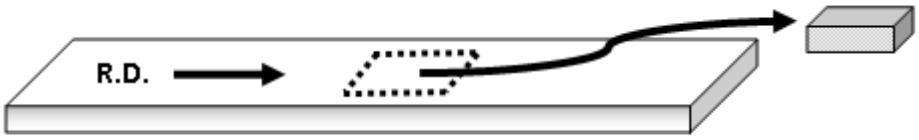

Fig. 3.4. A schematic drawing showing a rolled sample and specimen gathered for metallography

3.2.4. Age hardening methods

Development of new precipitates is necessary for enhancing the mechanical strength. For this purpose, two methods of age hardening were applied. First conventional aging treatment inside the furnace was conducted. The effect of aging under stress was investigated and compared with static aging as well.

3.2.4.1.Static aging

The static aging process was performed in a vacuum furnace to eliminate the adverse effect of the oxidation during the process. Samples were then quenched in water in order to preserve the structure. It is well established that the temperature and duration of the aging process can influence the size and density of precipitates in magnesium alloys [22, 87-89]. Based on the observations from previous works, a systematic scheme was arranged for temperature and time of static aging [22, 87-89]. Static aging was performed at 120℃,180℃, and 240℃. The aging time was ranged from 6 to 72 hours. The summarized experiments prepared for the static aging samples is illustrated in Table 3.2.

3.2.4.2.Stress aging

In order to investigate the effect of load direction on the orientation of the formed precipitates, conduction of aging under stress is required. For this purpose, an apparatus was designed and manufactured to apply elastic tensile load during the heat treatment. The designed apparatus consists of vacuum room, vacuum pump, loading mechanisms, heating unit and sample grips as shown in Fig. 3.5. To measure the applied load exposed to the sample, a load cell is located at the top of the center mill joined to the sample's grip. A vacuum pump is connected to the system to provide the vacuum condition during the process to avoid the effect of oxidation. For stress aging process, after the sample is loaded, the vacuum condition is

provided using the vacuum pump, and argon gas is injected into the chamber. Using temperature controlling system, the resistances is set to the desired value and the sample is heated using resistive heating.

Table 3.2. Experiments for static aged samples

No	Condition	Aging temperature (°C)	Aging Duration (h)
1	ST+rolled+annealed+aged	120	6
2	ST+rolled+annealed+aged	120	12
3	ST+rolled+annealed+aged	120	24
4	ST+rolled+annealed+aged	120	48
5	ST+rolled+annealed+aged	120	72
6	ST+rolled+annealed+aged	180	6
7	ST+rolled+annealed+aged	180	12
8	ST+rolled+annealed+aged	180	24
9	ST+rolled+annealed+aged	180	48
10	ST+rolled+annealed+aged	180	72
11	ST+rolled+annealed+aged	240	6
12	ST+rolled+annealed+aged	240	12
13	ST+rolled+annealed+aged	240	24
14	ST+rolled+annealed+aged	240	48
15	ST+rolled+annealed+aged	240	72

It is necessary to determine the loading level for stress aging along with setting the duration and temperature values. Elastic stress values of 25, 50 and 100 MPa were selected in this study. Aging temperatures of 120℃ and 180℃ were chosen and aging duration of 1 to 24 hours was selected. The experiments for the stress aged samples in summarized in Table 3.2. The limitations for selection of stress aging parameters is discussed. Visually it was observed that samples stress aged at 100 MPa for higher than 6 hours were fractured from the grip zone.

Previous literature suggests at that stress aging would be done in the elastic zone [90, 91]. Hence, the effect of applied stress was examined at lower stress values of 25 and 50 MPa based on the resullts obtained for mechanical testing at 100℃ and 200℃ . As it will be shown in the mechanical properties characterization section, the first trial at stress aging value of 50 MPa and aging time of 3 hours showed

better mechanical values relative to the 100 MPa stress aged ones. Hence, the applied loads of 50 and 25 MPa were pursued for further investigation of the effect of applied stress. The aging times of samples were selected step by step based on the comparative study in which the future aging time was selected based on the mechanical property trends. To select the parameters for stress aging, there is a critical lack of literature for stress aging of ZK60 alloy. There have been few research works on the effect of stress aging for Al-Zn-Mg and Al-Cu-Mg-Ag alloys [10]. However, the parameter selection is entirely dependent on the yield strength (YS) of material under investigation. Mechanical properties of the sample after rolling and annealing was investigated at 100℃ and 200℃ to identify the yield strength.

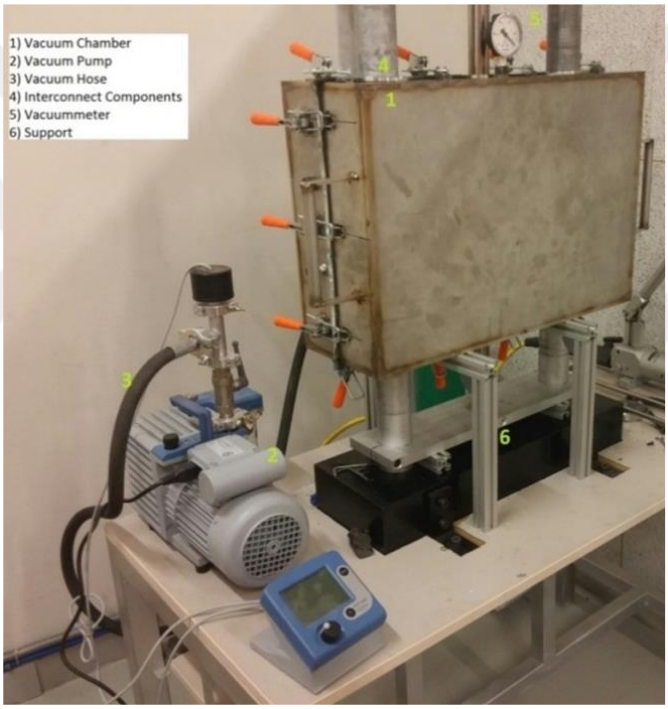

Fig. 3.5. Fabricated stress aging apparatus

For samples stress aged at 50 MPa at the aging temperature of 180℃, the effect of time was investigated for 1, 3,6,12, and 24 hours. For samples stress aged at 50 MPa at temperature of 120℃, the aging time of 1, 3, 6, and 12 hours were selected. Further investigation of time was stopped at 12h since the ultimate tensile strength (UTS) and elongation values were decreasing for samples by increasing the time up to 12h. For the samples stress aged at 25 MPa and 120℃, the effect of time was investigated at 3,6 and 12h. Finally, the effect of aging time for samples stress aged at 25 MPa and 180℃ were investigated at the aging times

of 3, 6, and 12 hours as similar to the 25Map and 120℃ condition. The experiments for stress aged samples is summarized in Table 3.3.

Table 3.3. Experiment for the stress aged samples

NO	Condition	Applied stress (MPa)	Aging temperature (C)	Aging time (h)
1	ST+rolled+annealed+aged	25	120	3
2	ST+rolled+annealed+aged	25	120	6
3	ST+rolled+annealed+aged	25	120	12
4	ST+rolled+annealed+aged	25	180	3
5	ST+rolled+annealed+aged	25	180	6
6	ST+rolled+annealed+aged	25	180	12
7	ST+rolled+annealed+aged	50	120	1
8	ST+rolled+annealed+aged	50	120	3
9	ST+rolled+annealed+aged	50	120	6
10	ST+rolled+annealed+aged	50	120	12
11	ST+rolled+annealed+aged	50	180	1
12	ST+rolled+annealed+aged	50	180	3
13	ST+rolled+annealed+aged	50	180	6
14	ST+rolled+annealed+aged	50	180	12
15	ST+rolled+annealed+aged	50	180	24
16	ST+rolled+annealed+aged	100	180	3
17	ST+rolled+annealed+aged	100	180	6

3.3. Microstructure Evaluation methods

3.3.1. Optical microscopy

Samples were cut down into dimensions of 10× 10 ×10 mm using a cutting machine in which silicon carbide disk was applied for rotation at cutting speed of 200 rpm. The samples for rolled slabs were chosen from the center of the rolled surface to eliminate the effect of edge cracks. Samples were then cold mounted using epoxy and hardener to handle the sample during mounting operation. Mounted samples of the alloy are presented in Fig. 3.6.

Conventional metallographic preparation method was used. Samples were ground with 500,800, 1200 and 2500 grits SiC papers. The water based lubricant was used to decrease the friction. Cloths of 3 and 1 μm were used for polishing by diamond suspension. During polishing with 1 μm clothes, ethanol based lubricant was used to prevent surface scratching and particle surrounding into the magnesium matrix.

Ground and polished samples were rinsed in ethanol and water after the operation. Samples were then etched in a solution of 5 gr picric acid, 10 ml acetic acid, 70 ml ethanol and 10 ml distilled water for 20 seconds to reveal grain boundaries. An optical microscope attached to the camera was utilized to reveal the grains in different magnifications.

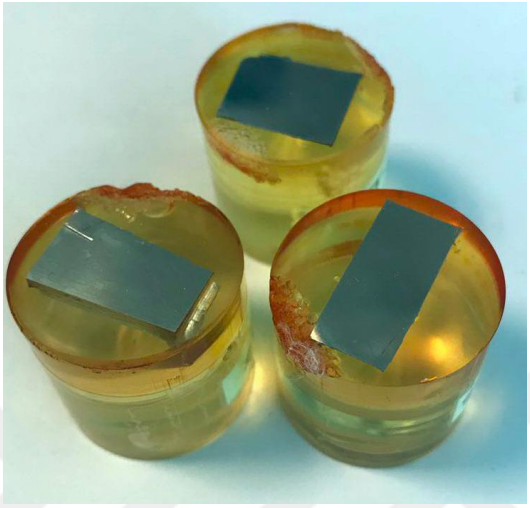

Fig.3.6. Cold mounted samples of Zk60

3.3.2. Scanning Electron Microscopy (SEM)

In order to reveal the concentration of alloying elements and sub-grains in the structure, Zeiss scanning electron microscopy (SEM) was applied. The samples for SEM were ground and polished as previously mentioned for the OM samples. The last grinding paper of #2500 was performed using the ethanol lubricant without water to restrict the oxidation. The samples were etched with the optical microscopy solution as mentioned in Section 3.3.1. Before SEM characterization, samples were rinsed with a plasma cleaner at the final step. SEM was performed in high magnifications to recognize the precipitates in micro-size. For energy dispersive X-Ray (EDX) analysis, a Field Emission Gun Scattering Electron Detector (FEGSEM) was used. Back-scattered electron detector (BSE) was applied to capture images in high magnifications. BSE was conducted at 15 kV accelerating voltage.

3.3.3. Transmission Electron Microscopy (TEM)

The samples were mechanically ground and polished down to 100µm. Prepared foils were then twin jet electro-polished using a solution of 60% methyl alcohol (CH3OH), 30% glycerin ($C_3H_8O_3$), and 10% nitric

acid (HNO_3) and then ion milled. Twin jet electro-polishing was conducted at 4 kV, and a tilting angle of 6° was used for ion milling.A JEOL 2010 microscope was used with an accelerating voltage of 200kV for imaging microscopic features and identifying the precipitates.

3.4. Crystallographic Texture measurement

3.4.1. X-Ray Diffraction

Samples for X- Ray diffraction (XRD) are ground, polished and then located on a tilting stage termed as goniometer. The dimension of samples for XRD are selected as 10×10×1mm which is a reliable area for measurements. The exact position of the peaks is firstly measured, then the location of the source and detector is changed from one single set of planes to an individual pole. The sample is tilted between 0 to 85° to reflect the measurements. This reflection is made to get the concentration of a single pole in various directions. The oscillation of sample may involve a large area of near 1 cm^2 to capture a broad scan [92]. Fig. 3.7 illustrates the schematic drawing of the XRD setup.

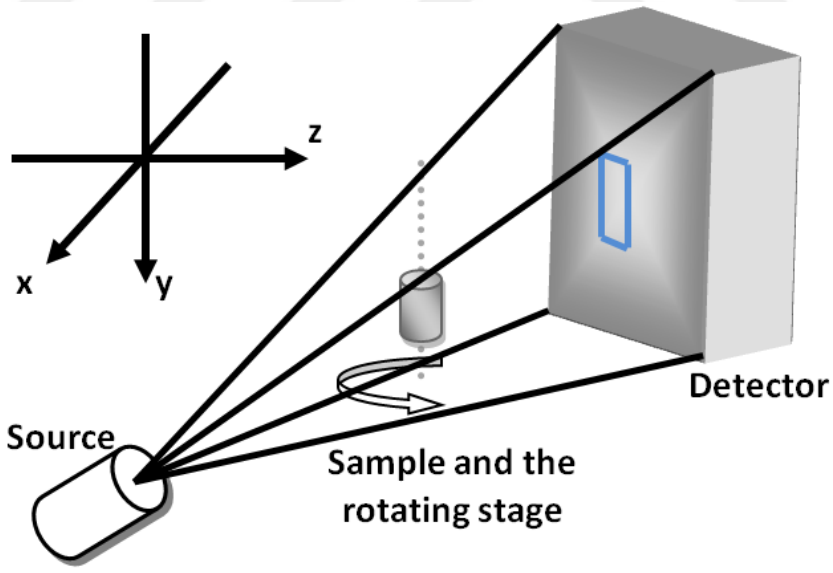

Fig. 3.7. Schematic drawing of XRD apparatus [92]

XRD is mainly used for macro-texture analysis in a broad range of sample oscillation. In this method, sample preparation is easy and measurement is performed relatively quickly. Since the samples are tilted 85°, information for remaining 5°of the pole is not available and needs to be calculated using the developed models. Moreover, XRD is not a suitable method for microtexture analysis where orientation in a micro-

scale area is required. Hence, the orientation of single grain and disorientation of adjacent grains can not be measured using this method.

3.4.2. Electron Backscattered Diffraction (EBSD)

The sample was located on a stage connected to a BSE detector equipped with a focused ion beam (FIB) apparatus and was tilted 70° from the horizontal direction. The backscattered electrons are captured on a phosphor screen using an electron backscattered diffraction (EBSD) camera. A measured background over broad area is subtracted from the observed backscatter pattern and Kikuchi patterns are captured. The ATOM software is used to analyze the Kikuchi bands to determine the crystal orientation in terms of Euler angles φ_1, ϕ and φ_2 [93, 94]. A schematic design of the EBSD is shown in Fig. 3.8.

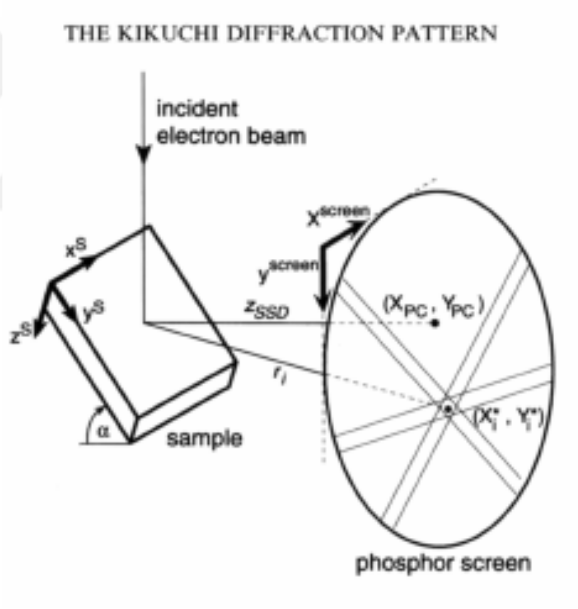

Fig. 3.8. Formation of Kikuchi bands on the phosphor screen used in an EBSD system [94]

It is necessary to calibrate the distance between the sample to the screen, sample tilt angle, specimen height and working distance in the camera. Tilting sample is needed to optimize the path length and to improve the pattern contrast. However tilting angle for more than 80° leads to distortion of the image. An angle near 70° is suitable to enhance both contrast and volume anisotropy of the sample.

EBSD gives helpful information about the misorientation between grain and grain boundary character distribution. In fine grained materials, utilization of EBSD can contribute to better understanding of the evolution of structure since the microstructure develops from dislocation cell boundaries [95]. Additionally, complete pole figures can be gained from a Kikuchi pattern to calculate the full orientation of a crystal. Since rolled materials have a high density of dislocations, it is a challenging effort to utilize EBSD characterization. For magnesium alloys due to high oxidation rate, it is hard to prepare EBSD samples using conventional metallographic preparation methods. Hence, FIB appratus connected to a Zeiss scanning electron microscope was applied to prepare samples for EBSD.

3.5. Mechanical testing

3.5.1. Hardness measurement

Samples for hardness tests were prepared based on the ASTM-E4 standard for hardness [96]. The samples were ground up to 2500 grits and then polished using the 1μm diamond suspension. Vickers microhardness test with intervals of 1 mm was performed using 1000 gf for 15 seconds. In order to assure the repeatability and accuracy of the results, five hardness tests were performed on every condition. The reported values for the hardness results are the mean value of obtained five points.

3.5.2. Uniaxial low temperature tensile tests

In order to investigate the temperature dependent deformation behavior of processed samples, low-temperature tensile tests were conducted. The tensile samples were electro-discharge machined with a gauge length of 15 mm. The samples were prepared in a direction in which extension direction was parallel to the rolling direction. Samples were ground and polished before tests in order to eliminate the adverse effect of scratches, and residual stressed formed during electro-discharge machining (EDM). Tensile tests were conducted at a strain rate of 10^{-3} s^{-1} at ambient temperature, -20°C and -60°C. All samples were cooled down to the deformation temperature and then deformed in a single loading stage. An Instron mechanical testing frame equipped with an environmental chamber was used. The specimen temperature

was measured using K-type thermocouples during deformation. The displacement of the samples were recorded using an extensometer.

In order to diagnose the elastic modulus of rolled samples for stress aging, high temperature tests were performed at temperatures of 100°C and 200°C. High temperature tensile tests were performed in the same mechanical testing frame as shown in Fig. 3.9. In order to assure the repeatability and accuracy of the results, three tensile tests were performed on every condition.

Fig. 3.9. high temperature set up [97]

Chapter 4

EFFECT OF ROLLING AND AGING PROCESSES ON THE MICROSTRUCTURE EVOLUTION OF ZK60 MAGNESIUM ALLOY

4.1. Optical microscopy characterization

4.1.1. Microstructure of solution treated sample (T4)

Fig. 4.1a and 4.1.b indicates the microstructure of solution treated (T4 condition) samples in two different regions. Coarse and equiaxed grains are apparent in both figures. Average grain size of 80μm was measured. It is hard to observe particles in micro-scale in solution treated samples due to the high amount of solubility of them into the matrix during the treatment. On the other hand, the twinning effect is hard to catch in T4, as it is shown in Fig. 4.1a and 4.1.b.

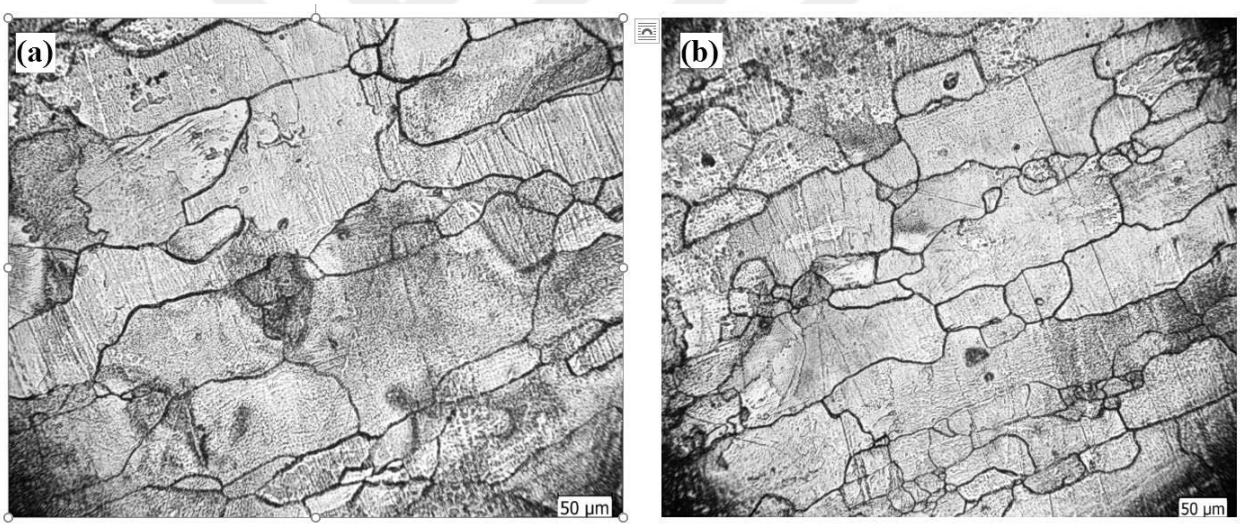

Fig. 4.1. Microstructure of solution treated sample in two different zones

4.1.3. Microstructure of solution treated and artificially aged samples (T6)

Fig. 4.2 indicates the microstructure of solution treated and subsequently artificially aged samples in two different zones at a temperature of 180℃ for 24 hours. As shown in Fig. 4.2, the grain size is relatively finer than solution treated sample (70μm) while the twinning is apparent in the microstructure of Fig. 4.2a. It is well known that twinning contributes to the deformation at ambient temperature due to limited slipping systems in magnesium alloys.

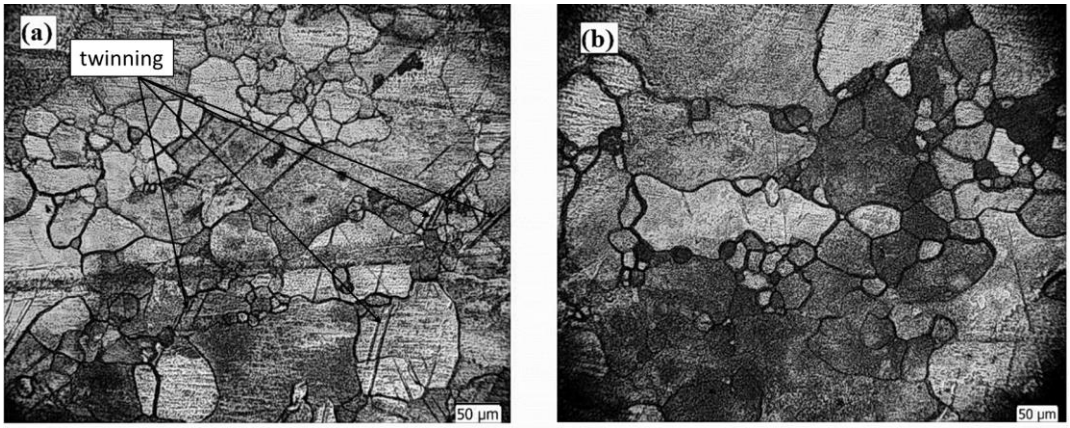

Fig. 4.2. Microstructure of solution treated and subsequently aged samples in 180℃ for 24 hours

4.1.4. Microstructure of rolled and annealed samples

Fig. 4.3a indicates the microstructure of solution treated and rolled samples while Fig.4.3b illustrates the microstructure for solution treated, rolled and annealed sample. The rolled sample have fine grains with average grain size of 6µm and high density of twinnings while for an annealed samples more stable structure with grain size of 25µm is observed. It is shown that the annealing can uniformly reduce the size of the grains which as described in the previous literature can increase the ductility value. Static recrystallization during the annealing process leads to more uniform and equiaxed grain distribution in the structure [60, 85]. For the rolled sample shear bands with high density and twinning effect are evident. In shear bands area, grain recrystallization is achieved with further processes such as aging and annealing.

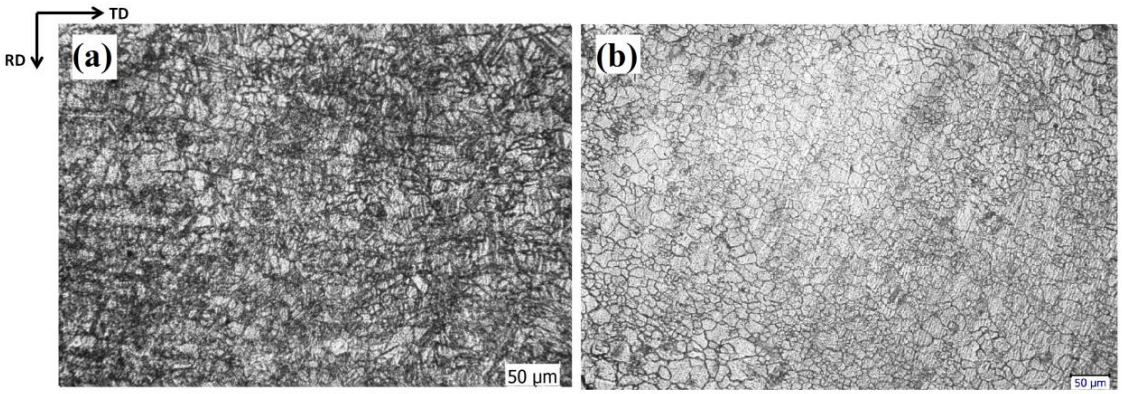

Fig. 4.3. Microstructure of (a) solution treated and rolled (b) solution treated, rolled and annealed sample

4.1.5. Microstructure of static aged samples

Microstructure of the static aged samples at various aging duration and temperatures are investigated as well. At the upcoming figures rolling and traverse directions (RD and TD) are marked. Aging temperature has no significant effect on grain size and structure uniformity. It is previously stated that the effect of aging treatment is trivial on the grain size change of the magnesium alloys [98]. On the other hand, the effect of aging treatment on the nucleation of precipitates and their distribution in the structure needs to be investigated. Using the optical microscope, the observation of the precipitates was not possible since the size of precipitates for the ZK60 alloy is in nanoscale and near 50 nm, which is observable only with the transmission electron microscope (TEM). Fig. 4.4 shows the microstructure of rolled, annealed and then statically aged samples at a temperature of 120℃. Aging time ranging from 6 to 72 hours was applied. The microstructure is relatively equiaxed with fine grains uniformly distributed with an average grain size of 12μm. Symptoms of shear bands are evident for samples aged for 24 hours as shown in Fig. 4.4c.

Fig. 4.5 Shows the microstructure of static aged samples at the temperature of 180℃. The aging time is ranging from 6 hours to 72 hours. By increasing the aging time from 6 hours to 24 hours more uniform and equiaxed grain are observed. For the aging time of 24 hours, shear bands along the rolling direction are observed with uniform grains distribution. Observation of uniform grains for rolled and aged samples of magnesium alloys is hard due to the high density of shear bands impeding the observation of dynamic recrystallized grains [99-101]. The average grain size of the samples aged at 180℃ is 20μm. Grain refinement as a common phenomenon for the rolled sample is evident at all aging durations.

Fig. 4.6 shows the microstructure of static aged samples at the temperature of 240℃. The aging time is ranging from 6 hours to 72 hours. Relative to the samples aged at 120℃ and 180℃, the grains of 240℃ static aged samples are coarser, and the uniformity of grains is decreased due to the high amount of heat input exposed to the structure. Shear bands start to reveal at the aging duration of 12 hours, and the shear bands density gets to its highest at the aging time of 48h. The average grain size of sample aged at 240℃

for duration of 12 hours is 35μm. However, coarse grains are observed at the aging duration of 48 hours. The average grain size for samples with duration of 72 hours is 42μm.

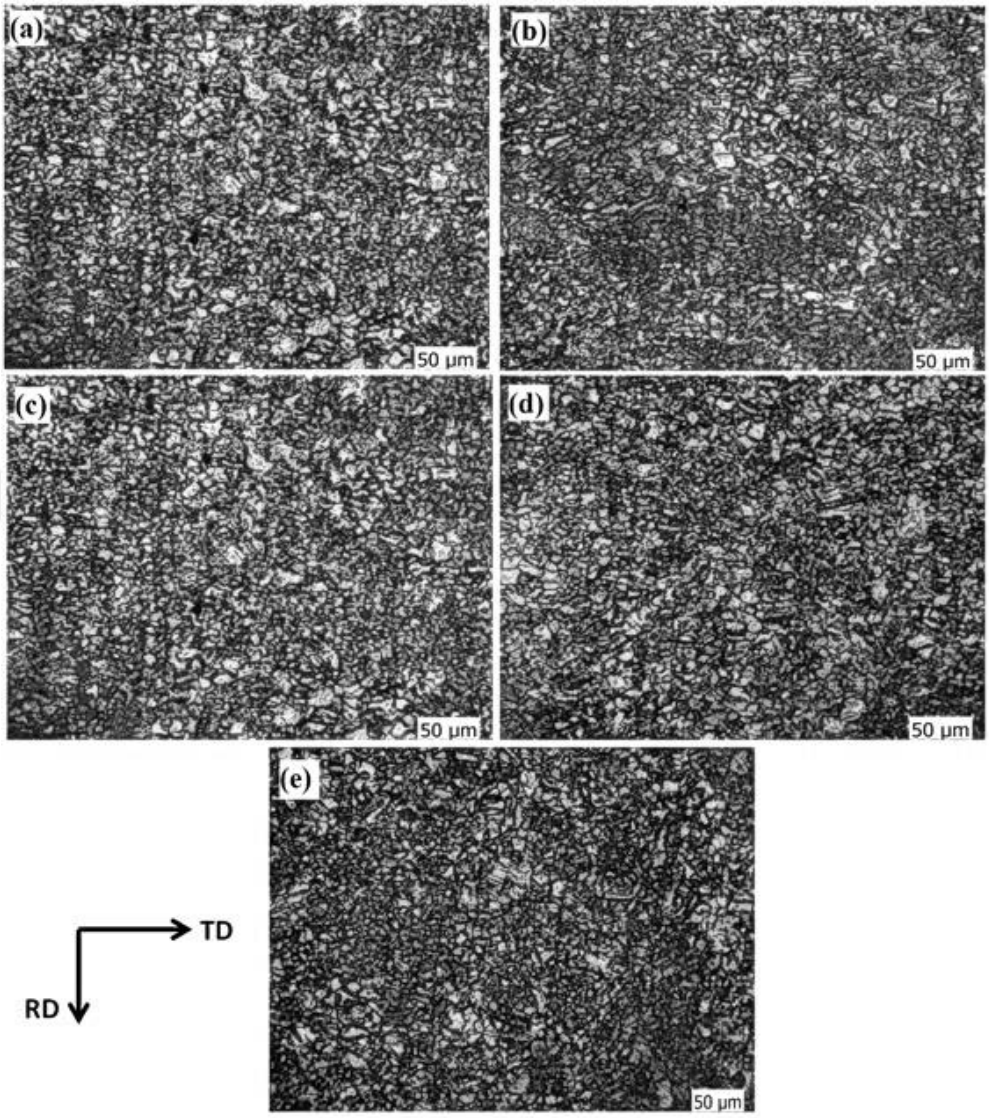

Fig. 4.4. Microstructure of samples aged at 120℃ for aging times of (a) 6h (b)12h (c) 24h (d) 48h (e) 72h

Temperature can easily cause recrystallization of grains at specified temperature while the aging time can limitedly influence the grain refinement and as a more efficient method can accelerate the formation and distribution of precipitates [69, 102, 103].

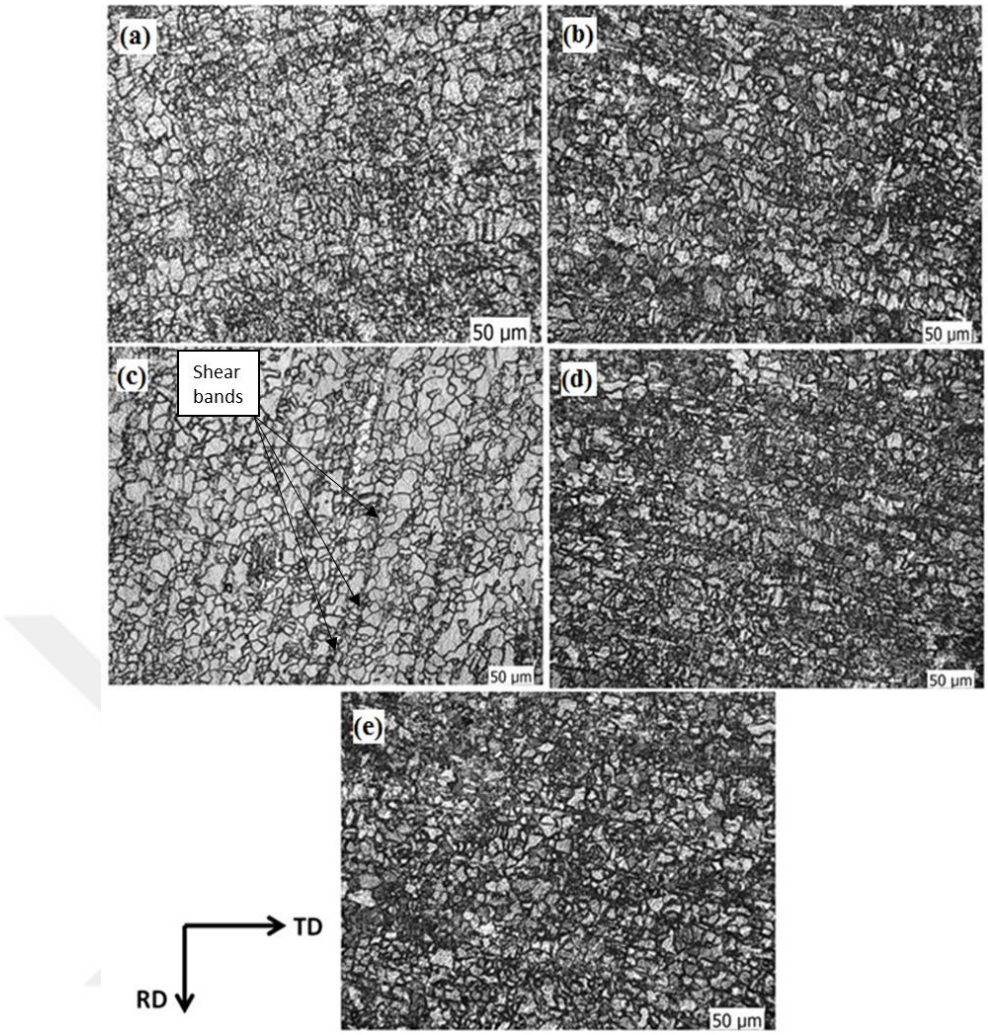

Fig. 4.5. Microstructure of samples aged at 180℃ for aging times of (a) 6h (b)12h (c) 24h (d) 48h (e) 72h

4.1.6. Microstructure of stress aged samples

The effect of aging time and the temperature is characterized for the stress aged samples at various applied stresses. The effect of amount of load on the microstructure of samples is investigated as well. Fig. 4.7 is presented to compare the microstructure of samples stress aged at applied loads of 25, 50 and 100 MPa. The average grain size of the sample stress aged at 25 MPa is 30µm. It can be seen that by increasing the amount of applied load the grain size decreases. Fully refined grains are observed for the sample stress aged at 100 MPa with average grain size of 20µm. Dynamic recrystallization is expected to occur during the stress aging, which can be the main reason for grain refinement at high loads [63, 104]. However,

recrystallization is also affected by the temperature of aging and its duration [105]. Hence, the effect of aging temperature and aging duration needs to be investigated for the stress aged samples.

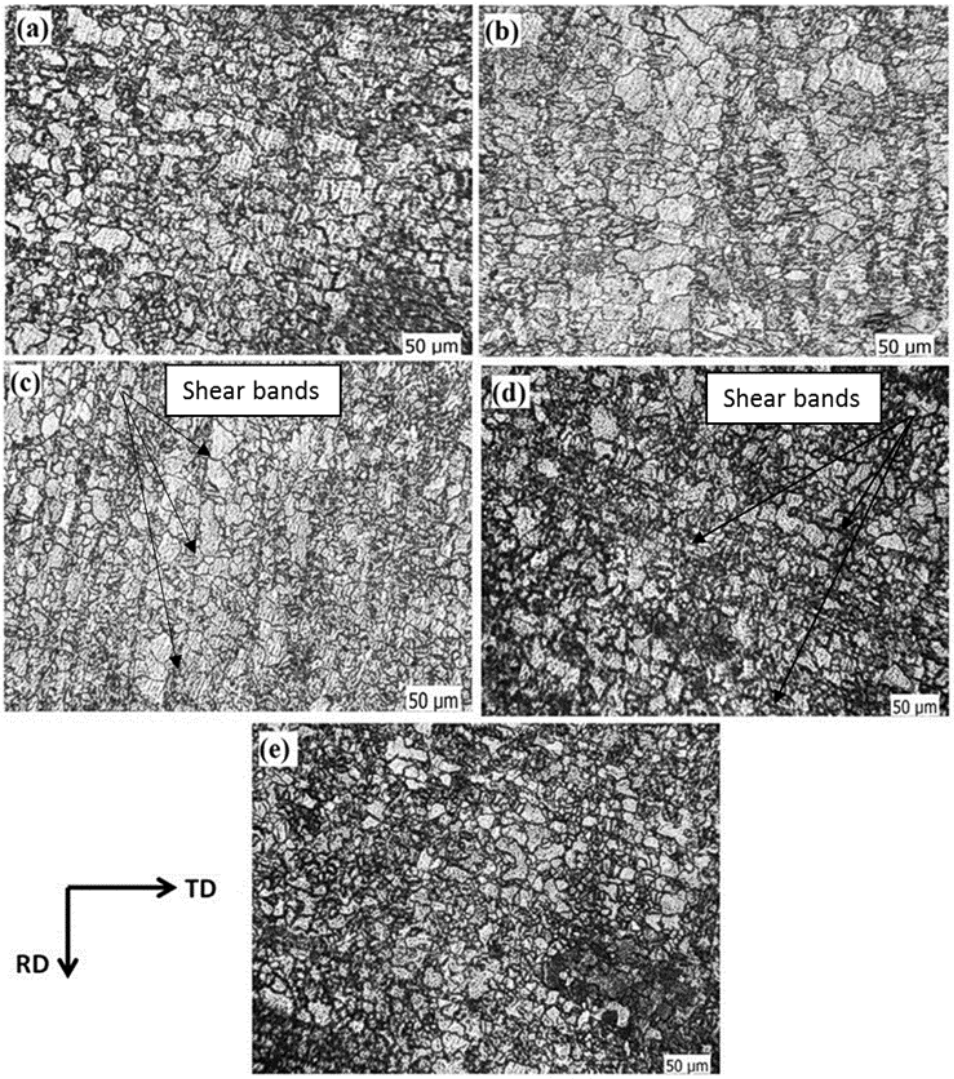

Fig. 4.6. Microstructure of samples aged at 240℃ for aging times of (a) 6h (b)12h (c) 24h (d) 48h (e) 72h

The effect of aging time for applied load of 100 MPa (Fig. 4.7) was examined only for samples stress aged at temperature of 180℃ due to the failure of samples for more than 6 hours. No obvious change in shear band density is observed by changing the aging duration from 3 to 6 hours. However, grain size has decreased from 25µm to 15µm by increasing the aging time from 3 to 6 hours due to the dynamic recrystallization of grains.

Fig. 4.9 shows the microstructure of samples stress aged under the stress value of 50 MPa and aging temperature of 120℃ at the different aging duration of 1, 3, 6 and 12 hours. For sample aged for one hour,

shear bands along with the elongated equiaxed grains are observed. At the aging time of 3 hours, the density of shear bands increases to the maximum value and the dynamic recrystallization of grains is hardly observable due to the high density of bands. This high density of shear bands can be the main reason for improved mechanical properties of samples aged at 50 MPa, 120℃ for 3 hours as it will be discussed in upcoming section. The existence of the shear bands can act as new nucleation sites during the static recrystallization, and this can lead to grain refinement and increase the mechanical properties of stress aged samples [106]. Dynamic recrystallization is observed for samples aged for 6 and 12 hours. Coarse grains with size of 46μm are observed at high duration of 72 hours. According to the results of Fig. 4.9, the effects of subsequent rolling and stress aging on the microstructure of the samples is improving grain size distribution and microstructural homogeneity.

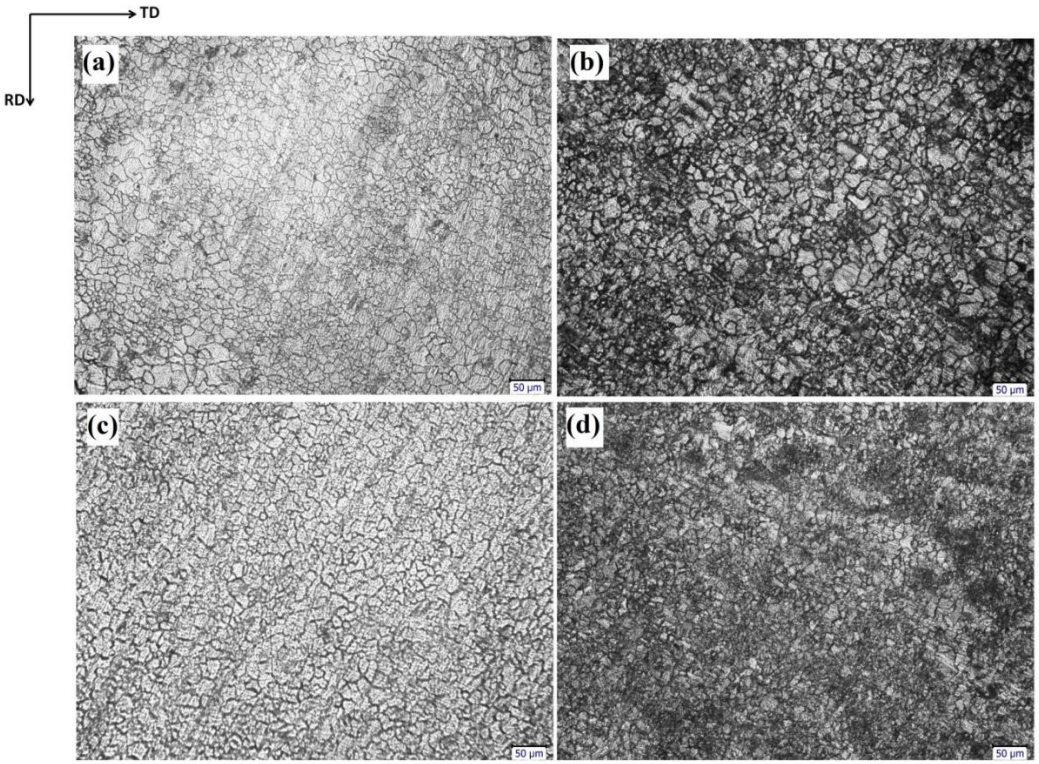

Fig. 4.7. Effect of applied load on the microstructure of stress aged samples (a) rolled- annealed samples (b) DA at applied load of 25 MPa (c) 50MPa (d) 100 MPa

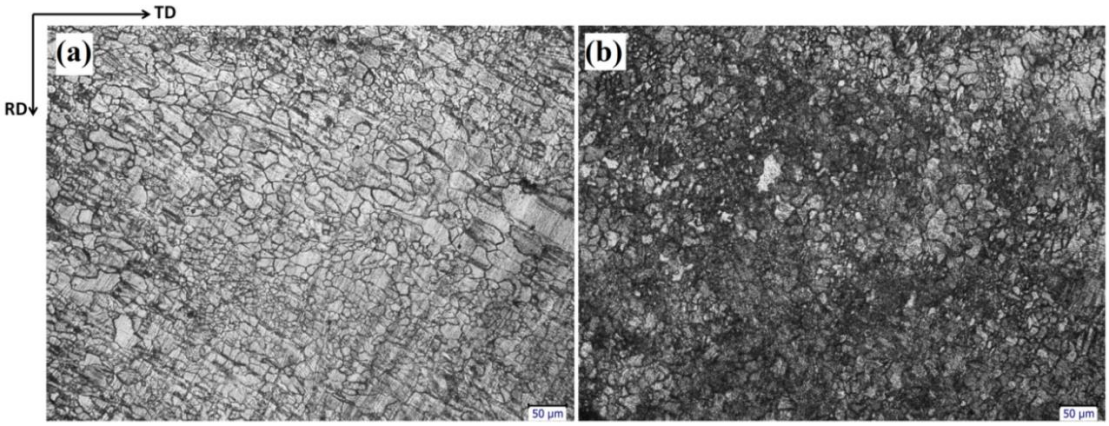

Fig. 4.8 Effect of aging time on the microstructure of samples under applied stress of 100 MPa and aged at 180℃ for period of (a) 3h (b) 6 h

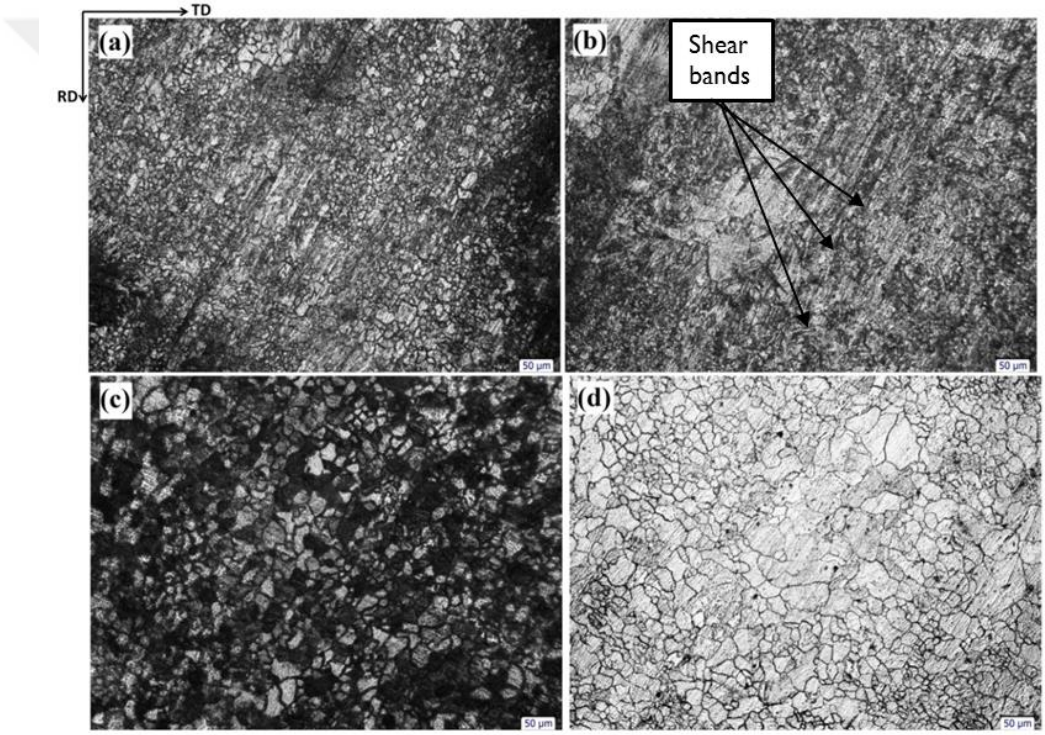

Fig. 4.9. Effect of aging time on the microstructure of samples under applied stress of 50 MPa and aged at 120℃ for period of (a) 1h (b) 3h (c) 6h (d) 12h

Fig. 4.10 shows the microstructure of samples stress aged under the stress value of 50 MPa and aging temperature of 180℃ at the various aging duration of 1, 3, 6 and 12 and 24 hours. For samples aged for 1 to 6 hours, the grain size is coarser relative to the sample aged under 120℃ due to higher temperature leading to higher heat input. While for sampled stress aged for 6 hours the grain size is 30µm, the grain size decreases to the 15µm for sample stress aged for 12 hours. Grain refinement is observed for samples

aged for duration of 12 hours as seen in Fig. 4.10d. For samples aged at 50 MPa and 180℃, it is hard to recognize the existence of shear bands.

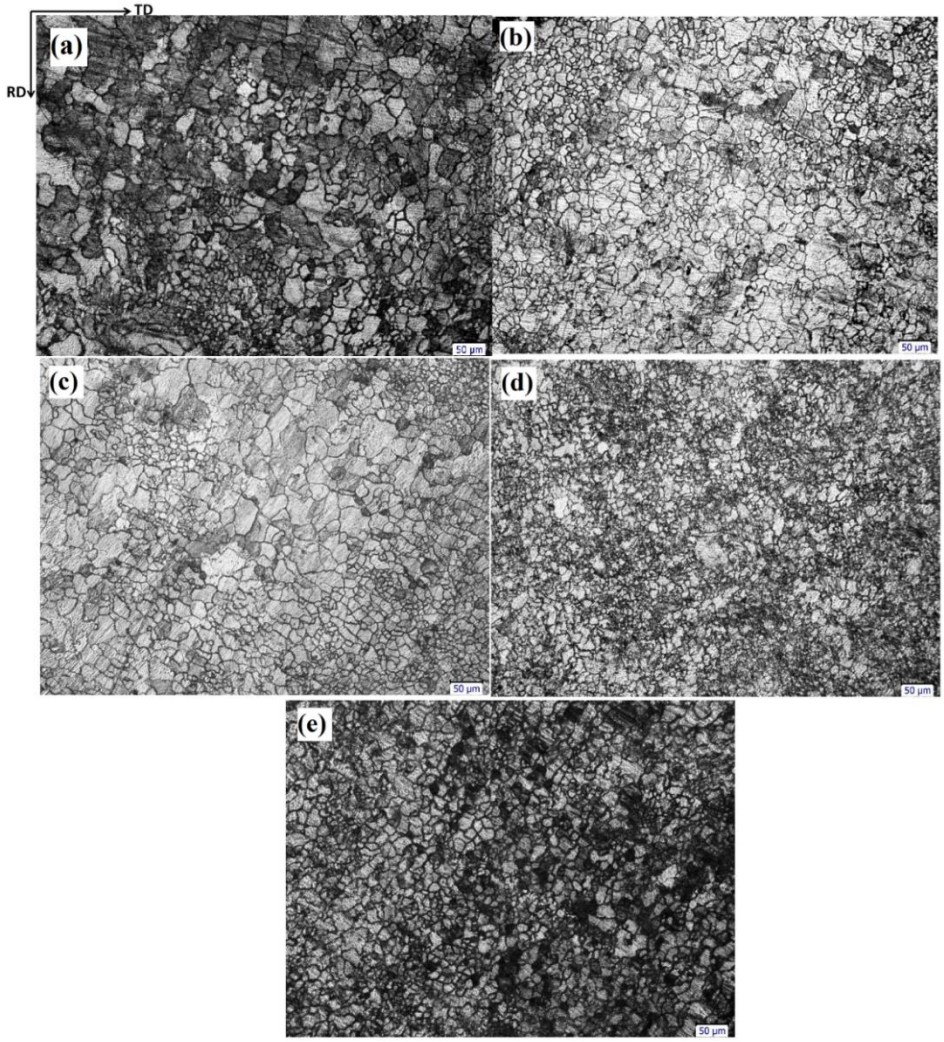

Fig. 4.10. Effect of aging time on the microstructure of samples under applied stress of 50MPa and aged at 180℃ for period of (a) 1h (b) 3h (c) 6h (d) 12h (e) 24 h

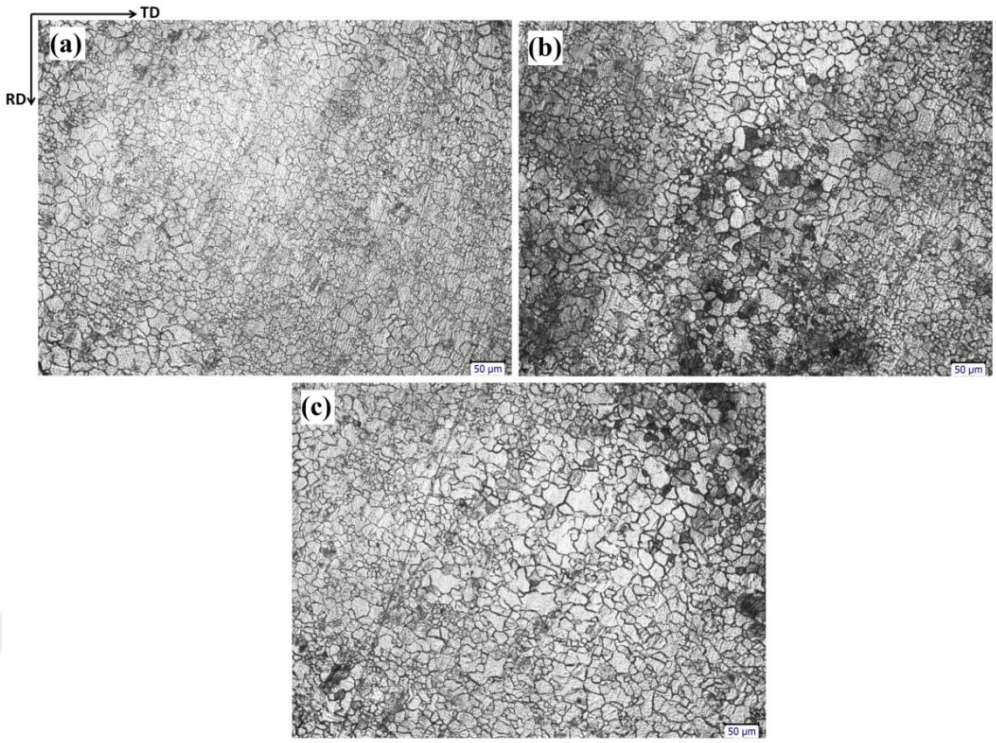

Fig. 4.11. Effect of aging time on the microstructure of samples under applied stress of 25 MPa and aged at 120℃ for period of (a) 3h (b) 6h (c) 12h

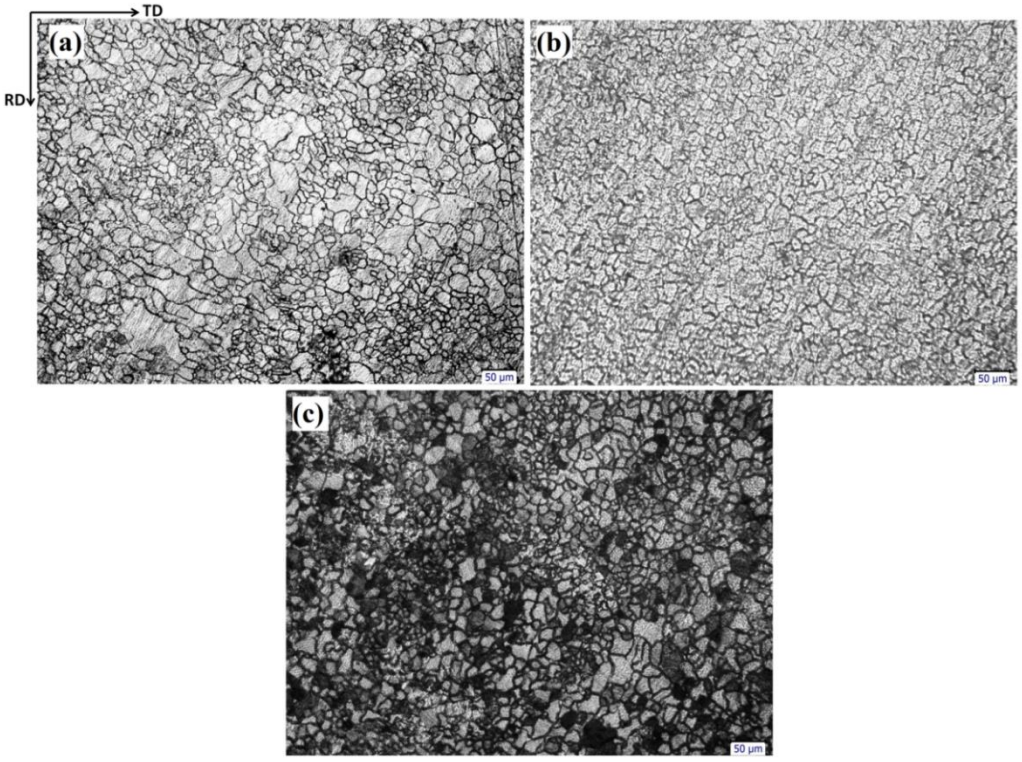

Fig. 4.12. Effect of aging time on the microstructure of samples under applied stress of 25 MPa and aged at 180℃ for period of (a) 3h (b) 6h (c) 12h

The microstructure of samples stress aged at 25 MPa is also investigated. Fig. 4.11 shows the microstructure of samples stress aged under the stress value of 25 MPa and aging temperature of 120℃ at the various aging duration of 3, 6 and 12 hours. It is indicated that by increasing the aging time up to 12 hours more stable structure is achieved. The grain size of sample aged for 12 hours is higher than the 3 and 6 hours counterparts which indicate the excessive exposure to the dynamic recrystallization. The average grain size for duration of 3 hours is10μm while for samples stress aged for duration of 6 and 12 hours grain size increases to 11 μm and 18 μm, respectively.

Table 4.1. Average grain size results of samples

Condition	Average grain size (μm)
Solution treated	80
Static aged-180℃-24h	70
Solution treated-Rolled	6
Solution treated-Rolled-Annealed	25
STAA-120℃-6h	13
STAA-120℃-12h	14
STAA-120℃-24h	12
STAA-120℃-48h	11
STAA-120℃-72h	14
STAA-180℃-6h	18
STAA-180℃-12h	19
STAA-180℃-24h	20
STAA-180℃-48h	22
STAA-240℃-6h	32
STAA-240℃-12h	35
STAA-240℃-24h	37
STAA-240℃-48h	38
STAA-240℃-72h	42
STRA-180℃-6h-100 MPa	15
STRA-180℃-3h-100 MPa	25
STRA-120℃-3h-25 MPa	10
STRA-120℃-6h-25 MPa	11
STRA-120℃-12h-25 MPa	18
STRA-180℃-3h-25 MPa	31
STRA-180℃-6h-25 MPa	22
STRA-180℃-12h-25 MPa	26
STRA-120℃-1h-50 MPa	43
STRA-120℃-3h-50 MPa	44
STRA-120℃-6h-50 MPa	45
STRA-120℃-12h-50 MPa	46
STRA-180℃-1h-50 MPa	29
STRA-180℃-3h-50 MPa	26
STRA-180℃-6h-50 MPa	30
STRA-180℃-12h-50 MPa	15
STRA-180℃-24h-50 MPa	19

Fig. 4. 12 shows the microstructure of samples stress aged under the stress value of 25 MPa and aging temperature of 180℃ at the aging duration of 3, 6 and 12 hours. Sample aged for 3 hours shows a uniform structure with no shear band, as the time of aging increases to the 12 hours crystallized grains are observed. Table 4.1. summarizes the average grain size results of all measured samples.

4.2. Scanning Electron Microscopy

Fig. 4.13 shows the SEM figure for the solution treated sample of ZK60. The composition of current slab contains magnesium matrix, and it is anticipated that significant amount of Mg-Zn and Zn-Zr precipitates would exist in this material. It is well established that due to aging process, wrought ZK60 alloy possesses high amount of $MgZn_2$ precipitates [107, 108]. Recognizing the existence of Zn-Zr particle is hard to be done using SEM analysis and TEM is required due to the nano-scale origin and distribution of Zn-Zr precipitates in the matrix [85, 108, 109]. However, previous works indicate that large particles of $MgZn_2$ may be observed using SEM [110]. Elemental mapping is used to characterize the intensity of every element to distinguish the existing particles. Solution treatment will lead to disappearing of Zn-Zr particles. However; bulk MgZn phases might remain in the solution treated ZK60 alloy. Hence, it is anticipated that MgZn phase exists in the matrix even in low density [67].

Fig 4.13 indicates the SEM micrograph for the solution treated, rolled and then statically aged sample at 180℃ for 24 hours. It is well known that rolling would help the nucleation of precipitates and the further aging process can lead to a more uniform distribution of precipitates along with their refinement. As shown in Fig. 4.14b and 4.14.c, higher concentration of Zn and Zr are evident. The high intensity of Zn in Fig. 4.14b can give symptoms about the formation Mg-Zn phase at these regions.

4.3. Transmission Electron Microscopy (TEM)

4.3.1. TEM Micrograph of the solution treated sample

The TEM micrograph of the solution treated sample is shown in Fig. 4.15. The corresponding diffraction pattern is added at the corner of the figure. A limited number of precipitates are demonstrated in the

micrograph of the solution treated sample as expected. Diffraction pattern for the zone shows a matrix while there is no visible precipitate on the diffraction pattern. It is clear that the solution treated sample has few precipitates relative to the processed sample due to disolving of the precipitates inside the matrix.

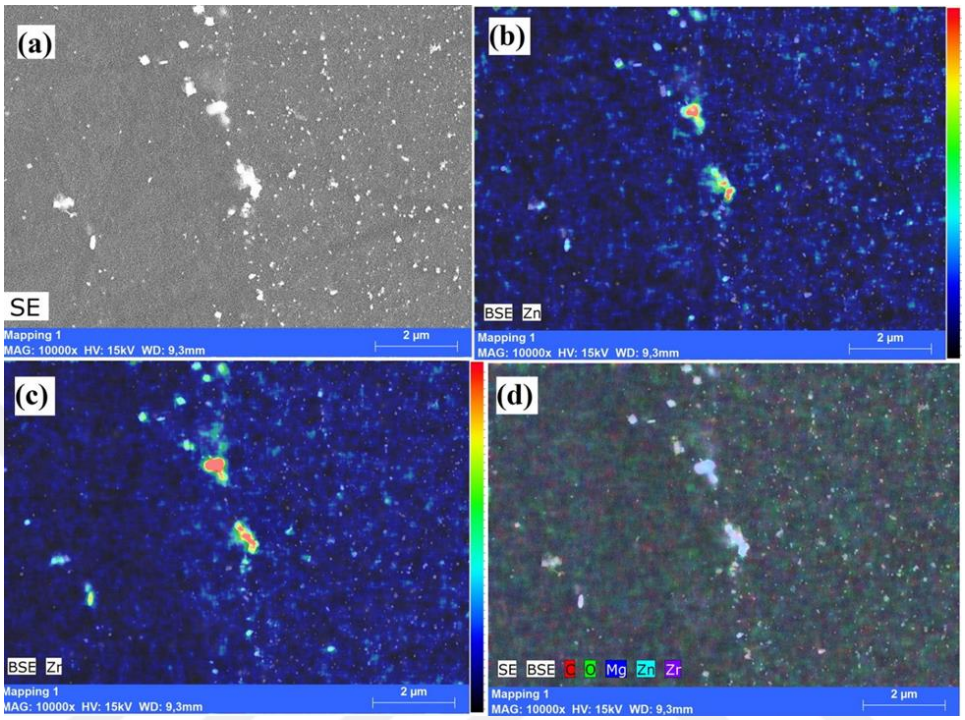

Fig. 4.13. (a) SEM micrograph of as solution treated sample (b) Zn concentration distribution in the ST condition (c) Zr concentration distribution in the ST condition (d) elemental mapping of the as ST sample.

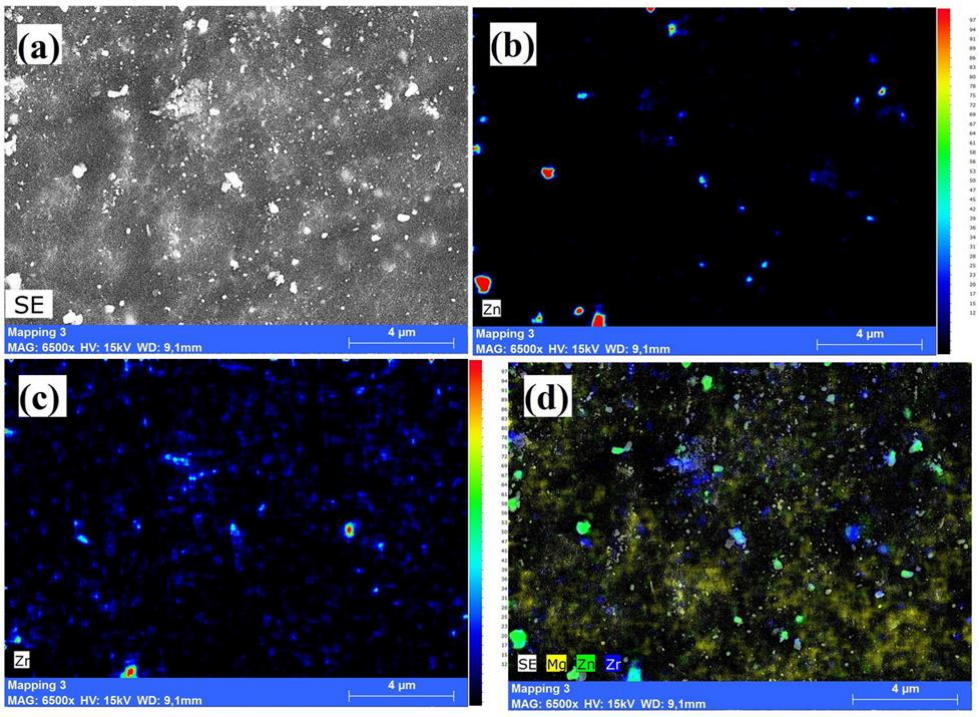

Fig. 4.14. (a) SEM micrograph of rolled and statically aged sample in 180℃ for 24h (b) Zn concentration distribution (c) Zr concentration distribution (d) elemental mapping of the sample.

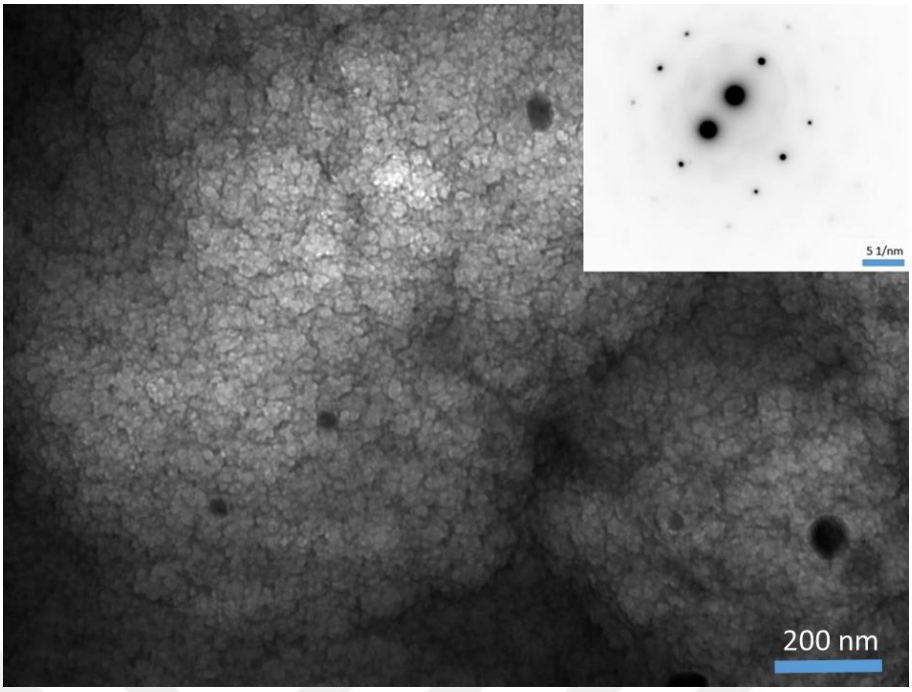

Fig. 4.15. TEM micrograph and diffraction pattern of ST sample

4.3.2. TEM Micrograph of the static aged sample

The TEM micrograph and diffraction pattern of the rolled and static aged sample is shown in Fig. 4.16. Fine precipitates with more uniform distribution and density are observed for the static aged sample. It is observed that static aging process has led to the formation of more precipitates in good distribution in the matrix. Signs of precipitates are clear in the diffraction pattern of the static aged samples.

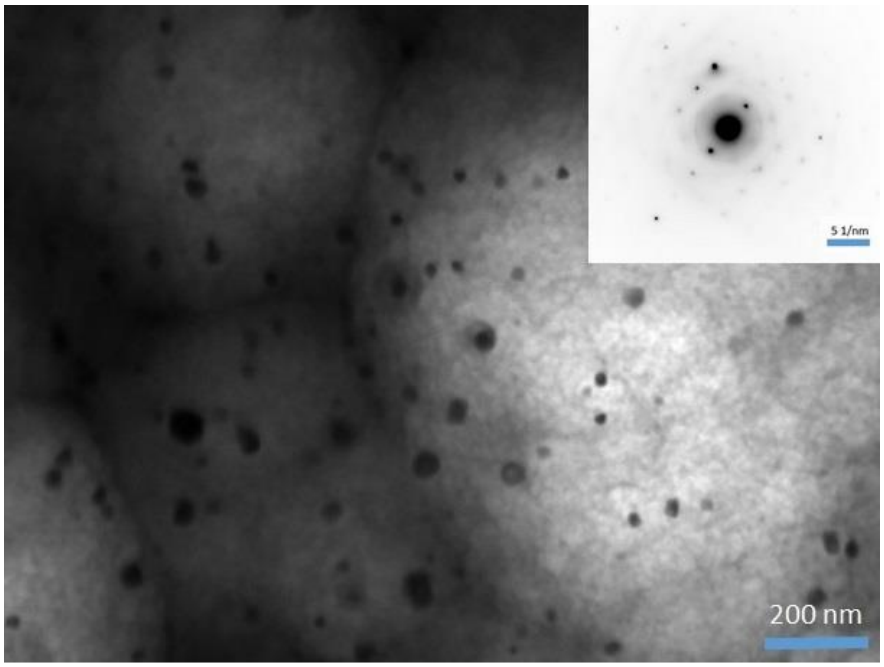

Fig. 4. 16. TEM micrograph and diffraction pattern of rolled and static aged sample

4.3.3. TEM Micrograph of stress aged samples

The TEM micrograph and diffraction pattern of the rolled and stress aged sample are shown in Fig. 4.17. During the stress aging, localization of stress can occur due to extension of the sample. High density of precipitates with small size and uniform distribution can be seen for the stress aged sample. The high density of precipitates along with their smaller size contributes to the hardening of this microstructure. It is expected for the stress aged samples to have precipitates oriented along the extension direction. Precipitate indexing is needed to demonstrate the misorientation of the precipitates along the corresponding plane. It is estimated that for ZK60 alloy two types of precipitates ($\acute{\beta}_1$ and $\acute{\beta}_2$) with different shapes and orientation habit planes may form during the aging process. $\acute{\beta}_1$ forms in the shape of rods with axis being parallel to the (0002) direction of matrix. $\acute{\beta}_2$ is formed in the shape of disks lying on the basal plane. The difference between these two types can be distinguished if a fovored plane is recognized. At the early stage of aging $\acute{\beta}_2$ precipitates are active while later $\acute{\beta}_1$ ones are involved [111]. Morphology of exisiting precipitates in the ZK60 alloy is shown in Fig. 4.18. Previous studies revealed that shape and amount of precipitates is dependent to the aging time and temperature [22, 112]. Hence, it can be estimated that an optimized value can be found for aging temperature and duration in which high density of fine precipitaes would form. Based on the observations, it is clear that stress aging supports the formation of precipitates.

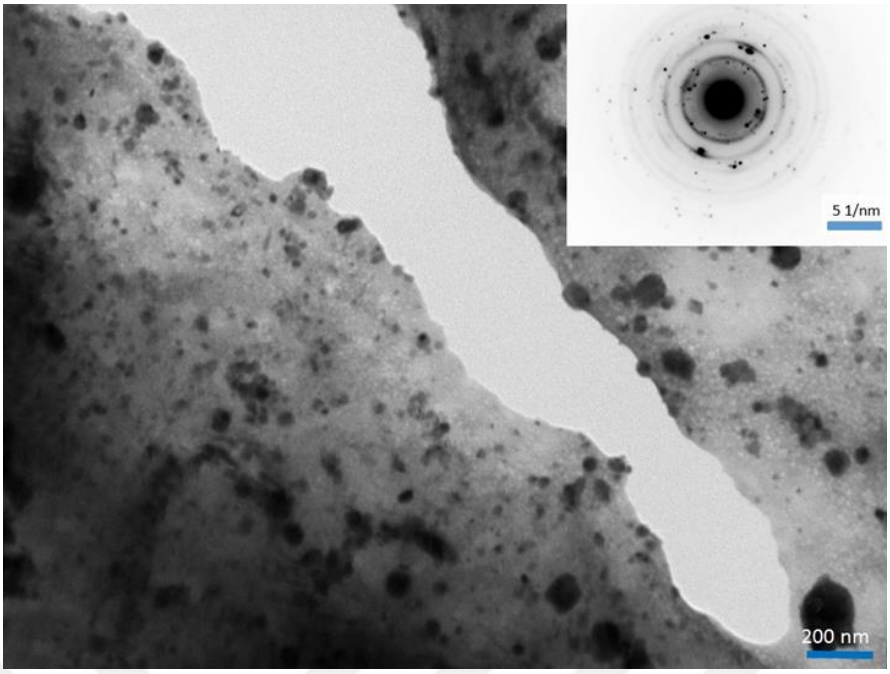

Fig. 4.17. TEM micrograph and diffraction pattern of rolled and stress aged sample

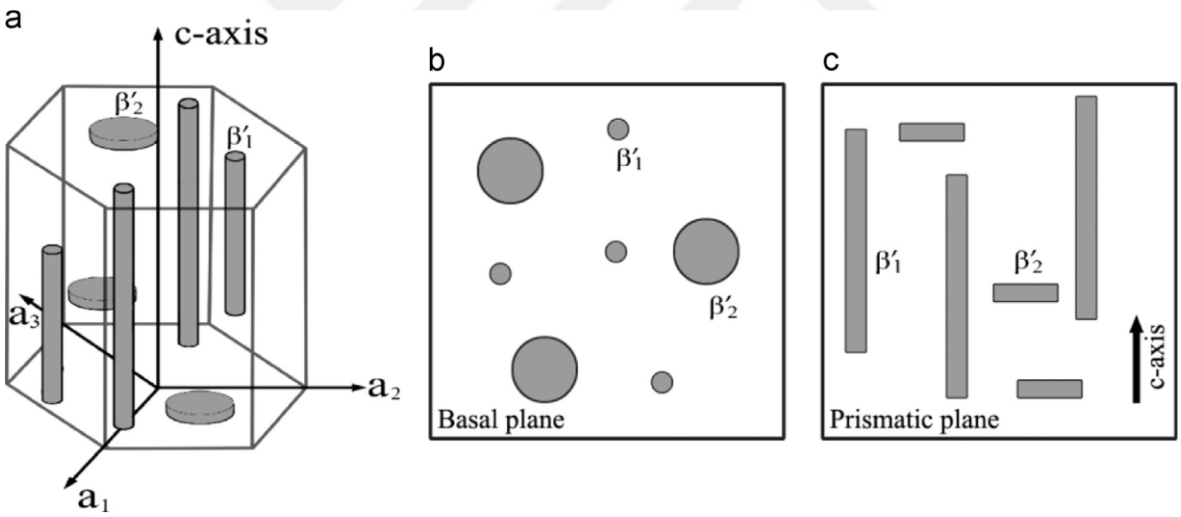

Fig. 4.18. Schematic illustration of the morphologies of precipitates [22]

Chapter 5

EFFECT OF ROLLING AND AGING PROCESSES ON THE MECHANICAL PROPERTIES OF ZK60 MAGNESIUM ALLOY

5.1. Hardness Results

The hardness results for static and stress aged samples are summarized in Table 5.1 and 5.2. It is evident that hardness of processed samples is higher than solution treated material in all conditions. The hardness of the ST is 48 while the statically aged one is 65 in the best condition and 66 for stress aged sample in the best condition.

For static aged samples, the hardness results are higher in aging temperature of 180℃, while at 120℃ and 240℃, the maximum hardness value decreases to 53. The same trend is observed for the stress aged samples, and in temperature of 120℃ and applied stress of 50 MPa, hardness is the highest. However, the resolution of the hardness results was not in a manner to investigate the effect of aging time of every temperature, since the results were very near to each other in any temperature. It is reported that the aging enhances the hardness properties of processed samples. Meanwhile, high hardness is reported for the rolled samples of ZK60 [25, 113, 114]. Formation of precipitates along with nucleation of new grains increases the hardness response of ZK60 alloy [115].

Table 5.1. Hardness results of static aged samples

No	condition	Aging Temperature (C)	Aging Duration (h)	Hardness (Hv)
1	ST	RT	0	63
2	ST-Rolled-Annealed-Aged	120	6	65
3	ST-Rolled-Annealed-Aged	120	12	65
4	ST-Rolled-Annealed-Aged	120	24	68
5	ST-Rolled-Annealed-Aged	120	48	67
6	ST-Rolled-Annealed-Aged	120	72	68
7	ST-Rolled-Annealed-Aged	180	6	78
8	ST-Rolled-Annealed-Aged	180	12	79

9	ST-Rolled-Annealed-Aged	180	24	80
10	ST-Rolled-Annealed-Aged	180	48	80
11	ST-Rolled-Annealed-Aged	180	72	75
12	ST-Rolled-Annealed-Aged	240	6	66
13	ST-Rolled-Annealed-Aged	240	12	67
14	ST-Rolled-Annealed-Aged	240	24	67
15	ST-Rolled-Annealed-Aged	240	48	66
16	ST-Rolled-Annealed-Aged	240	72	65

Table 5.2. Hardness results of stress aged samples

No	Condition	Applied stress (MPa)	Aging Temperature (C)	Aging Duration (h)	Hardness Results (Hv)
1	ST	0	RT	0	63
2	ST-Rolled-Annealed-Aged	100	180	3	64
3	ST-Rolled-Annealed-Aged	100	180	6	65
4	ST-Rolled-Annealed-Aged	25	120	3	77
5	ST-Rolled-Annealed-Aged	25	120	6	76
6	ST-Rolled-Annealed-Aged	25	120	12	75
7	ST-Rolled-Annealed-Aged	25	180	3	76
8	ST-Rolled-Annealed-Aged	25	180	6	75
9	ST-Rolled-Annealed-Aged	25	180	12	76
10	ST-Rolled-Annealed-Aged	50	120	1	78
11	ST-Rolled-Annealed-Aged	50	120	3	82
12	ST-Rolled-Annealed-Aged	50	120	6	80
13	ST-Rolled-Annealed-Aged	50	120	12	82
14	ST-Rolled-Annealed-Aged	50	180	1	79
15	ST-Rolled-Annealed-Aged	50	180	3	69
16	ST-Rolled-Annealed-Aged	50	180	6	71
17	ST-Rolled-Annealed-Aged	50	180	12	71
18	ST-Rolled-Annealed-Aged	50	180	24	69

5.2. Uniaxial Tensile Properties of Processed samples

5.2.1. Tensile properties of static aged samples

Tensile properties of the solution treated (ST) sample is shown in Fig. 5.1. The ultimate tensile strength (UTS) of solution treated sample is 255 MPa while the strain to failure is 11%. The observed behavior has good agreements with the previous literature. Chen at al. and He et al. [22, 89] reported that the tensile strength of solution treated ZK60 alloy is 273 MPa.

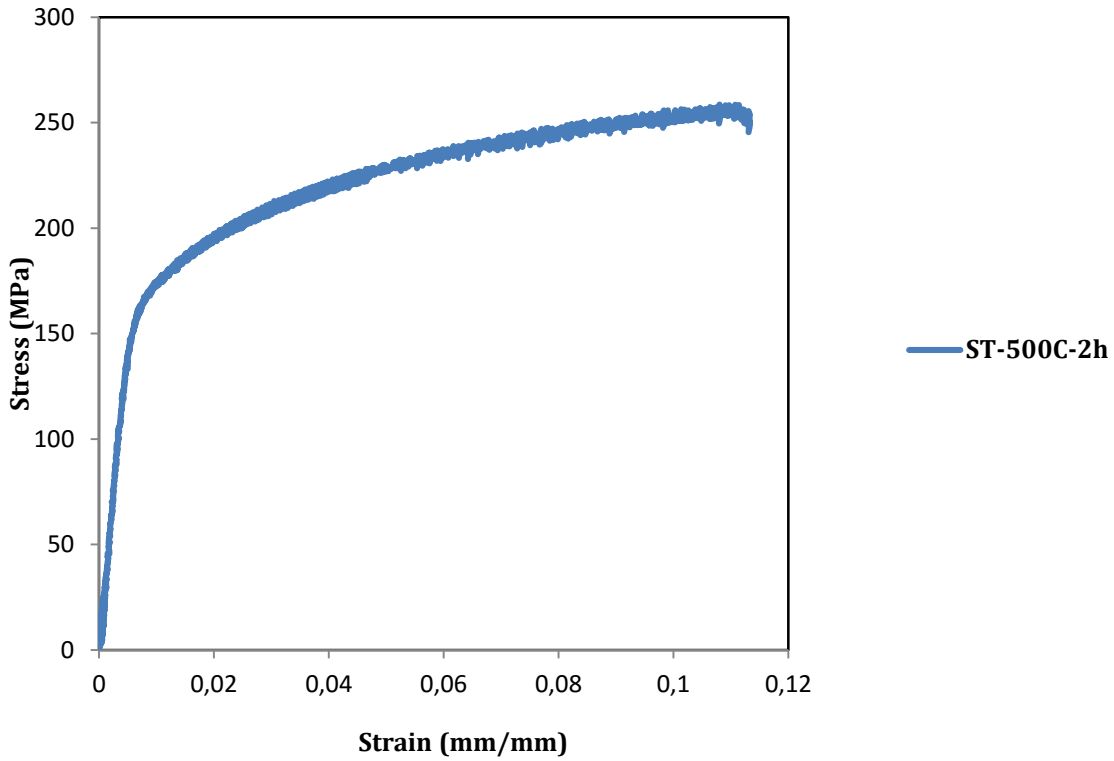

Fig. 5.1. Stress-strain curve for the solution treated sample at 500℃ and 2 hours

Effect of annealing heat treatment on the tensile properties of processed samples is investigated. The temperature of 350℃ and 400℃ are analyzed to find the best condition for the annealing treatments after rolling. As it is seen in Fig. 5.2, sample annealed at 350℃ for 2 hours has better ductility and strength response. However, the tensile strength of sample annealed at 350℃ for 20 minutes is nearly the same while the ductility is much lower. Since the aim of annealing is to recover the formability of rolled sheets, the condition with the highest amount of ductility recovery is chosen as the annealing parameter for the upcoming samples.

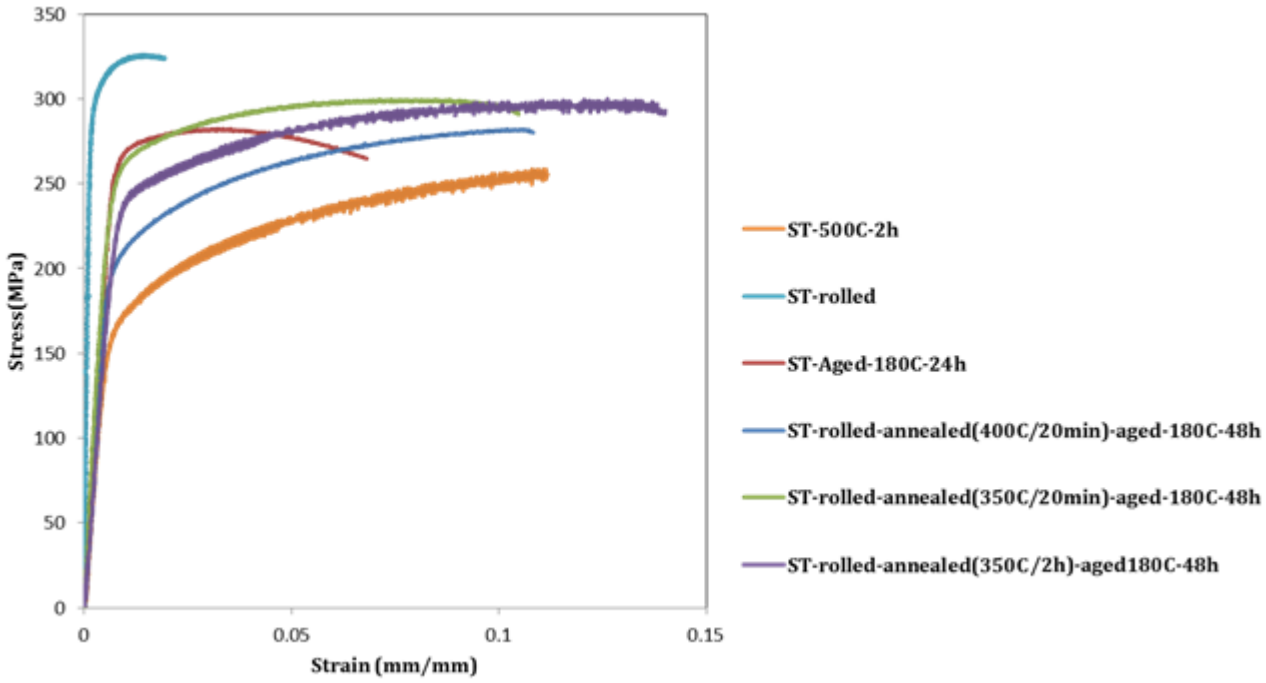

Fig. 5.2. The effect of annealing treatment on the tensile behavior of solution treated and rolled samples

The static aging investigations have been performed at temperatures of 120℃, 180℃, and 240℃ for aging durations ranging from 6 to 72 hours. The tensile tests for the static aged samples are performed parallel to the rolling direction. Fig. 5.3 shows the tensile results for the samples aged at 120℃. At the aging temperature of 120℃ and aging duration of 24 hours, best tensile strength with high ductility is achieved. Fig. 5.4 shows the tensile results for the samples aged at 180℃. The best tensile performance is observed for the sample aged for 24 hours. This sample has the elongation to failure of 25% and tensile strength of 305 MPa. For sample aged for 6 hours, tensile strength of 290 MPa and strain to the failure of 20% are obtained. The elongation for the 12 hours aged sample decreases to 12%. Sample aged for 72 hours exhibit low ductility and strength as well.

The stress-strain curves for samples aged at 240℃ are illustrated in Fig. 5.5. The highest tensile strength is observed for the sample aged for 24 hours, while at higher aging durations, the elongations are nearly the same.

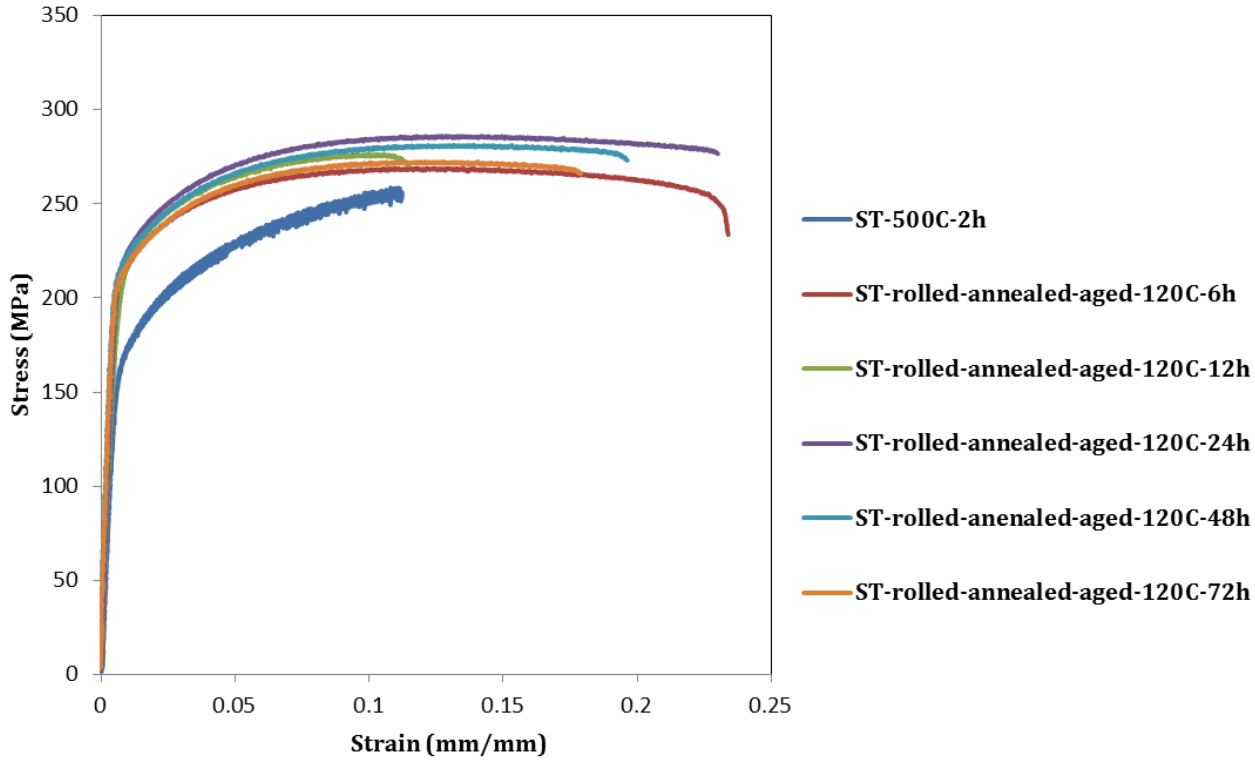

Fig. 5.3. Effect of aging duration on the tensile strength of aged samples at 120℃

Fig. 5.6 shows the tensile strength of samples versus the aging time at three different aging temperatures. It is clear that the tensile strength of samples aged at 180℃ is higher than those aged at 120℃ and 240℃. The highest strength is achieved at aging time ranging between 24 to 48 hours. The static aged sample's micrograph of TEM presented in Chapter 4 is related to sample aged at 180℃ for 24 hours. As mentioned this sample has fine precipitates distributed along the matrix. Hence, It is possible to reach fine grains with good precipitate distribution in this condition. considering the elongation, the best condition for static aging is at a temperature of 180℃ and aging duration of 24 hours.

5.2.2. Tensile properties of stress aged samples

Tensile properties of stress aged samples were characterized at different temperatures with different applied loads and aging durations. The mechanical behavior of stress aged samples was compared with the corresponding static aged counterparts.

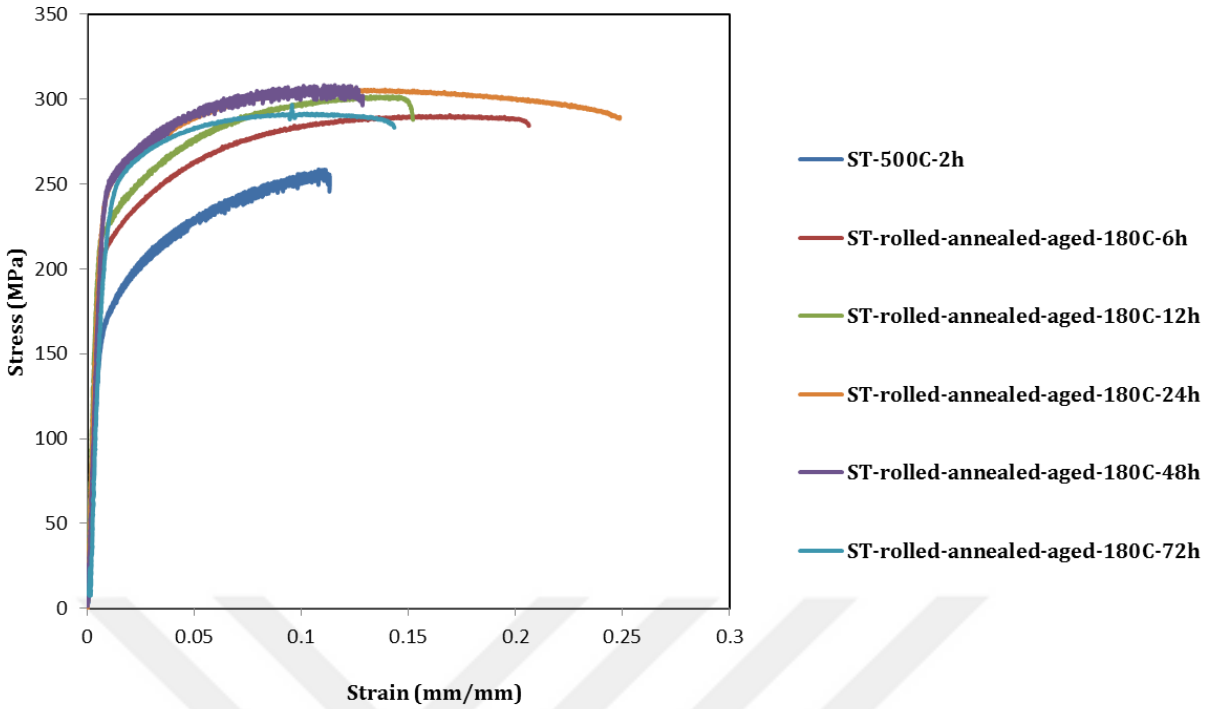

Fig. 5.4. Effect of aging duration on the tensile strength of aged samples at 180℃

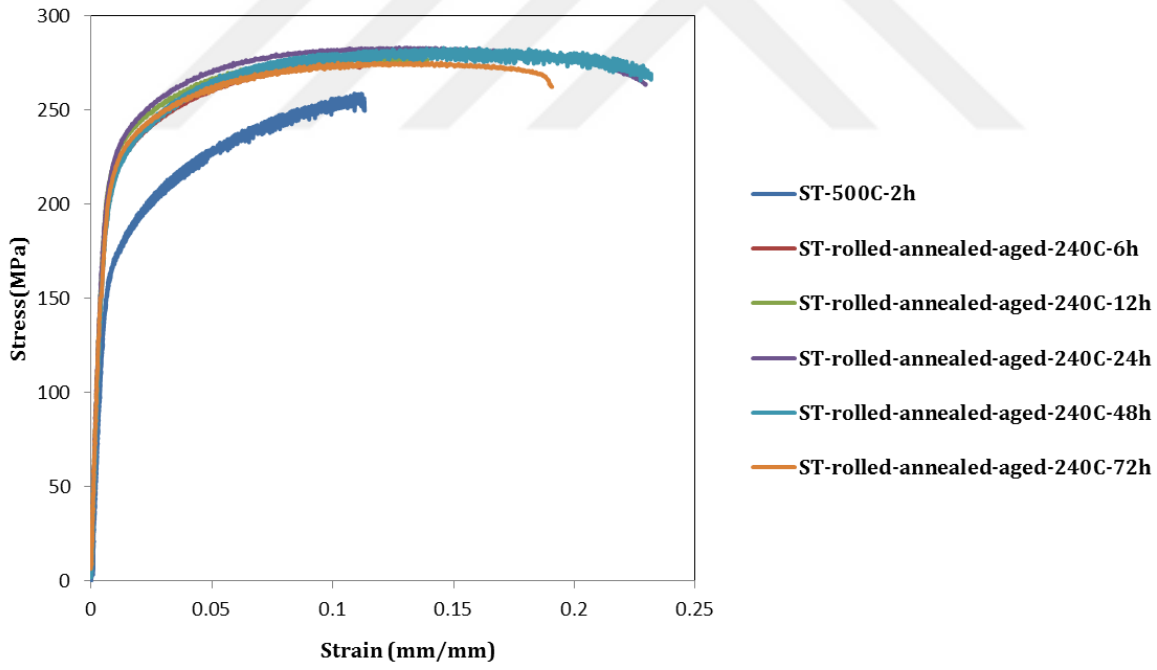

Fig. 5.5. Effect of aging duration on the tensile strength of aged samples at 240℃

In order to determine the aging stress, it is necessary to know the high temperature deformation behavior. The material before stress aging process is solution treated, rolled and then subsequently annealed. It is hard to find the mechanical properties of a sample in this condition in the literature. Hence, tensile

properties of the samples at the stress aging range of 100℃ to 200℃ is investigated. Hence the high temperature tests were conducted at these temperatures.

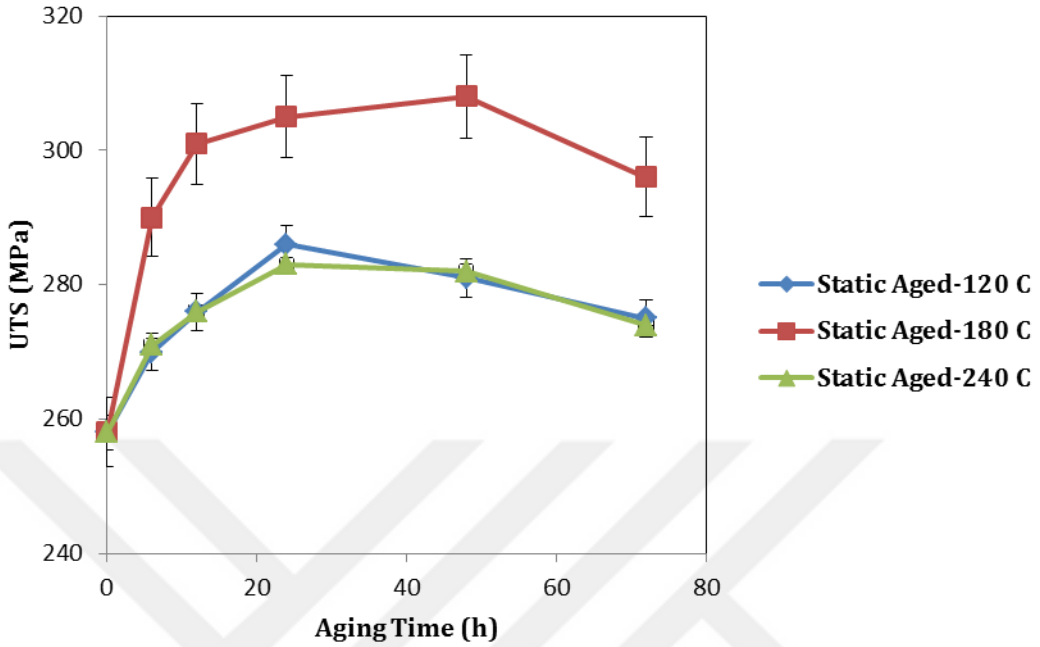

Fig. 5.6. Strength of processed samples versus aging time at different aging temperatures

The results of stress-strain curves for 100℃ and 200℃ and ambient temperature are illustrated in Fig. 5.7. The YS of the sample at ambient temperature is near 170 MPa while at 100℃ it decreases to 150 MPa and for 200℃ to near 100 MPa. It is worth noting that no superplastic behavior was seen in these temperature ranges since the elongation was near 23% for the 200℃ and 27% for 200℃ samples. High superplasticity was observed for the previous or hardened sheets of ZK60 alloys [116]. Based on these results it was concluded that the applied stress should not exceed the 100 MPa for the samples.

Fig. 5.8 shows the mechanical properties of stress aged samples under the load of 100 MPa. For sample stress aged for 3 hours, the UTS value is near 304 MPa, and the elongation is 7%. By increasing the aging time, the UTS decreases to the 285 MPa while the elongation increases to 12%. It is reported that the orientation of the precipitates can be favored based on the direction of applied load under the elastic stress regime [90]. Depending on the orientation of the precipitate habit plane with respect to the stress axis, precipitation may or may not be favored, thus leading to a preferentially oriented precipitate structure [117,

118]. It is noted that the samples stress aged at 100 MPa are deformed under the applied load and also may fracture from the grip zone at long aging durations. Stress localization at higher aging times (here at 6 hours) may lead to a decrease in the strength of the sample while localized points can function to increase the elongation. However, stress aging is recommended to be performed in the elastic region. Hence, the applied load needs to be decreased to impede the formation of localized stress.

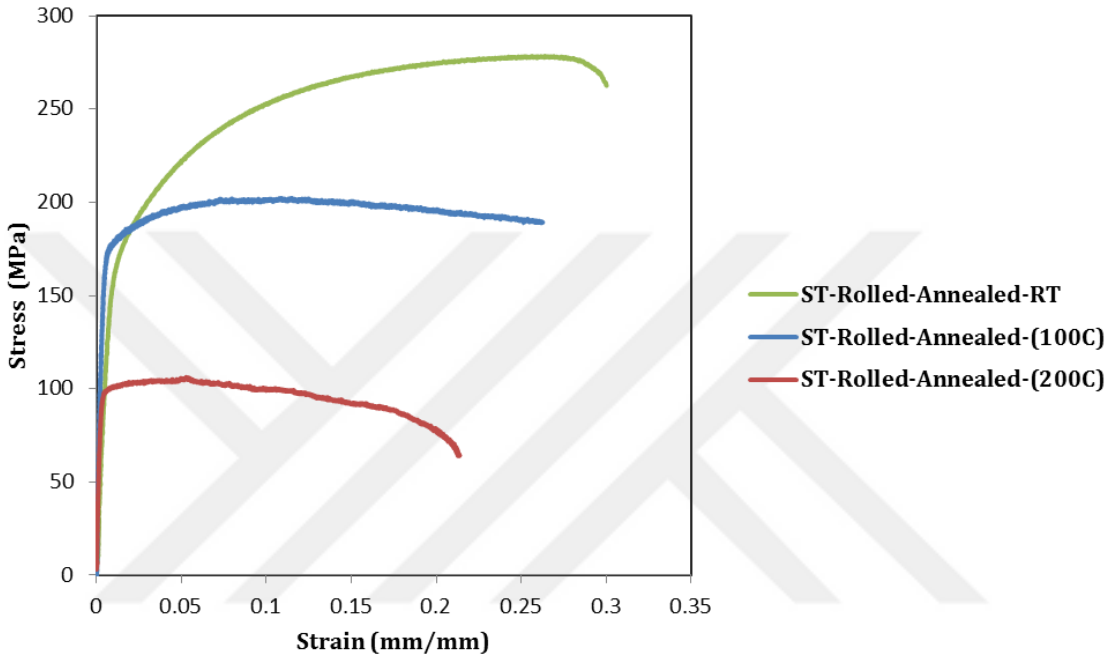

Fig. 5.7. Tensile properties of solution treated rolled and annealed ZK60 samples at high temperature

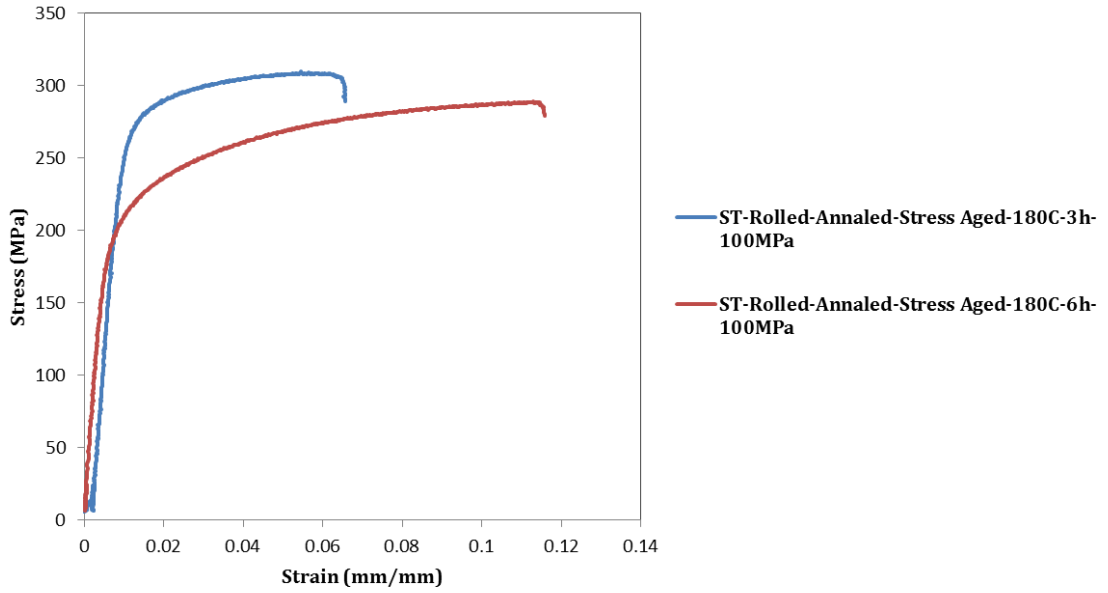

Fig. 5.8. Tensile properties of samples stress aged at 100 MPa

It was observed that the effect of stress aging with a value of 100 MPa resulted in UTS and elongation values that are nearly the same with those of static aged samples. On the other hand, stress aged samples were fractured from the grip regions for an aging time more than 6 hours since it can be assumed that under the stress of 100 MPa samples could not yield for more than 6 hours. Hence, the effect of stress aging was investigated under the stress values of 25 and 50 MPa to achieve improved tensile behavior.

Fig. 5.9 illustrates the stress- strain curves for the stress aged samples stress aged at 25 MPa at a temperature of 180℃. Tensile strengths of the samples increase while increasing the aging time from 3 to 12 hours. This shows that formation of fine precipitates needs more time for samples aged at 25 MPa. Tensile strength of this condition in overall is not satisfying and less than most cases in static aging condition. Hence further investigation of aging time in 180℃ would not be the case of interest [119]. On the other hand, the role of stress may be explained by elastic changes on the lattice dimensions of the matrix decreasing the coherency strains between matrix and precipitate, thereby favoring nucleation on certain planes [119, 120]. Previous works state that as the density of precipitates increases the tensile strength and elongation of the sample increases in the applied direction.

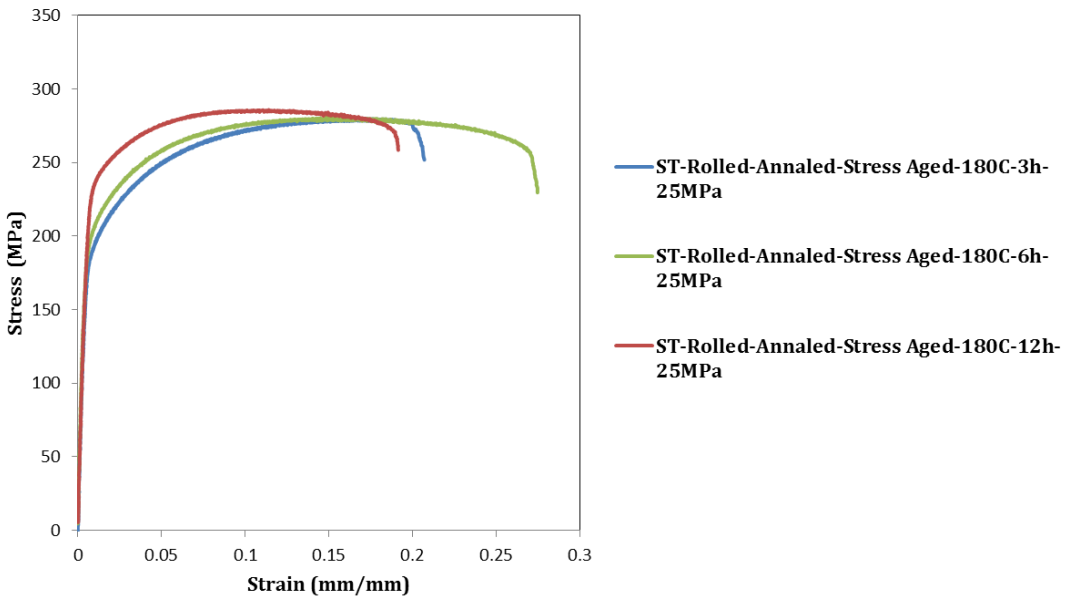

Fig. 5.9. Effect of aging duration on tensile properties of samples stress aged at 180℃ and 25 MPa

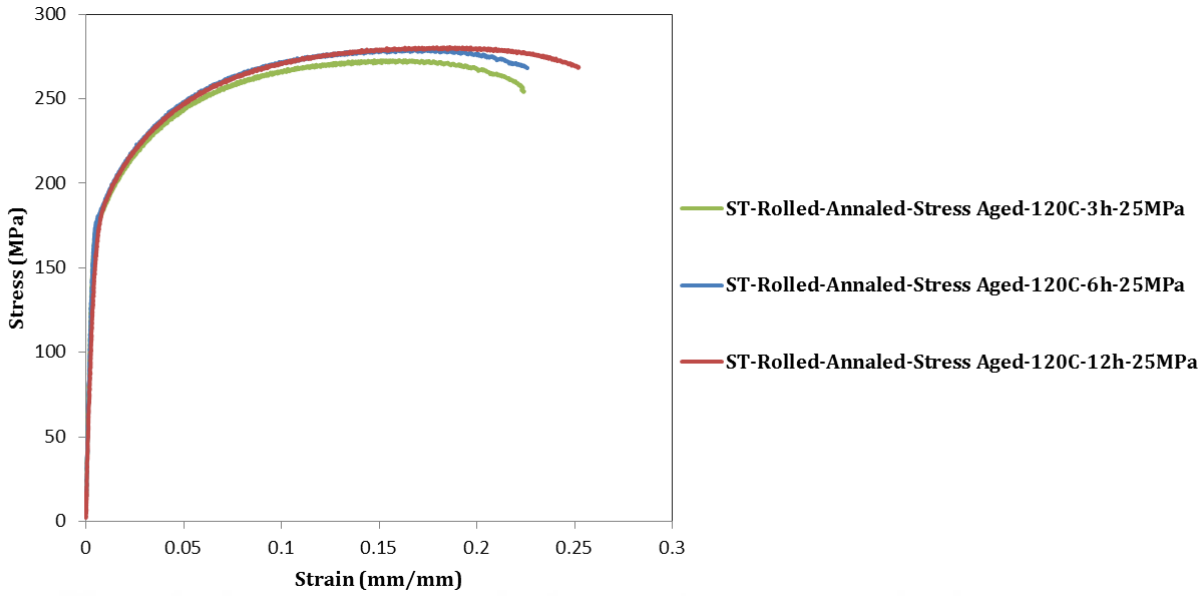

Fig. 5.10. Effect of aging duration on tensile properties of samples stress aged at 120℃ and 25 MPa

Fig.5.10 shows the tensile properties of samples stress aged at 120℃ and 25 MPa. It is clear that by increasing the aging time, tensile strength of the samples decrease while elongation to failure values remain nearly the same.

Effect of stress aging under stress value of 50 MPa is discussed next. Fig. 5.11, illustrates the stress-strain curves for the stress aged samples at 50 MPa and temperature of 120℃. By increasing the aging time to 3 hours, the tensile strength of the sample reaches to the maximum value. The best mechanical properties are achieved for stress aged sample at 120℃ for 3 hours under the applied stress of 50 MPa. This sample has a UTS of 352 MPa and an elongation of 13 percent. By further increase of the aging time, tensile strengths of the samples decreased. However, mechanical performance of the samples in this condition is better than the other conditions. The combination of applied stress and aging temperature as discussed, influences the mechanical properties by changing the density of precipitates. Precipitate hardening can effectively increase the yield and tensile strength. As observed at the TEM micrograph of stress aged sample, fine precipitates with good distribution are obtained after stress aging of sample. Hence, the high strength of this condition is attributed to the formation and distribution of precipitates.

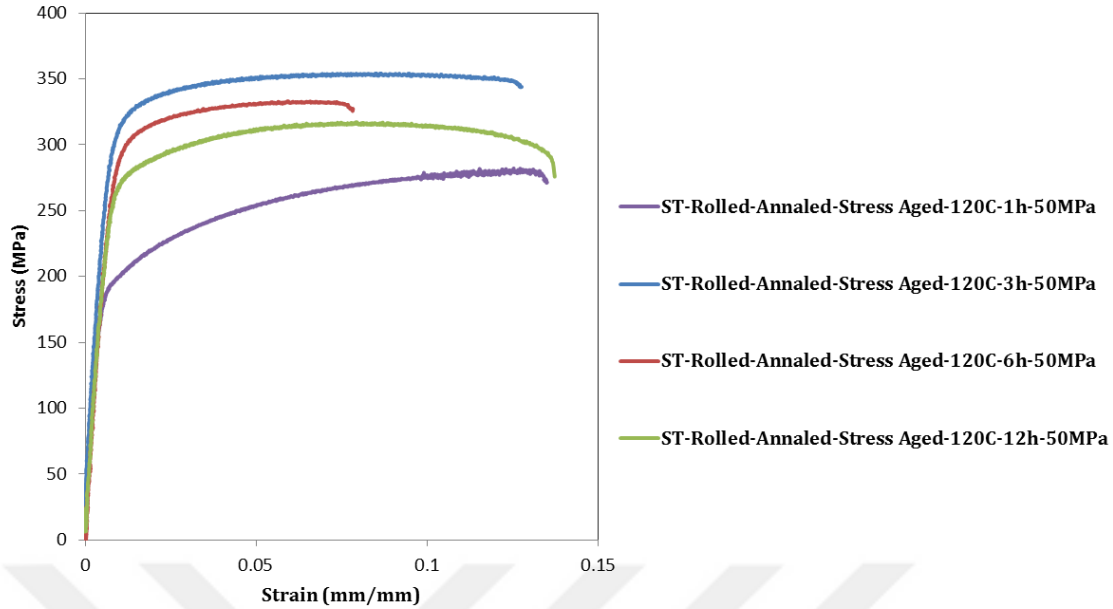

Fig. 5.11. Effect of aging duration on tensile properties of samples stress aged at 120℃ and 50 MPa

Fig. 5.12 illustrates the stress-strain curves for the stress aged samples at 50 MPa and at a temperature of 180℃. The same trend as for the samples aged at 50 MPa, 120℃ is also observed here. By increasing the aging time, tensile strength is increased up to a maximum value of 321 MPa at 3 hours aging duration. Further aging decreases the tensile strength and ductility of stress aged samples, overall strength and ductility of the sample aged for 1 hour are better though.

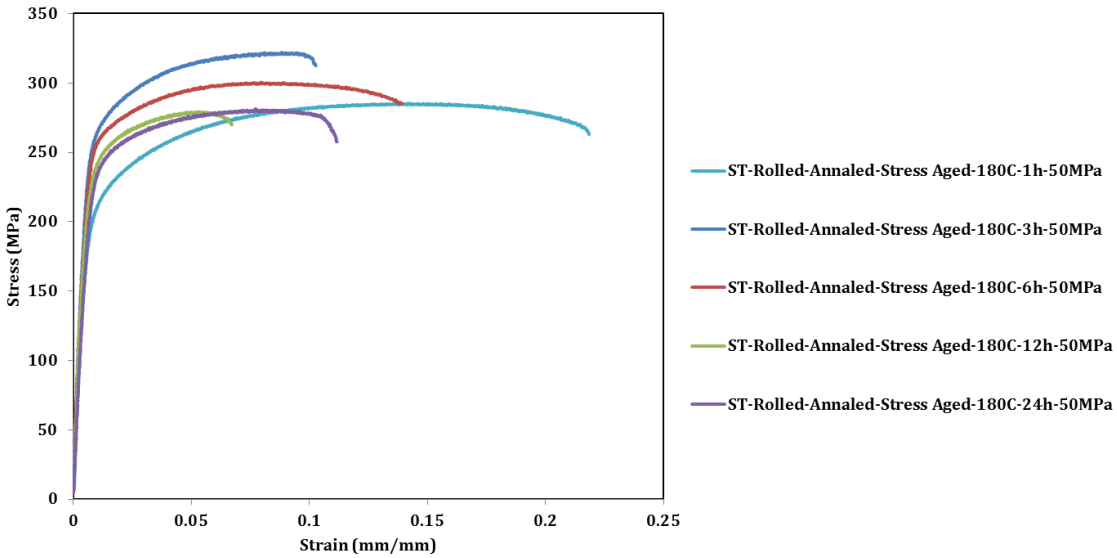

Fig. 5.12. Effect of aging duration on tensile properties of samples stress aged at 180℃ and 50 MPa

As a conclusion, the tensile behavior of all conditions are compared as shown in Fig. 5.13. The ST sample has the UTS value of 258 MPa and elongation of 11% which is a weak tensile performance. Rolled sample exhibited high tensile strength of 327 MPa, while the ductility is very low (1.8%). Annealing process improved the ductility of the rolled sample while a sudden decrease in tensile strength is observed dropping down to 270 MPa. For the sample static aged at the 180℃ for 24 hours, an improvement is observed for the UTS and elongation values to 304 MPa and 25%, respectively. Applying the stress aging process, UTS and elongation values of the sample are improved to 352 MPa and 12%, respectively.

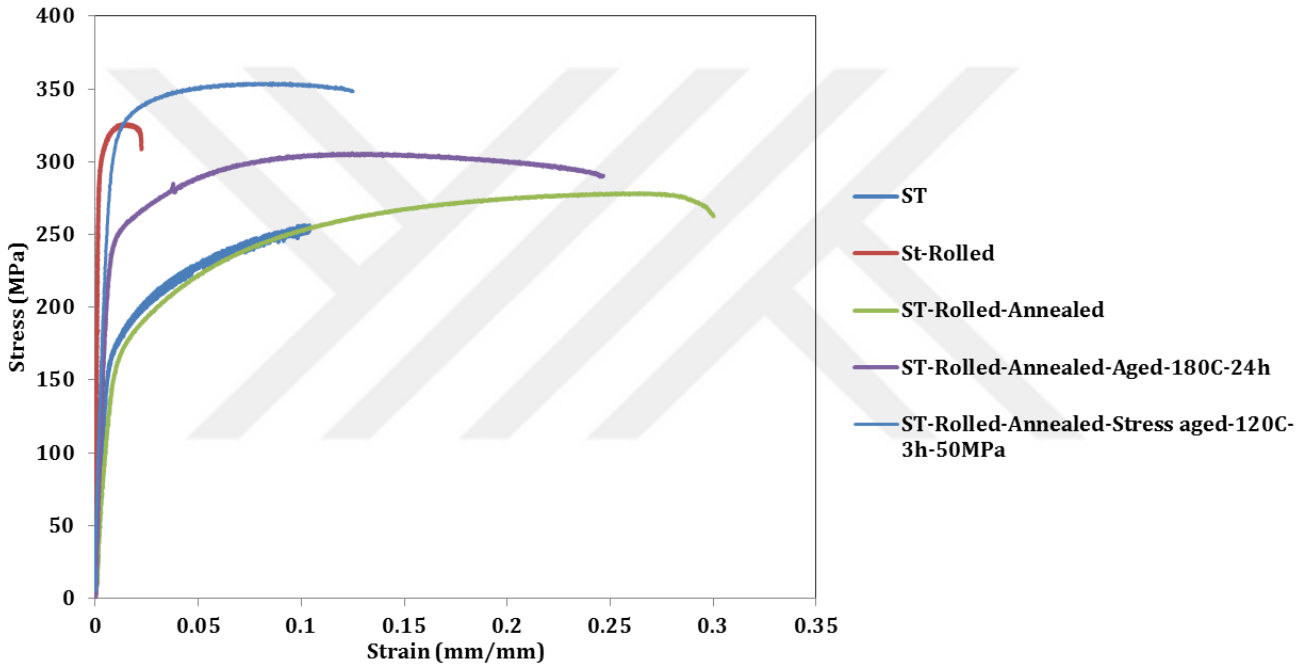

Fig. 5.13. Comparison of tensile properties of (a) ST (b) rolled (c) rolled and annealed (d) best static aged sample (e) best stress aged sample

Fig. 5.14 indicates the tensile properties of stress aged samples at a temperature of 120℃ and duration of 3 hours at two applied load values of 25 and 50 MPa. As discussed in Chapter 4, By increasing the applied load of stress aged samples, finer grains with more uniform structure are achieved. Finer grains can lead to better ductility response as shown in Fig. 5.12. During the static recrystallization, fine grain can be formed leading to better formability [121]. The sample, stress aged under the load of 50 MPa has better ductility than its 25 MPa counterpart. However, the UTS of sample aged at 50 MPa is 352 MPa and far better than the sample aged at 25 MPa.

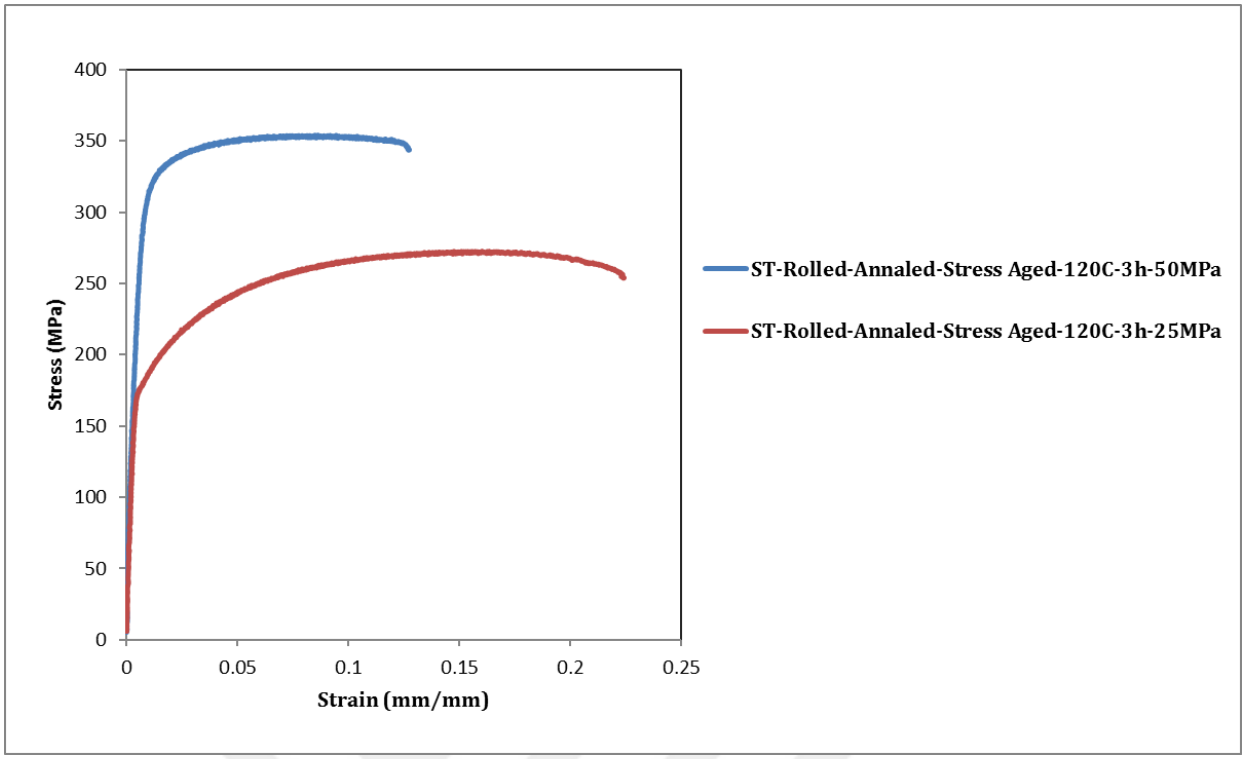

Fig. 5.14. Effect of applied stress on the tensile response of the processed samples.

5.2.3. Low temperature mechanical behavior

The effect of temperature on the tensile properties is investigated in this section. Fig. 5.15 shows the tensile performance of the solution treated sample at room temperature, -20℃ and -60℃. It is clear that by decreasing the testing temperature down to -60℃, the tensile strength is increased with a decrease in ductility. For static aged and solution treated samples higher elastic modulus is observed at -60℃ relative to ambient condition. The ductility of static aged samples drops dramatically by decreasing the temperature. The ductility of static aged sample at ambient temperature is 11% while it decreases to 3% for the sample tested at -60℃. For the stress aged sample, ductility of ambient temperature and the -20℃ sample are relatively the same, while for the -60℃ sample, the ductility decreases to 9%. Stress aged sample exhibits better mechanical strength at ambient temperature, while strength is nearly the same for samples aged at -20℃ and -60℃.

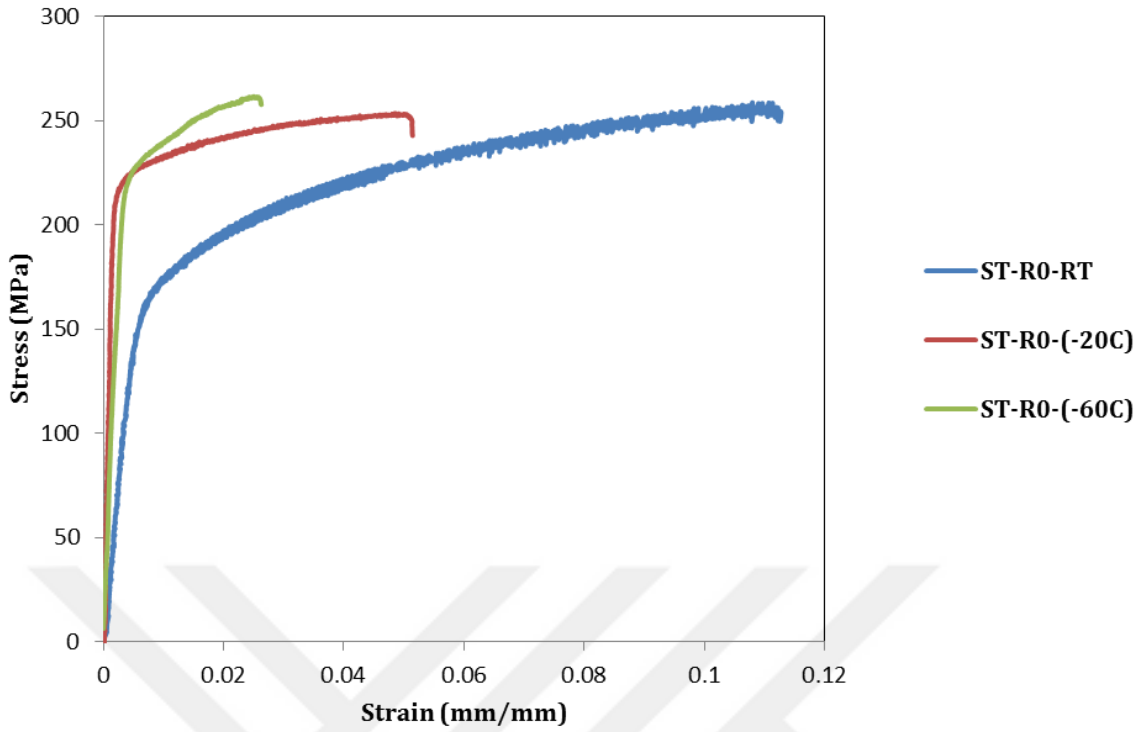

Fig. 5.15. Effect of testing temperature on the tensile properties of solution treated sample

It is observed that elastic modulus of solution treated and static aged sample increases significantly at low temperatures. The elastic modulus of solution treated sampe is 30 GPa , while by decreasing temperature to -20℃ , the elastic modulus increases to 98 GPa. However, for sample deformed at -60℃, the elastic modulus decreases to 67 GPa. For stress aged samples, the elastic modulus of samples at ambient and -20℃ is nearly the same (37 GPa) while the elastic modulus of sample deformed at -60 ℃ has increased to 125 GPa. Many materials experience a decrease in the elastic modulus at higher temperature since it becomes easier to stretch the atomic bonds [122, 123]. For example, the temperature dependence of the elastic stiffness constants of metals is a well-known phenomenon. It is shown for aluminum alloy that by decreasing the temperature the elastic modulus increases due to difficult stretch of the atomic bonds [124, 125].

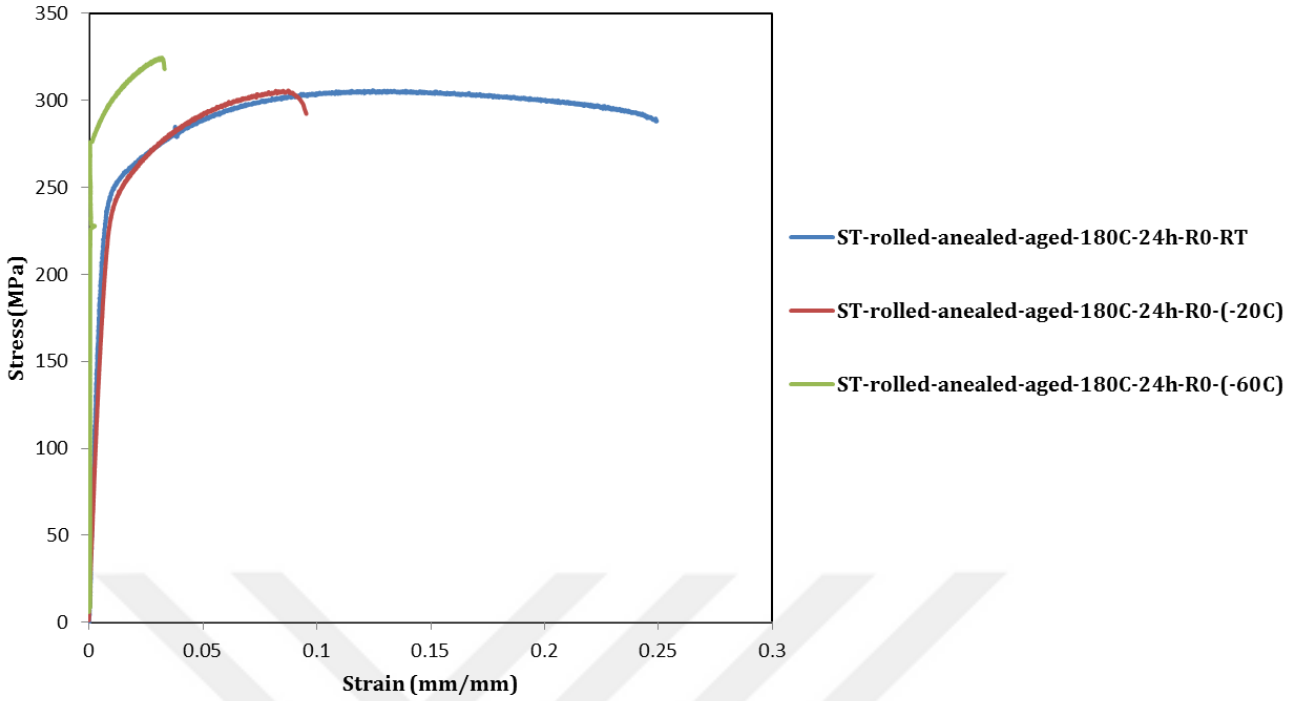

Fig. 5.16. Effect of testing temperature on the tensile properties of static aged samples

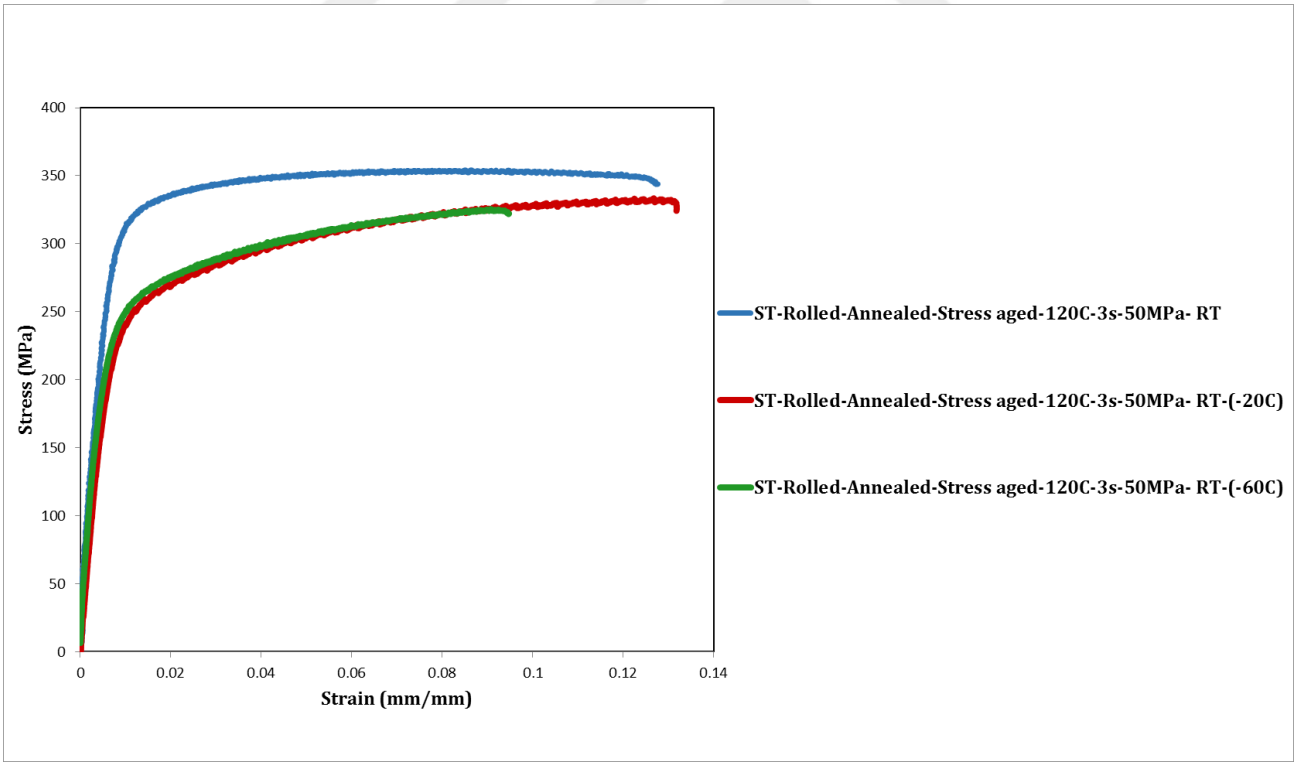

Fig. 5.17. Effect of testing temperature on the tensile properties of stress aged samples

The mechanical behavior of the sample stress aged at the best condition is investigated at -20℃. Tensile strength of the sample is 342 MPa with the elongation of 17%. Mechanical properties of the stress aged

sample at -20℃ implies the high strength of the sample at low temperatures. The stress-strain curve for the stress aged sample at -60℃ also implies reasonable mechanical response of the sample. This sample exhibits good ductility of 10% along with a reasonable UTS of 332 MPa. Microstructure analysis reveals that the alloy deforms by slip and twinning at low temperatures while at high temperatures additional slip systems are activated leading to improved ductility. At room temperature, the decomposition of precipitates leads to a detrimental effect on the mechanical properties of the alloy [83].

Mechanical properties of solution treated and best condition samples are compared at -20℃ and -60℃ as well. Fig. 5.18 compares the tensile properties of samples at -20℃. It is clear that the stress aged sample has better formability along with favorable strength relative to the static aged and solution treated samples. It can be inferred that the tensile properties of aged samples are improved significantly by thermo-mechanical process relative to the solution treated sample. The same trend is shown for -60℃ condition, where the tensile strength of stress aged sample is improved and formability is twice that of the solution treated sample. Mechanical properties of processed samples are summarized in Table. 5.3.

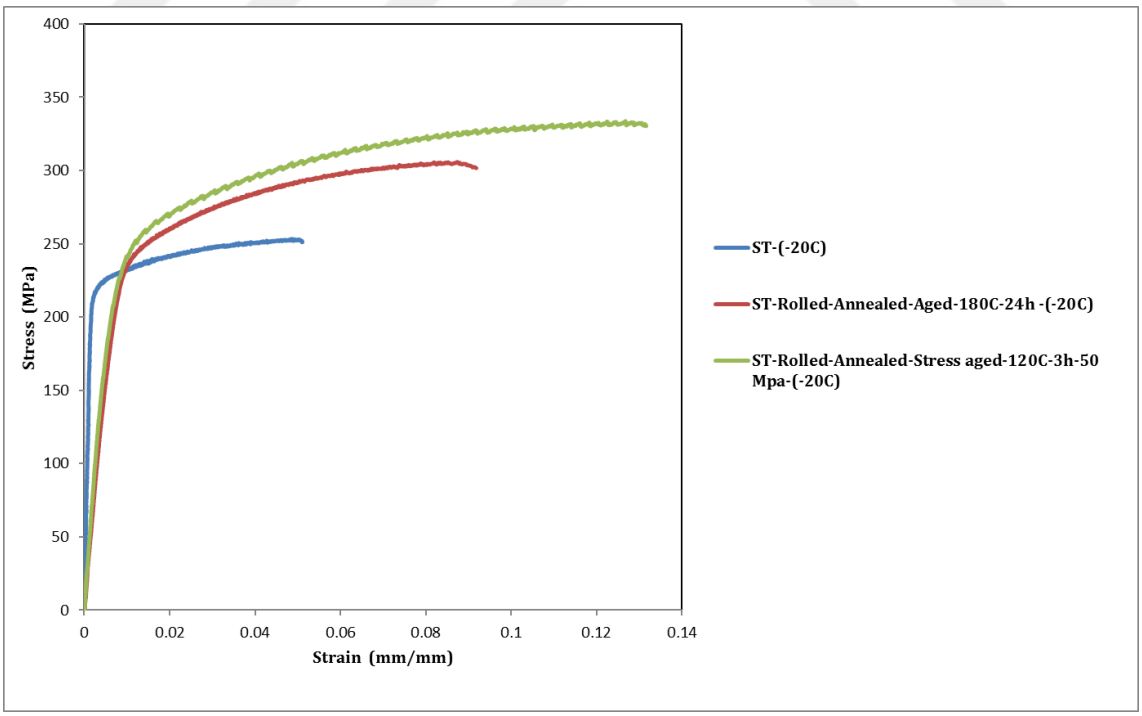

Fig. 5.18. Tensile behavior of solution treated, static aged best condition, and the stress aged best condition in -20℃

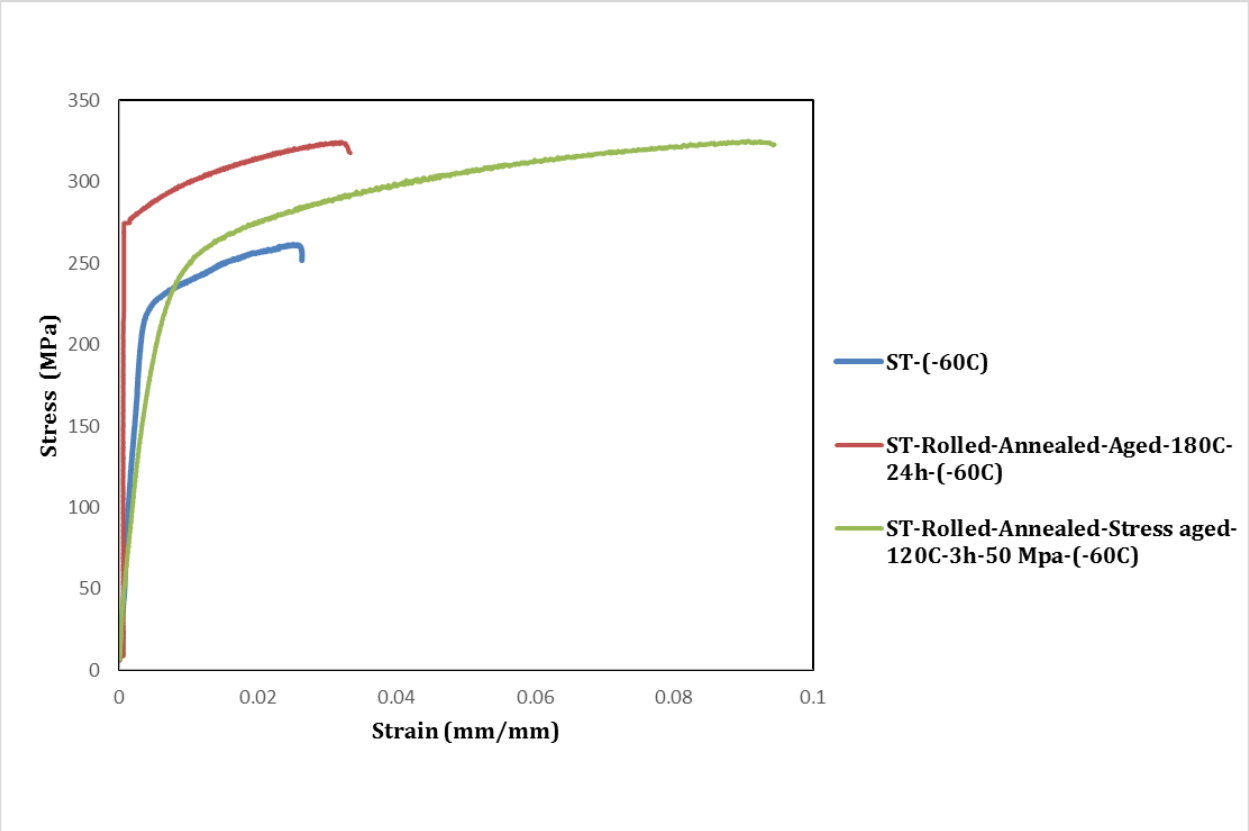

Fig. 5.19. Tensile behavior of solution treated, static aged best condition and the stress aged best condition in -60℃

Table. 5.3. Mechanical properties of developed samples

Condition	Yield Strength (MPa)	UTS (MPa)	Elongation (%)
Solution treated	162.8	255.3	11.4
Solution treated (-20℃)	187.2	251.6	5.1
Solution treated (-60℃)	179.2	262.4	2.6
Static aged-180℃-24h	225.2	254.3	9.3
Solution treated-Rolled	268.4	327.5	1.8
Solution treated-Rolled-Annealed(350C/2h)-Static aged-180℃-48h	184.5	306.9	13.7
Solution treated-Rolled-Annealed(400C/20min)-Static aged- 180℃-48h	189.3	273.4	11.1
Solution treated-Rolled-Annealed(350C/20min)- Static aged-180℃-48h	213.2	299.2	10.3
STAA-120℃-6h	176.2	269.7	23.3
STAA-120℃-12h	153.3	277.2	11.6
STAA-120℃-24h	199.2	286	23.2
STAA-120℃-48h	202.3	282.3	20.1
STAA-120℃-72h	182.5	272.3	18.4
STAA-180℃-6h	168.2	289.3	20.1
STAA-180℃-12h	184.2	301.2	15.1
STAA-180℃-24h-(-20℃)	210.1	305.7	9.2
STAA-180℃-24h-(-60℃)	243.2	322.8	3.3
STAA-180℃-24h	205.8	304.8	25.2
STAA-180℃-48h	175.2	291.2	14.4
STAA-240℃-6h	165.4	271.2	11.5
STAA-240℃-12h	177.2	276.5	17.4
STAA-240℃-24h	188.2	283.2	22.3
STAA-240℃-48h	180.3	283	23.5
STAA-240℃-72h	175.2	274.7	18.9
Solution treated-Rolled-Annealed	158.3	275	30
Solution treated-Rolled-Annealed-100℃	155.4	202	25.9

Solution treated-Rolled-Annealed-200℃	101.2	106.5	21.2
STRA-180℃-6h-100 MPa	183.4	282.1	12.2
STRA-180℃-3h-100 MPa	212.2	309.4	6.6
STRA-120℃-3h-25 MPa	160.4	278.4	22.4
STRA-120℃-6h-25 MPa	158.4	280.6	23.6
STRA-120℃-12h-25 MPa	161.2	283.1	26.1
STRA-180℃-3h-25 MPa	131.2	278.1	20.2
STRA-180℃-6h-25 MPa	157.6	280.2	26.9
STRA-180℃-12h-25 MPa	156.3	285.2	19.4
STRA-120℃-1h-50 MPa	135.2	280.17	13.4
STRA-120℃-3h-50 MPa	162.4	353.3	12.5
STRA-120℃-3h-50 MPa-(-20℃)	158.1	333.7	13
STRA-120℃-3h-50 MPa-(-60℃)	150.3	337.9	9.2
STRA-120℃-6h-50 MPa	150.2	330.4	7.85
STRA-120℃-12h-50 MPa	163.7	315.4	13.4
STRA-180℃-1h-50 MPa	151.3	284.6	21.2
STRA-180℃-3h-50 MPa	166.7	321.3	10.1
STRA-180℃-6h-50 MPa	142.6	299.6	13.9
STRA-180℃-12h-50 MPa	122.8	278.7	6.5
STRA-180℃-24h-50 MPa	163.1	280.2	11.2

*STTA represents the solution treated, rolled, annealed and static aged samples
*STRA represents the solution treated, rolled, annealed and stress aged samples

The SEM images of the fracture surfaces are illustrated in Fig. 5.20 for solution treated, static aged and stress aged conditions at ambient and -60℃ temperatures. The fracture surfaces are composed of several small dimples and few lamellar quasi-cleavage planes for solution treated samples at ambient temperature. Large cracked particles can be observed on the fracture surface of -60℃. It is reported that lamellar cleavage planes are formed due to the formation of coarse rod like precipitates of $\acute{\beta}_1$ that lead to stress concentration at their interfaces with Mg matrix [126]. Solution treated samples as discussed in TEM characterization section have few coarse precipitates. Hence, formation of semi-cleavage planes is supported with precipitates formation as well [127]. Many small dimples with few cracked voids are observed for the static aged samples at ambient temperature deformation which is the characteristic of ductile fracture supporting high ductility of static aged sample. At -60℃ the number and size of voids are in line with lower formability of static aged sample. Dimples and voids are observed for the stress aged samples deformed at ambient temperature. Large void cracks propagated along the fracture zone is observed for the stress aged sample deformed at -60℃ while no dimples are observed. Formability of stress aged sample is better than static aged sample which can be attributed to the propagation of crack along the applied load direction [111].

5.2.4. The strengthening mechanism of formed precipitates under applied load

It has been reported that the habit plane of $\acute{\beta}_1$ precipitates is prismatic plane of $(10\bar{1}0)$ with $[0001]_{Mg}$ growth direction [128]. Fig. 5.21 exhibits the schematic representations of $\acute{\beta}_1$ rod like precipitates and $\acute{\beta}_2$ disk-shaped ones under the forces of different directions. When the basal planes of grains are perpendicular to the tensile direction, $\acute{\beta}_1$ precipitates can act as semi-fibers and strengthen Mg matrix greatly as shown in Fig. 5.21a. However, in Fig. 5.21b, when the basal planes of grains are parallel to the tensile direction, the interface between $\acute{\beta}_1$ precipitates and matrix bears more load, which will degrade the mechanical properties and with $\acute{\beta}_1$ rods coarsening, the adherence strength between $\acute{\beta}_1$ rods and matrix will degrade, which lowers the mechanical properties.

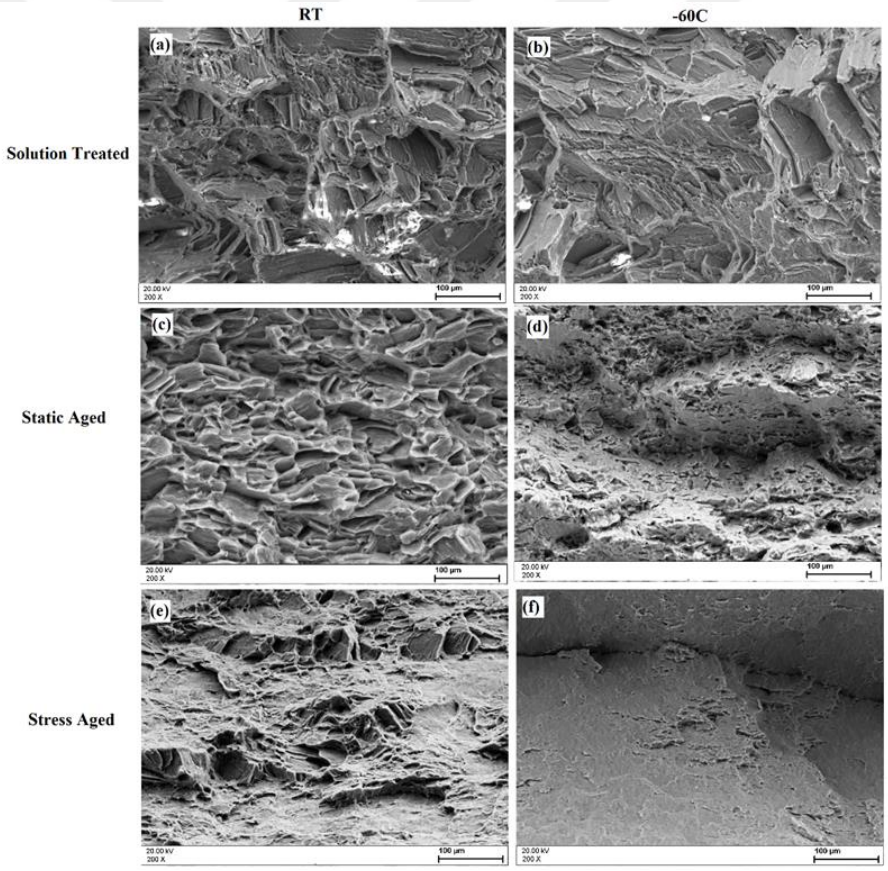

Fig. 5.20. Fracture surface of samples after tensile tests (a) solution treated sample at ambient temperature and (b) -60℃, STAA-180℃-24 sample at (c) ambient temperature (d) -60℃ and STRA-120℃-3h-50 MPa sample at (e) ambient temperature (f) -60℃

For solution treated sample, few $\acute{\beta}_1$ precipitates were observed and mechanical properties are not influenced by precipitate orientation in general. For static and stress aged samples high density of

precipitates were observed. Therefore, the mechanical properties depend on the variation of the size of the $\acute{\beta}_1$ rods.

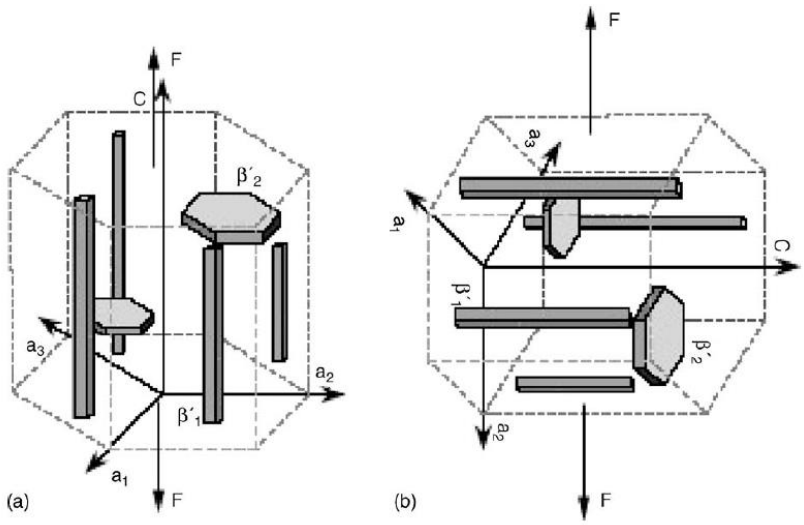

Fig. 5.21. Schematic morphology representations of $\acute{\beta}_1$ and $\acute{\beta}_2$ precipitates [129]: (a) the basal plane perpendicular to and (b) parallel to the tensile direction

Chapter 6

EFFECT OF ROLLING AND AGING PROCESSES ON THE TEXTURE OF ZK60 MAGNESIUM ALLOY

6.1. X-Ray Diffraction pattern analysis

X-Ray diffraction (XRD) as a rapid analytical technique primarily used for phase identification of a crystalline material can provide information on unit cell dimensions. In the current work, XRD is used to investigate the existence of precipitates in the microstructure of samples. Phase analysis using XRD shows the presence of $MgZn_2$ precipitates.

XRD results indicate that the ST samples mainly consisted of α-Mg and $MgZn_2$ phases as shown in Fig. 6.1. For the ST sample, very low peaks are observed for the $MgZn_2$ precipitates which indicates a good solution of precipitates inside the α-Mg phase. This means that an almost single phase solid solution is formed in ZK60-ST and good formability is obtained during rolling deformation. As shown in Fig. 6.2, the XRD pattern of the rolled sample has higher peaks for $MgZn_2$ precipitates which prove the nucleation of precipitates during the rolling process. It should be noted that precipitates consisting of Zn-Zr phases are hard to be detected with XRD due to the low amount of Zr in the alloy composition.

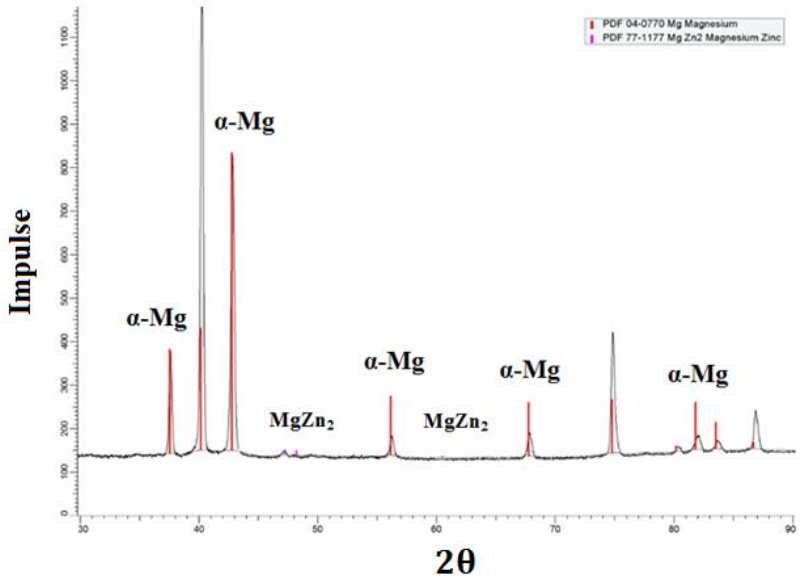

Fig. 6.1. X-ray diffraction pattern of the ST sample.

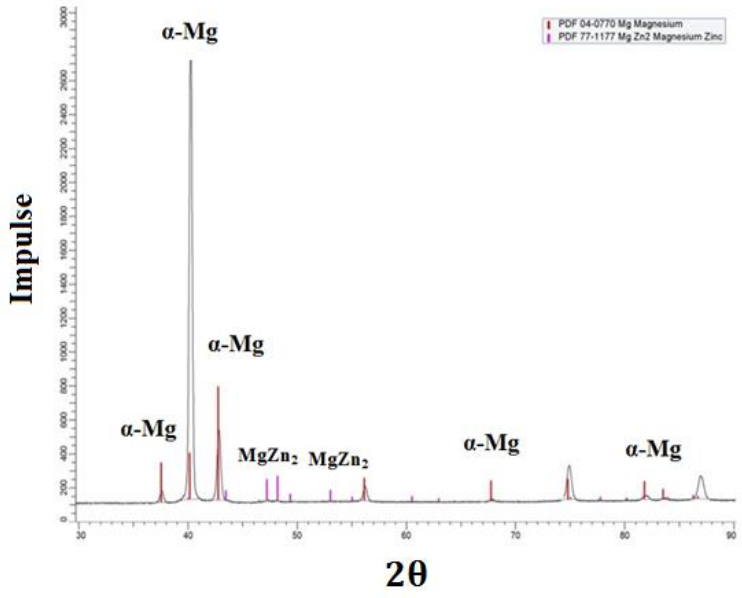

Fig. 6.2. X-ray diffraction pattern of the rolled sample.

Fig. 6.3 shows the XRD pattern for the solution treated sample and static aged at temperature of 180℃ for 24 hours. This sample is not rolled, and it is anticipated that the precipitate formation is limited. As it is clear in the figure, a limited number of peaks are evident showing the existence of the $MgZn_2$ phase. Higher peaks are observed for the rolled and then static aged samples at a temperature of 180℃ for 24 hours as shown in Fig. 6.4.

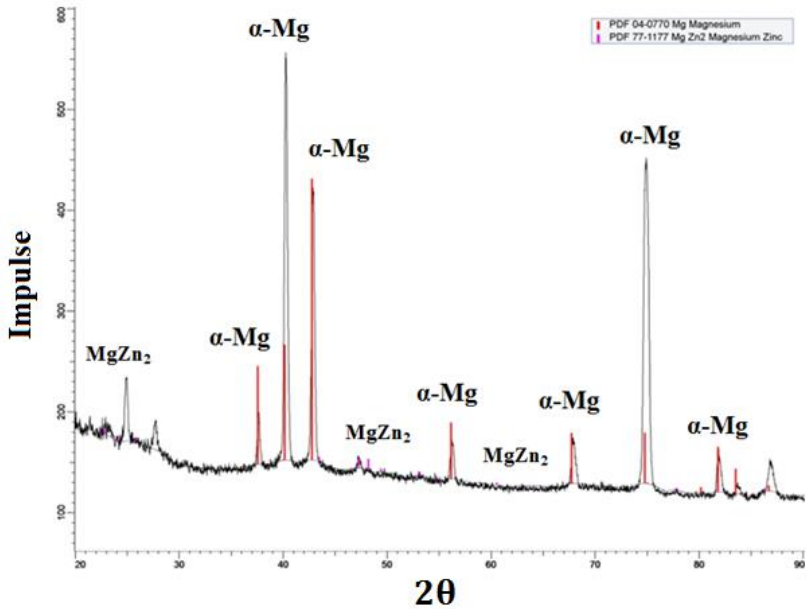

Fig. 6.3. X-ray diffraction pattern of the aged sample 180℃ for 24h

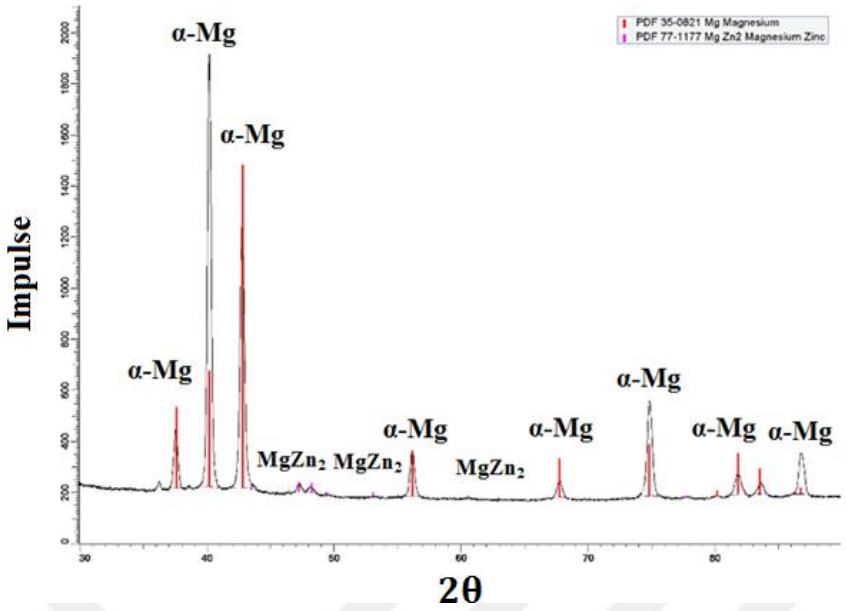

Fig. 6.4. X ray diffraction pattern of the rolled and aged sample at 180℃ for 24h

The XRD pattern for the stress aged sample shows high and intense peaks for the $MgZn_2$ phase. It can be inferred that more precipitates of $MgZn_2$ are formed during the stress aging process. Peaks for the stress aged sample are the highest among all samples indicating that precipitate formation can be accelerated using the stress aging method.

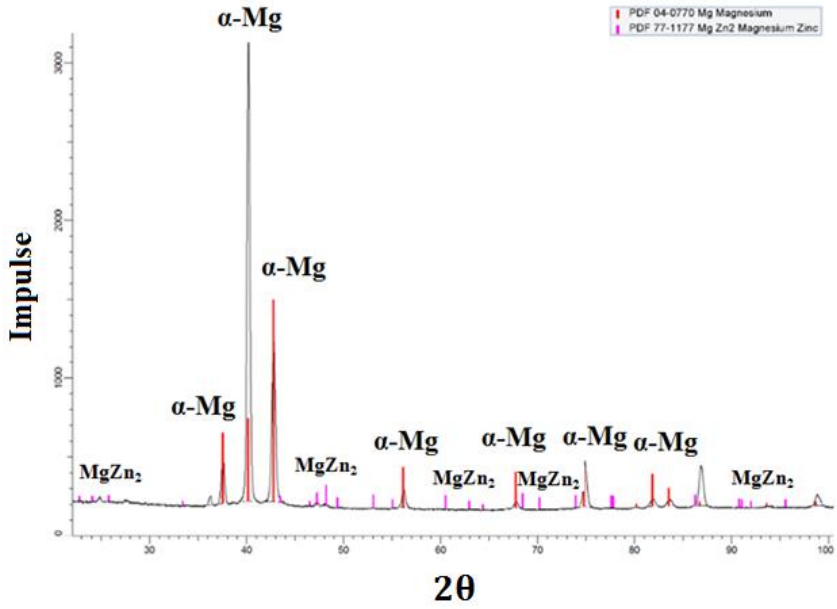

Fig. 6.5. X-Ray diffraction pattern of the rolled and stress aged sample at 120℃ for 3h and 50 MPa

6.2. Pole figure characterization by X-Ray Diffraction

XRD data are used to extract the pole figures for the (0002) basal plane and $(10\bar{1}0)$ prismatic planes. Fig.6.6 illustrates the pole figure for the basal plane for processed samples. The solution treated sample exhibits an inhomogeneous texture; the basal poles tend to align along the rolling direction. For sample solution treated and aged at 180℃ for 24h, the basal component is tilted 10 degrees from the RD (Fig. 6.6b). The basal texture variation is attributed to the arrangement of precipitates plates in the Mg matrix. It is estimated that during the static aging process, arrangement of cubic and rod like precipitates in an hcp structure can change both in direction and density [130]. The precipitates in the form of [0001] rods are most effective in increasing the precipitate number density per unit area of slip plane of the magnesium matrix phase.

The directions of the rolled samples are designated in order to characterize the effect of rolling on the texture. Hence the direction parallel to the rolling is termed as RD, transverse to the rolling as TD and the direction perpendicular to the rolling surface as ND. Rolled sample has a strong basal texture aligned in the ND direction (Fig. 6.6c). During rolling of magnesium, both basal slip and tension twinning reorient the c-axis of grains so that c-axis becomes approximately parallel to the compression axis (ND or sheet thickness direction). This leads to a favorable alignment of basal planes parallel to the RD. Rolled and static aged sample for 24 hours at 180℃ has basal component aligned in the ND direction which is elongated along the TD direction. The stress aged samples were exposed to the extension in the rolling direction and thus exhibited strong basal texture elongated along the RD. Stress aging extends the sample in the RD direction making the same effect as rolling on the texture and leading to an alignment of grains with c-axis. This intensifies the basal texture in stress aged samples.

The intensity of pole figures in basal plane is characterized. The intensity of solution treated sample is 3.55 at the highest. For solution treated and static aged sample at 180℃ for 24 hours the intensity increases significantly to 6.8. High intensity of basal component at this condition means that the precipitates are located in the basal plane. Alignment of both, $\acute{\beta}_1$ and $\acute{\beta}_2$ precipitates to the basal plane is possible, since

$\acute{\beta}_1$ is located on this plane and $\acute{\beta}_2$ is perpendicular to it. Rolled sample exhibits higher intensity relative to the aged samples. However, the stress aging intensifies the intensity more significantly relative to the static aging on the basal plane.

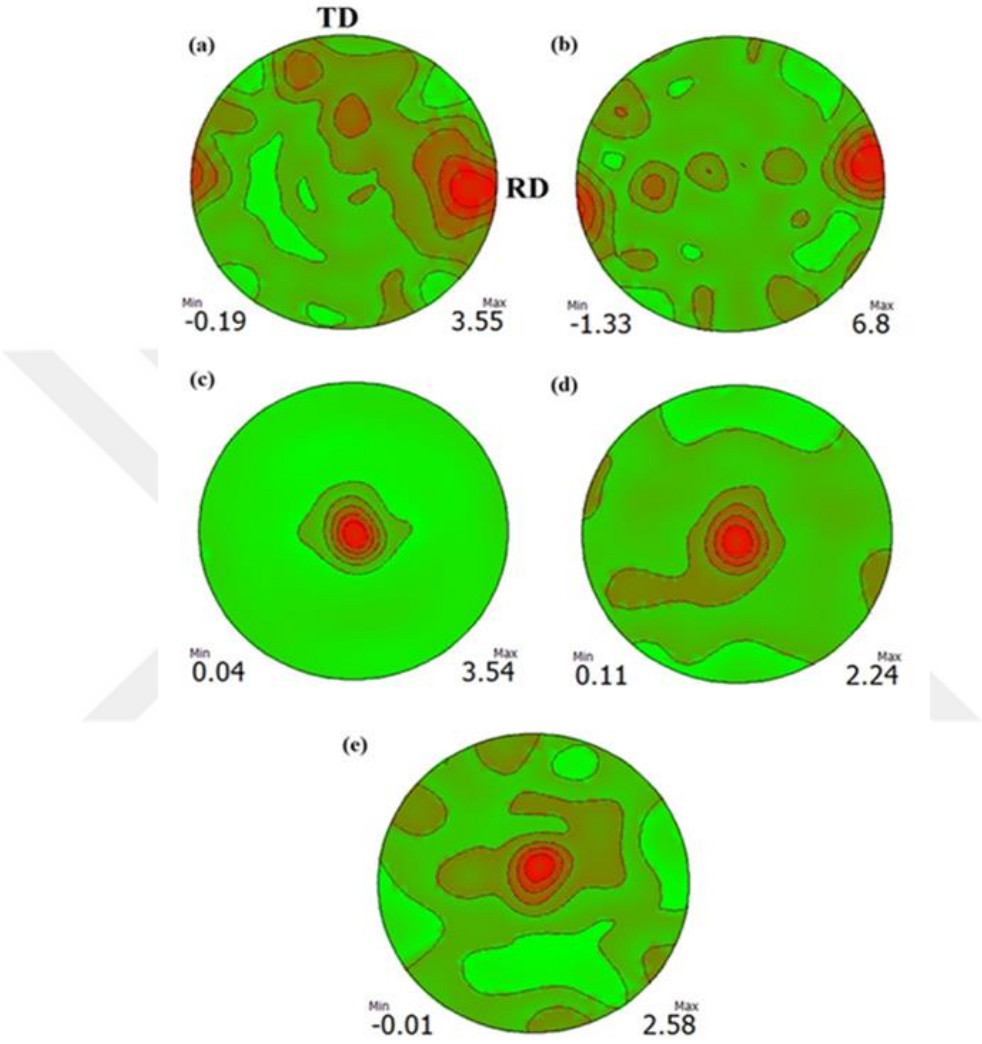

Fig. 6.6. Pole figures extracted from XRD data along the (0002) direction for (a) solution treated sample (b) solution treated and aged sample at 180℃ for 24h (c) solution treated and rolled sample (d) solution treated, rolled and aged sample at 180℃ for 24h (e) solution treated, rolled and stress aged at 120℃ for 3h

Fig.6.7 illustrates the pole figure showing the orientation of the prismatic $(10\bar{1}0)$ plane for the processed samples. The solution treated sample exhibits an inhomogeneous texture; the prismatic poles are distributed around directions. However, there are more poles aligned with the ND direction. For solution treated and aged at 180℃ for 24 hours sample, the poles are aligned with the traverse direction (TD), while the intensity of poles is increased relative to the solution treated sample. Alignment of prismatic poles along the TD

reveals the fact that in the case of plastic deformation with the extension in TD, the prismatic slip will be activated. The rolled sample shows high intensity poles in the TD and RD (Fig. 6.7c). For rolled and static aged and stress aged samples (Fig. 6.7d and 6.7e), the same trend is observed, and the poles are aligned with the RD and TD.

6.3. Texture analysis using the EBSD method

6.3.1. Texture analysis for the solution treated sample

Fig. 6.8a and b illustrate the misorientation of grains and the inverse pole figure (ipf) of solution treated sample. Solution treated sample exhibits bimodal structure with coarse grains with size of 20 μm and fine grains with size of 1-4 μm. The misorientation angle of grain boundaries for the solution treated samples indicate high fraction of grain boundaries (HAGB) which is attributed to the occurrence of DRX during deformation process for the wrought alloy. The grains with the prismatic orientation of $(21\bar{1}0)$ are dominant in the microstructure. High intensity with the maximum magnitude of 18.37 is calculated from the EBSD results for the ST sample for rolling direction (RD) on the basal plane of (0001) as shown in Fig. 6.8b. ST sample exhibits basal texture aligned with the RD direction. The same trend was observed in the pole figures extracted from the XRD results for solution treated samples. This can be attributed to the forging or extrusion process applied to the wrought slab of ZK60. While ST sample shows strong basal texture, no evident pole intensity is observed in $(10\bar{1}0)$ and $(10\bar{1}1)$ planes. Hence, it can be inferred that no obvious prismatic or first order pyramidal pole texture exists for the ST sample.

6.3.2. Texture analysis for the best condition of static aged sample

Fig. 6.9a and 6.9.b illustrate misorientation of grains and the inverse pole figure (ipf) of rolled and static aged sample. Finer grains with average grain size of 10 μm and more equixed structure is observed for this sample. However, some coarse grains along with existence of fine grains representing the residual of original bimodal structure are observed for static aged sample. Grains exhibit distinct misorientation rather random while the basal texture is still observed in ipfs and pole figures. It is clear from the (0002) basal

pole figure that alignment of rolled and static aged sample is changed. While the basal poles were aligned with the RD, for the rolled and static aged sample they are tilted toward the ND. However, it is inferred from Fig. 6.9c that the basal poles are distorted from the ND with the angle of near 45 degrees.

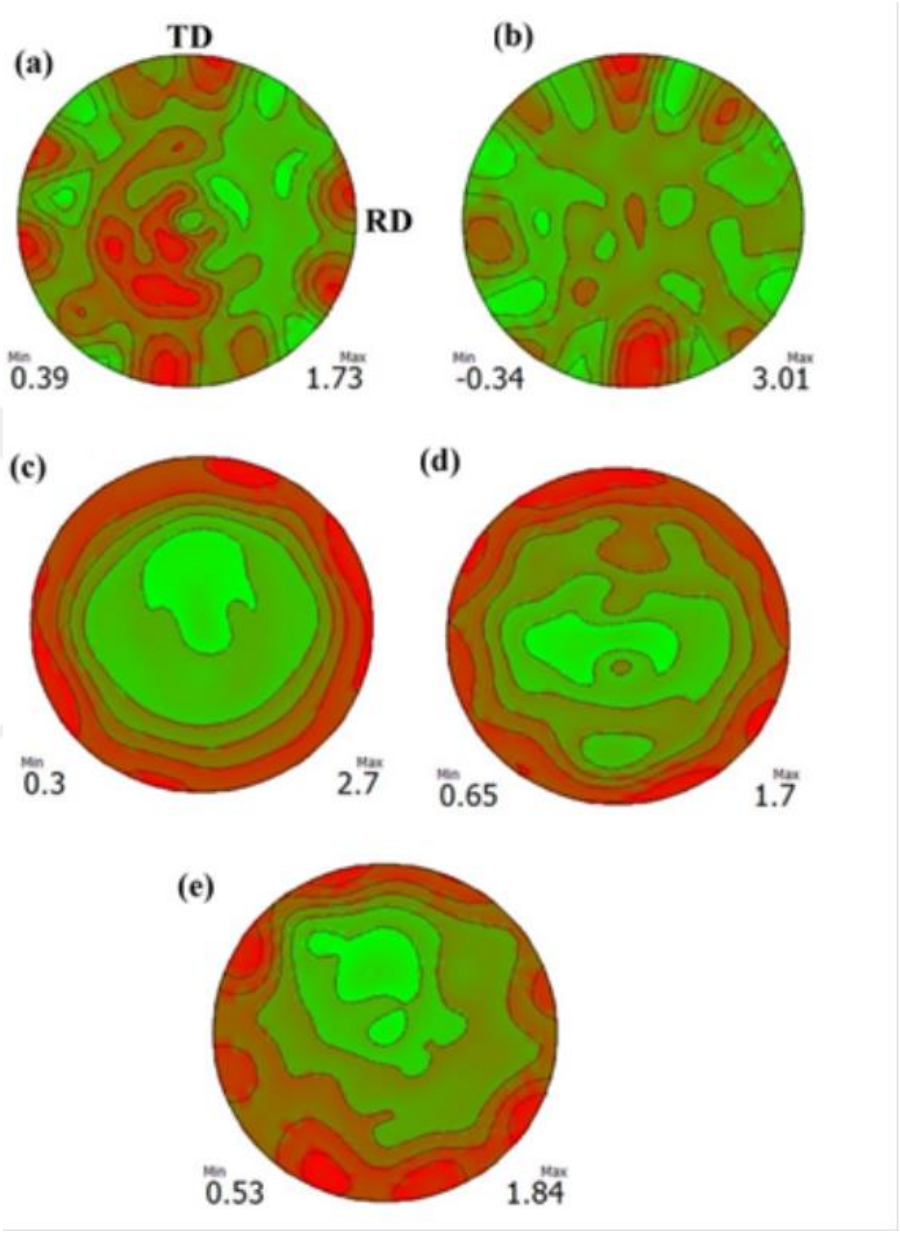

Fig. 6.7. Pole figures extracted from XRD data along the $(10\bar{1}0)$ plane for (a) solution treated sample (b) solution treated and aged sample at 180℃ for 24h (c) solution treated and rolled sample (d) solution treated, rolled and aged sample at 180℃ for 24h (e) solution treated, rolled and stress aged at 120℃ for 3h

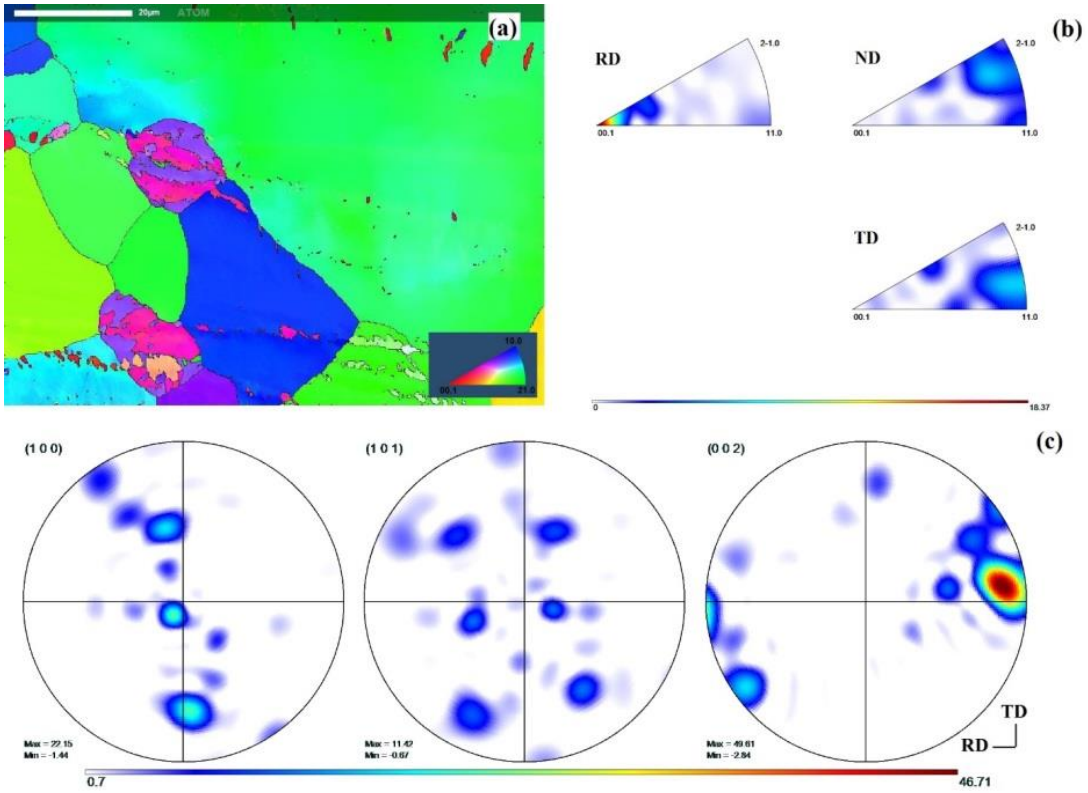

Fig. 6.8. (a) Misorientation of grain (b) inverse pole figure (c) pole figures for the ST sample extracted from the EBSD results.

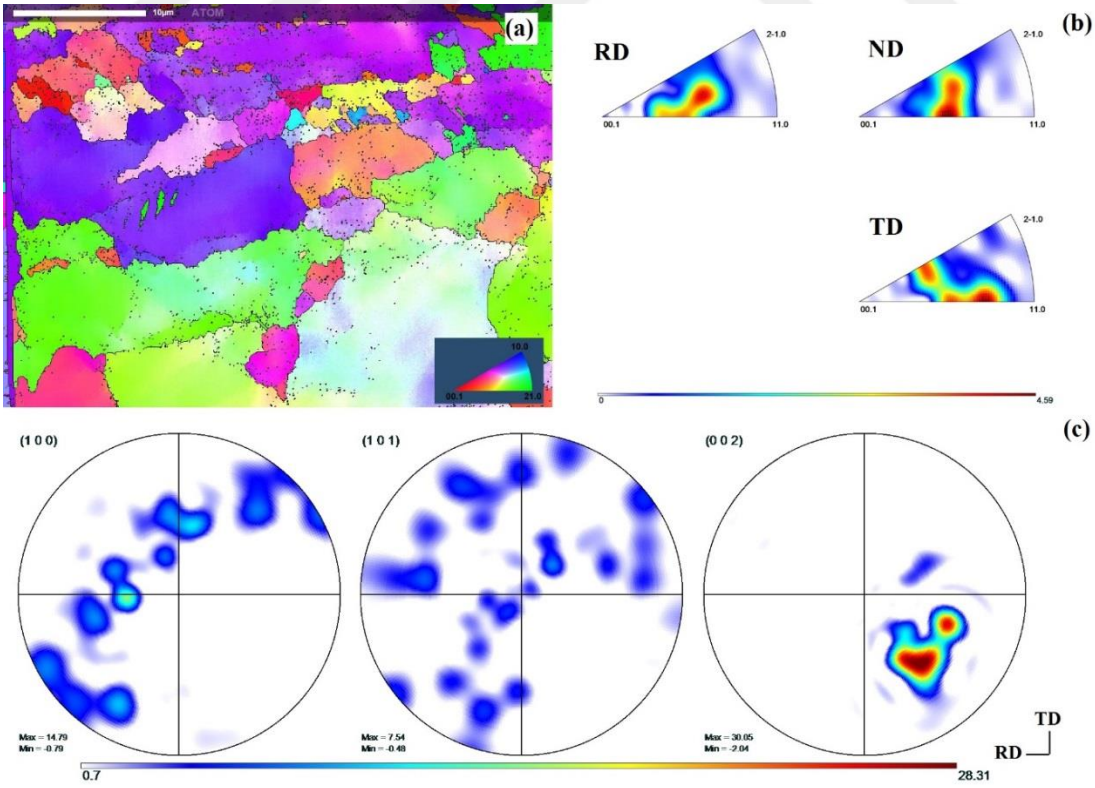

Fig. 6.9. Misorientation of grain (b) inverse pole figure (c) pole figures for the rolled and static aged sample extracted from the EBSD results.

6.3.3. Texture analysis for the best condition of stress aged sample

Fig. 6.11 a and 6.11b illustrates the misorientation of grains and the inverse pole figure (ipf) of rolled and stress aged samples. The large grains are fully eliminated and fine and equixed grains with average grain size of 5μm are achieved. Crystals tend to orient with the (0002) basal plane as shown in Fig. 6.11a. A strong basal texture usually seen for the rolled samples is exhibited for this condition. The basal plane is aligned with the ND while the intensity of ipf is 6.66 at the highest. Since stress aging leads to the contraction of the c-axis, and alignment of the basal poles with the ND, stress aging has the same effect as rolling on the texture. Hence it can be inferred that while rolling and static aging could not fully orient the basal poles, further stress aging led to the formation of a strong basal texture along the ND.

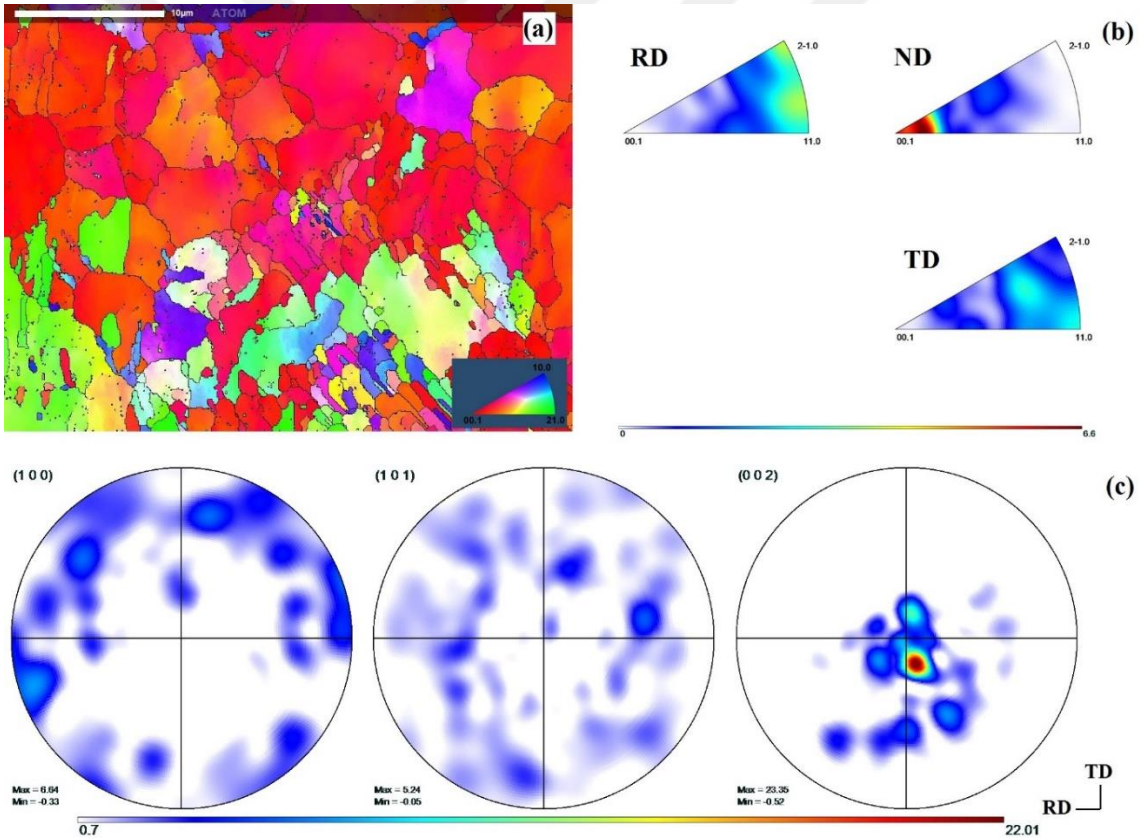

Fig. 6.10. Misorientation of grain (b) inverse pole figure (c) pole figures for the rolled and stress aged sample extracted from the EBSD results.

6.3.4. Texture analysis for the deformed best condition of stress aged sample

Fig. 6.20 shows the pole figures for the deformed stress aged sample after tensile test. It is clear that the basal poles are strong in the ND where the c-axis was contracted during the deformation. The low ductility

of samples at low temperature can be attributed to the limited deformation mechanism restricted with strong basal texture. Basal slip is activated for the low temperature samples and extension in c-axis is restricted leading to the low formability. While the sample is loaded along the RD, it has the same effect as the compression on the texture and activation of tension twinning and/or <c+a> slip mode are required for higher ductility of the deformed samples. Hence, due to limitation of activated slip modes formability of stress aged sample (STRA-120℃-3h-50 MPa) is restricted to 12.5% and is nearly the same with the solution treated sample at ambient temperature.

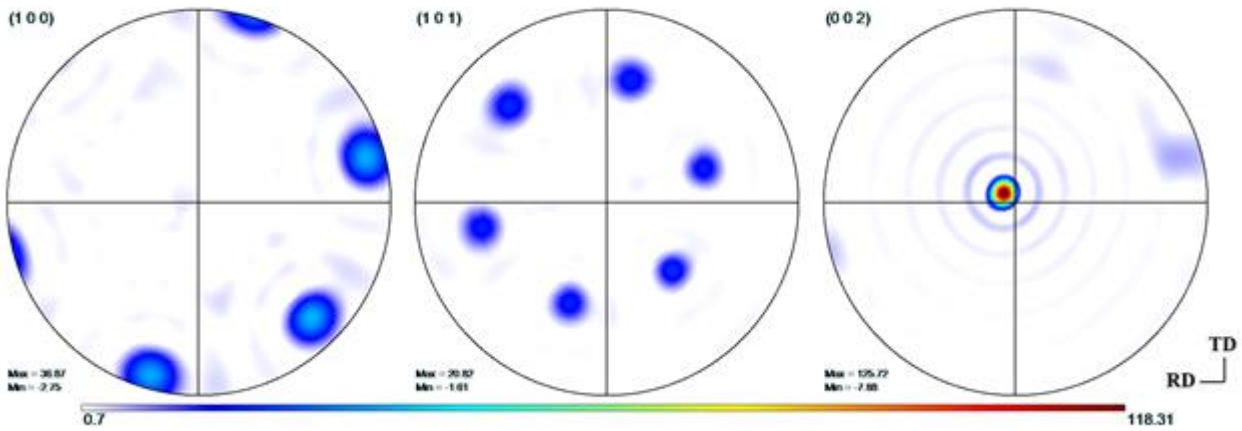

Fig. 6.11. Pole figures for the sample stress aged and then strained at 10^{-3} s^{-1}

6.3.5. Effect of textue on the orientation of precipitates and the mechanical response

As discussed above the basal pole figures are aligned with the RD for the solution treated samples. Basically, in the case of existence of rod precipitates, solution treated samples can exhibit high tensile strength due to the alignment of rod precipitates with the loading direction parallel to the prismatic plane. However, due to lack of precipitates in the solution treated sample, low strength and ductility are achieved. To some degree, texture can interpret the mechanical response of the static aged samples [126]. Since the basal poles are tilted 45° from the ND, it is expected that combination of stress concentration at the interphase of rod-shaped precipitate and Mg matrix along with semi-fiber strengthening parallel to load direction make the role in determining the mechanical response and activated slip mode [126]. While stress concentration at interphase degrades the tensile properties, fibrous precipitates parallel to the prismatic

planes strengthen the tensile properties [129]. Strong basal texture is seen for the stress aged sample. High stress concentration at the interphase of rod precipitates with Mg matrix is expected, however high density of fine precipitates increases the hardening of the samples. Low ductility of stress aged samples at ambient temperature relative to the static aged sample is due to the alignment of rod precipitates perpendicular to the load direction [129]. However, activation of non-basal slip modes along with twinning can be the main reason for higher formability for stress aged samples at low temperatures [126].

CONCLUSION

Wrought slabs of ZK60 magnesium alloy was exposed to a thermo-mechanical process. A systematic rolling and aging process were applied to enhance the mechanical properties of solution treated samples of ZK60. Based on the conducted experiments and observed results, the following conclusion can be drawn:

i. Thermo-mechanical process containing rolling, annealing and aging treatment was found as an effective method to refine the microstructure and enhance the mechanical properties. Fine and equiaxed grains were observed for the static and stress aged samples while the solution treated sample had coarse grains with inhomogeneous structure.

ii. The solution treated sample exhibited low mechanical properties while the enhanced mechanical properties were achieved for both static aged and stress aged samples. The solution treated sample had the UTS of 255 MPa and elongation of 11%. The best sample of rolled and static aged condition exhibit UTS of 305 MPa and elongation of 25%. The enhancement for the stress aged sample was even more, and 353 MPa and 15% were achieved for UTS and strain to failure, respectively.

iii. High strength along with significant increase in elongation for the static aged sample is attributed to the nucleation of grains during the rolling process and formation of fine precipitates of $MgZn_2$ during the aging process. The high strength was achieved for the stress aged sample attributed to the formation of uniform and fine precipitates with more density along with possibility of activation of tension twinning.

iv. While the precipitates were nearly dissolved into the matrix for the solution treated sample, high density of precipitates was shown for the rolled and static aged sample. Fine, uniform and denser precipitates were observed for the stress aged samples. The indexing of the observed precipitates reveals that $MgZn_2$ precipitates are dominant in the matrix of stress aged sample. Precipitation hardening as an effective method has contributed to the improvement of mechanical properties of processed samples.

v. The solution treated sample exhibits random texture along with basal pole figure aligned in the RD of the processed samples. The rolled sample shows strong basal texture as the grain are oriented along the c-axis. The rolled and static aged sample shows basal texture oriented 45 degrees from the ND. The stress aged sample demonstrates strong basal texture aligned with the ND where the basal planes are parallel to the RD. It is inferred that stress aging can enforce the effect of rolling on the texture by orienting the crystals along the c-axis.

vi. Tensile behavior of solution treated and processed samples were characterized at low temperatures. It was observed that at low temperature deformation mechanism is limited to the basal slip. Hence at low temperatures, formability of strained samples is low. Suppression of tension twinning at low temperature decreases the formability. Stress aged sample exhibited high strength (337 MPa) and good ductility (9.2%) while mechanical response of solution treated sample was limited to 262 MPa and 2.6% at -60°C temperature.

RECOMMENDATIONS FOR FUTURE WORKS

Although some efforts were made to study thermo-mechanical processing of magnesium alloys in the present work, these methods are not limited to the performed experiments and achieved findings. Therefore, there are few suggestions for upcoming research works.

i. The high temperature tensile behavior of developed samples can be characterized to investigate whether superplasticity is observed at high temperatures for the developed samples. The constitutive modeling of high temperature can be made to predict the strength of samples at high temperatures.

ii. The impact properties of the processed samples can be investigated. A comparison between tensile toughness and impact toughness energy can be made.

REFERENCES

[1] Luo AA. Recent magnesium alloy development for automotive powertrain applications. Materials Science Forum: Trans Tech Publ; 2003. p. 57-66.

[2] Easton M, Beer A, Barnett M, Davies C, Dunlop G, Durandet Y, et al. Magnesium alloy applications in automotive structures. JOM Journal of the Minerals, Metals and Materials Society. 2008;60:57-62.

[3] Luo AA. Recent magnesium alloy development for elevated temperature applications. International materials reviews. 2004;49:13-30.

[4] Kulekci MK. Magnesium and its alloys applications in automotive industry. The International Journal of Advanced Manufacturing Technology. 2008;39:851-65.

[5] Luo AA. Magnesium: current and potential automotive applications. Jom. 2002;54:42-8.

[6] Stalmann A, Sebastian W, Friedrich H, Schumann S, Dröder K. Properties and processing of magnesium wrought products for automotive applications. Advanced Engineering Materials. 2001;3:969-74.

[7] Kim W-J, Chung S, Chung C, Kum D. Superplasticity in thin magnesium alloy sheets and deformation mechanism maps for magnesium alloys at elevated temperatures. Acta Materialia. 2001;49:3337-45.

[8] Agnew S, Tomé C, Brown D, Holden T, Vogel S. Study of slip mechanisms in a magnesium alloy by neutron diffraction and modeling. Scripta Materialia. 2003;48:1003-8.

[9] Koike J, Kobayashi T, Mukai T, Watanabe H, Suzuki M, Maruyama K, et al. The activity of non-basal slip systems and dynamic recovery at room temperature in fine-grained AZ31B magnesium alloys. Acta materialia. 2003;51:2055-65.

[10] Wang Y, Huang J. The role of twinning and untwinning in yielding behavior in hot-extruded Mg–Al–Zn alloy. Acta materialia. 2007;55:897-905.

[11] Brown D, Agnew S, Bourke M, Holden T, Vogel S, Tomé C. Internal strain and texture evolution during deformation twinning in magnesium. Materials Science and Engineering: A. 2005;399:1-12.

[12] Lowe TC, Valiev RZ. The use of severe plastic deformation techniques in grain refinement. JOM Journal of the Minerals, Metals and Materials Society. 2004;56:64-8.

[13] Valiev RZ, Alexandrov IV. Development of severe plastic deformation techniques for the fabrication of bulk nanostructured materials. Annales de Chimie Science des Materiaux: Elsevier; 2002. p. 3-14.

[14] Chen H, Kang SB, Yu H, Kim HW, Min G. Microstructure and mechanical properties of Mg–4.5 Al–1.0 Zn alloy sheets produced by twin roll casting and sequential warm rolling. Materials Science and Engineering: A. 2008;492:317-26.

[15] Huang X, Suzuki K, Saito N. Enhancement of stretch formability of Mg–3Al–1Zn alloy sheet using hot rolling at high temperatures up to 823K and subsequent warm rolling. Scripta Materialia. 2009;61:445-8.

[16] Wang Y, Kang SB, Cho J. Microstructure and mechanical properties of Mg–Al–Mn–Ca alloy sheet produced by twin roll casting and sequential warm rolling. Journal of Alloys and Compounds. 2011;509:704-11.

[17] Styczynski A, Hartig C, Bohlen J, Letzig D. Cold rolling textures in AZ31 wrought magnesium alloy. Scripta Materialia. 2004;50:943-7.

[18] Yin D, Zhang K, Wang G, Han W. Warm deformation behavior of hot-rolled AZ31 Mg alloy. Materials Science and Engineering: A. 2005;392:320-5.

[19] Ji Y, Park J. Formability of magnesium AZ31 sheet in the incremental forming at warm temperature. Journal of materials processing technology. 2008;201:354-8.

[20] Watanabe H, Mukai T, Ishikawa K, Higashi K. Low temperature superplasticity of a fine-grained ZK60 magnesium alloy processed by equal-channel-angular extrusion. Scripta Materialia. 2002;46:851-6.

[21] Bussiba A, Artzy AB, Shtechman A, Ifergan S, Kupiec M. Grain refinement of AZ31 and ZK60 Mg alloys—towards superplasticity studies. Materials Science and Engineering: A. 2001;302:56-62.

[22] Xu D, Liu L, Xu Y, Han E. The effect of precipitates on the mechanical properties of ZK60-Y alloy. Materials Science and Engineering: A. 2006;420:322-32.

[23] Chen X, Pan F, Mao J, Wang J, Zhang D, Tang A, et al. Effect of heat treatment on strain hardening of ZK60 Mg alloy. Materials & Design. 2011;32:1526-30.

[24] Xin R, Song B, Zeng K, Huang G, Liu Q. Effect of aging precipitation on mechanical anisotropy of an extruded Mg–Y–Nd alloy. Materials & Design. 2012;34:384-8.

[25] Chen H, Kang SB, Yu H, Cho J, Kim HW, Min G. Effect of heat treatment on microstructure and mechanical properties of twin roll cast and sequential warm rolled ZK60 alloy sheets. Journal of Alloys and compounds. 2009;476:324-8.

[26] Zheng K, Dong J, Zeng X, Ding W. Effect of pre-deformation on aging characteristics and mechanical properties of a Mg–Gd–Nd–Zr alloy. Materials Science and Engineering: A. 2008;491:103-9.

[27] Hong S-G, Park SH, Lee CS. Strain path dependence of {10− 12} twinning activity in a polycrystalline magnesium alloy. Scripta Materialia. 2011;64:145-8.

[28] Xin Y, Wang M, Zeng Z, Nie M, Liu Q. Strengthening and toughening of magnesium alloy by {10− 12} extension twins. Scripta Materialia. 2012;66:25-8.

[29] Brewer Jr H, Holman M. World Aerospace Structure Technology'90. London, UK. 1990;41.

[30] Cassada W, Shiflet G, Starke E. Mechanism of Al2CuLi (T1) nucleation and growth. Metallurgical transactions A. 1991;22:287-97.

[31] Eto T, Sato A, Mori T. Stress-oriented precipitation of GP Zones and θ′ in an Al‧ Cu alloy. Acta Metallurgica. 1978;26:499-508.

[32] Von Batchelder F, Raeuchle R. Lattice constants and Brillouin Zone overlap in dilute magnesium alloys. Physical Review. 1957;105:59.

[33] Davis JR, Allen P, Lampman S, Zorc TB, Henry SD, Daquila JL, et al. Metals handbook: properties and selection: nonferrous alloys and special-purpose materials: ASM International; 1990.

[34] Avedesian MM, Baker H. ASM specialty handbook: magnesium and magnesium alloys: ASM international; 1999.

[35] Housh S, Mikucki B, Stevenson A. Metals handbook. ASM International, Ohio. 1990:455.

[36] Polmear I. Magnesium alloys and applications. Materials science and technology. 1994;10:1-16.

[37] Horst EF, Mordike B. Magnesium technology. metallurgy, design data, application. Springer-Verlag, Berlin Heidelberg; 2006.

[38] Doege E, Dröder K. Sheet metal forming of magnesium wrought alloys—formability and process technology. Journal of Materials Processing Technology. 2001;115:14-9.

[39] Agnew SR. Wrought magnesium: a 21st century outlook. JOM Journal of the Minerals, Metals and Materials Society. 2004;56:20-1.

[40] Robson J, Paa-Rai C. The interaction of grain refinement and ageing in magnesium–zinc–zirconium (ZK) alloys. Acta Materialia. 2015;95:10-9.

[41] Davies C, Barnett M. Expanding the extrusion limits of wrought magnesium alloys. JOM Journal of the Minerals, Metals and Materials Society. 2004;56:22-4.

[42] Clark J. Age hardening in a Mg-9 wt.% Al alloy. Acta Metallurgica. 1968;16:141-52.

[43] Cáceres C, Blake A. The strength of concentrated Mg–Zn solid solutions. physica status solidi (a). 2002;194:147-58.

[44] Luo A, Pekguleryuz M. Cast magnesium alloys for elevated temperature applications. Journal of materials science. 1994;29:5259-71.

[45] Sun M, Easton MA, StJohn DH, Wu G, Abbott TB, Ding W. Grain refinement of magnesium alloys by Mg–Zr master alloys: the role of alloy chemistry and Zr particle number density. Advanced Engineering Materials. 2013;15:373-8.

[46] StJohn DH, Qian M, Easton MA, Cao P, Hildebrand Z. Grain refinement of magnesium alloys. Metallurgical and Materials Transactions A. 2005;36:1669-79.

[47] Koike J, Ohyama R, Kobayashi T, Suzuki M, Maruyama K. Grain-boundary sliding in AZ31 magnesium alloys at room temperature to 523 K. Materials Transactions. 2003;44:445-51.

[48] Koike J. Enhanced deformation mechanisms by anisotropic plasticity in polycrystalline Mg alloys at room temperature. Metallurgical and Materials Transactions A. 2005;36:1689-96.

[49] Dieter GE, Bacon DJ. Mechanical metallurgy: McGraw-hill New York; 1986.

[50] Groves G, Kelly A. Independent slip systems in crystals. Philosophical Magazine. 1963;8:877-87.

[51] Barnett M. A Taylor model based description of the proof stress of magnesium AZ31 during hot working. Metallurgical and materials transactions A. 2003;34:1799-806.

[52] Barnett M. Forming of magnesium and its alloys. Fundamentals of magnesium alloy metallurgy Cambridge: Woodhead Publishing Limited. 2013:197-231.

[53] Obara T, Yoshinga H, Morozumi S. {11$\bar{2}$2}< 1123> Slip system in magnesium. Acta Metallurgica. 1973;21:845-53.

[54] Al-Samman T. Comparative study of the deformation behavior of hexagonal magnesium–lithium alloys and a conventional magnesium AZ31 alloy. Acta Materialia. 2009;57:2229-42.

[55] Yi S, Bohlen J, Heinemann F, Letzig D. Mechanical anisotropy and deep drawing behaviour of AZ31 and ZE10 magnesium alloy sheets. Acta Materialia. 2010;58:592-605.

[56] Christian JW, Mahajan S. Deformation twinning. Progress in materials science. 1995;39:1-157.

[57] Smallman RE, Bishop RJ. Modern physical metallurgy and materials engineering: Butterworth-Heinemann; 1999.

[58] Ecob N, Ralph B. The effect of grain size on deformation twinning in a textured zinc alloy. Journal of Materials Science. 1983;18:2419-29.

[59] Barnett M, Keshavarz Z, Beer A, Atwell D. Influence of grain size on the compressive deformation of wrought Mg–3Al–1Zn. Acta materialia. 2004;52:5093-103.

[60] Gong X, Kang SB, Li S, Cho JH. Enhanced plasticity of twin-roll cast ZK60 magnesium alloy through differential speed rolling. Materials & Design. 2009;30:3345-50.

[61] Lou X, Li M, Boger R, Agnew S, Wagoner R. Hardening evolution of AZ31B Mg sheet. International Journal of Plasticity. 2007;23:44-86.

[62] Agnew S, Yoo M, Tome C. Application of texture simulation to understanding mechanical behavior of Mg and solid solution alloys containing Li or Y. Acta Materialia. 2001;49:4277-89.

[63] Ion S, Humphreys F, White S. Dynamic recrystallisation and the development of microstructure during the high temperature deformation of magnesium. Acta Metallurgica. 1982;30:1909-19.

[64] Gehrmann R, Frommert MM, Gottstein G. Texture effects on plastic deformation of magnesium. Materials Science and Engineering: A. 2005;395:338-49.

[65] Humphreys FJ, Hatherly M. Recrystallization and related annealing phenomena: Elsevier; 2012.

[66] Mwembela A, Konopleva E, McQueen H. Microstructural development in Mg alloy AZ31 during hot working. Scripta Materialia. 1997;37:1789-95.

[67] Galiyev A, Kaibyshev R, Gottstein G. Correlation of plastic deformation and dynamic recrystallization in magnesium alloy ZK60. Acta materialia. 2001;49:1199-207.

[68] Chen H, Zang Q, Yu H, Zhang J, Jin Y. Effect of intermediate annealing on the microstructure and mechanical property of ZK60 magnesium alloy produced by twin roll casting and hot rolling. Materials Characterization. 2015;106:437-41.

[69] Hongmei C, Huashun Y, Bong KS, Guanghui M, Yunxue J. Effect of forming process on microstructure and mechanical properties of ZK60 alloy sheet. Rare Metal Materials and Engineering. 2011;40:1708-12.

[70] Barnett M, Keshavarz Z, Nave M. Microstructural features of rolled Mg-3Al-1Zn. Metallurgical and Materials Transactions A. 2005;36:1697-704.

[71] Del Valle J, Pérez-Prado MT, Ruano O. Texture evolution during large-strain hot rolling of the Mg AZ61 alloy. Materials Science and Engineering: A. 2003;355:68-78.

[72] Chuvil'Deev V, Nieh T, Gryaznov MY, Sysoev A, Kopylov V. Low-temperature superplasticity and internal friction in microcrystalline Mg alloys processed by ECAP. Scripta Materialia. 2004;50:861-5.

[73] Figueiredo RB, Langdon TG. The development of superplastic ductilities and microstructural homogeneity in a magnesium ZK60 alloy processed by ECAP. Materials Science and Engineering: A. 2006;430:151-6.

[74] Lapovok R, Cottam R, Thomson P, Estrin Y. Extraordinary superplastic ductility of magnesium alloy ZK60. Journal of materials research. 2005;20:1375-8.

[75] Dumitru F-D, Higuera-Cobos OF, Cabrera J. ZK60 alloy processed by ECAP: Microstructural, physical and mechanical characterization. Materials Science and Engineering: A. 2014;594:32-9.

[76] Torbati-Sarraf SA, Langdon TG. Properties of a ZK60 magnesium alloy processed by high-pressure torsion. Journal of Alloys and Compounds. 2014;613:357-63.

[77] Kai M, Horita Z, Langdon TG. Developing grain refinement and superplasticity in a magnesium alloy processed by high-pressure torsion. Materials Science and Engineering: A. 2008;488:117-24.

[78] Choi I-C, Lee D-H, Ahn B, Durst K, Kawasaki M, Langdon TG, et al. Enhancement of strain-rate sensitivity and shear yield strength of a magnesium alloy processed by high-pressure torsion. Scripta Materialia. 2015;94:44-7.

[79] Handbook A. Forming and forging. ASM International. 1988;14:483.

[80] Chawla KK, Meyers M. Mechanical behavior of materials: Prentice Hall; 1999.

[81] Friedrich HE, Mordike BL. Magnesium technology: Springer; 2006.

[82] Sylwestrowicz W, Hall E. The deformation and ageing of mild steel. Proceedings of the Physical Society Section B. 1951;64:495.

[83] Ahmad I, Jing X, Shu D. Effect of temperature on the mechanical behaviour of magnesium alloy AZ91D in the range between− 30° C and 250° C. International Journal of Mechanical Sciences. 2014;86:34-45.

[84] Wang H, Dong S, Lv G. Plastic deformation characteristics of an Mg–3Al–1Zn alloy at low temperatures. Materials & Design. 2016;92:143-50.

[85] Chen H, Yu H, Kang SB, Cho JH, Min G. Optimization of annealing treatment parameters in a twin roll cast and warm rolled ZK60 alloy sheet. Materials Science and Engineering: A. 2010;527:1236-42.

[86] Watanabe H, Mukai T, Kohzu M, Tanabe S, Higashi K. Low temperature superplasticity in a ZK60 magnesium alloy. Materials Transactions, JIM. 1999;40:809-14.

[87] Chen H, Liu T, Zhang Y, Song B, Hou D, Pan F. The yield asymmetry and precipitation behavior of pre-twinned ZK60 alloy. Materials Science and Engineering: A. 2016;652:167-74.

[88] Wang S-R, Min W, Kang S-B, Cho J-H. Microstructure comparison of ZK60 alloy under casting, twin roll casting and hot compression. Transactions of Nonferrous Metals Society of China. 2010;20:763-8.

[89] Chen X-H, Huang X-W, Pan F-S, Tang A-T, Wang J-F, Zhang D-F. Effects of heat treatment on microstructure and mechanical properties of ZK60 Mg alloy. Transactions of Nonferrous Metals Society of China. 2011;21:754-60.

[90] Zhu A, Starke E. Stress aging of Al–xCu alloys: experiments. Acta materialia. 2001;49:2285-95.

[91] Swann P, Pickering H. Implications of the stress aging yield phenomenon with regard to stress corrosion cracking. Corrosion. 1963;19:369t-72t.

[92] Wenk H, Van Houtte P. Texture and anisotropy. Reports on Progress in Physics. 2004;67:1367.

[93] Dingley DJ, Wright SI. Determination of crystal phase from an electron backscatter diffraction pattern. Journal of Applied Crystallography. 2009;42:234-41.

[94] Humphreys J. Texture Analysis: Macrotexture, Microtexture and Orientation Mapping. Journal of Microscopy. 2001;203:231-2.

[95] Mishin O, Juul Jensen D, Hansen N. Mater Sci Eng A 342: 320. doi: 10.1016. S0921-5093 (02). 2003:00311-8.

[96] Standard Test Methods for Vickers Hardness and Knoop Hardness of Metallic Materials. ASTM International; 2017.

[97] Shojaei K, Sajadifar S, Yapici G. On the mechanical behavior of cold deformed aluminum 7075 alloy at elevated temperatures. Materials Science and Engineering: A. 2016;670:81-9.

[98] Song B, Xin R, Sun L, Chen G, Liu Q. Enhancing the strength of rolled ZK60 alloys via the combined use of twinning deformation and aging treatment. Materials Science and Engineering: A. 2013;582:68-75.

[99] Kim W, Kim M, Wang J. Superplastic behavior of a fine-grained ZK60 magnesium alloy processed by high-ratio differential speed rolling. Materials Science and Engineering: A. 2009;527:322-7.
[100] Gu M, Wu Z, Jin Y, Koçak M. Effects of Reinforcements on the Aging Response of a ZK60-based Hybrid Composite. Materials Science and Engineering: A. 1999;272:257-63.
[101] Wang Y, Xin Y, Yu H, Lv L, Liu Q. Formation and microstructure of shear bands during hot rolling of a Mg–6Zn–0.5 Zr alloy plate with a basal texture. Journal of Alloys and Compounds. 2015;644:147-54.
[102] Agnew S, Mehrotra P, Lillo T, Stoica G, Liaw P. Texture evolution of five wrought magnesium alloys during route A equal channel angular extrusion: Experiments and simulations. Acta Materialia. 2005;53:3135-46.
[103] Bhattacharjee T, Mendis C, Sasaki T, Ohkubo T, Hono K. Effect of Zr addition on the precipitation in Mg–Zn-based alloy. Scripta Materialia. 2012;67:967-70.
[104] HE Y-b, PAN Q-l, Qin C, ZHANG Z-y, LIU X-y, LI W-b. Modeling of strain hardening and dynamic recrystallization of ZK60 magnesium alloy during hot deformation. Transactions of Nonferrous Metals Society of China. 2012;22:246-54.
[105] Hono K, Mendis C, Sasaki T, Oh-Ishi K. Towards the development of heat-treatable high-strength wrought Mg alloys. Scripta Materialia. 2010;63:710-5.
[106] Rollett A, Humphreys F, Rohrer GS, Hatherly M. Recrystallization and related annealing phenomena: Elsevier; 2004.
[107] Mendis C, Oh-Ishi K, Kawamura Y, Honma T, Kamado S, Hono K. Precipitation-Hardenable Mg–2.4 Zn–0.1 Ag–0.1 Ca–0.16 Zr (at.%) Wrought Magnesium Alloy. Acta Materialia. 2009;57:749-60.
[108] Yu W, Liu Z, He H, Cheng N, Li X. Microstructure and mechanical properties of ZK60–Yb magnesium alloys. Materials Science and Engineering: A. 2008;478:101-7.

[109] Li B, Joshi S, Azevedo K, Ma E, Ramesh K, Figueiredo R, et al. Dynamic testing at high strain rates of an ultrafine-grained magnesium alloy processed by ECAP. Materials Science and Engineering: A. 2009;517:24-9.

[110] Clark J. Transmission electron microscopy study of age hardening in a Mg-5 wt.% Zn alloy. Acta Metallurgica. 1965;13:1281-9.

[111] Song B, Xin R, Guo N, Xu J, Sun L, Liu Q. Dependence of tensile and compressive deformation behavior on aging precipitation in rolled ZK60 alloys. Materials Science and Engineering: A. 2015;639:724-31.

[112] Xie G, Ma Z, Geng L. Effect of microstructural evolution on mechanical properties of friction stir welded ZK60 alloy. Materials Science and Engineering: A. 2008;486:49-55.

[113] Yan L, Zhang Z-M, Yong X. Influence of aging on microstructure and mechanical properties of AZ80 and ZK60 magnesium alloys. Transactions of Nonferrous Metals Society of China. 2011;21:739-44.

[114] Orlov D, Raab G, Lamark TT, Popov M, Estrin Y. Improvement of mechanical properties of magnesium alloy ZK60 by integrated extrusion and equal channel angular pressing. Acta Materialia. 2011;59:375-85.

[115] Kang SB, Cho JH, Kim HW, Jin Y. Effect of heat treatment on microstructure and mechanical properties in ZK60 alloy sheet. Materials Science Forum: Trans Tech Publ; 2008. p. 361-4.

[116] Mehrotra P, Lillo T, Agnew S. Ductility enhancement of a heat-treatable magnesium alloy. Scripta materialia. 2006;55:855-8.

[117] Eggeler G, Khalil-Allafi J, Neuking K, Dlouhý A. Creep of binary Ni-rich NiTi shape memory alloys and the influence of pre-creep on martensitic transformations: Dedicated to Professor Dr. Haël Mughrabi on the occasion of his 65th birthday. Zeitschrift für Metallkunde. 2002;93:654-60.

[118] Zhu A, Chen J, Starke E. Precipitation strengthening of stress-aged Al–xCu alloys. Acta Materialia. 2000;48:2239-46.

[119] Hosford WF, Agrawal SP. Effect of stress during aging on the precipitation of θ′ in Al-4 Wt pct Cu. Metallurgical Transactions A. 1975;6:487-91.

[120] Oblak J, Paulonis D, Duvall D. Coherency strengthening in Ni base alloys hardened by DO22 γ′ precipitates. Metallurgical Transactions. 1974;5:143.

[121] Chao H, Sun H, Chen W, Wang E. Static recrystallization kinetics of a heavily cold drawn AZ31 magnesium alloy under annealing treatment. Materials Characterization. 2011;62:312-20.

[122] Brammer J, Percival C. Elevated-temperature elastic moduli of 2024 aluminum obtained by a laser-pulse technique. Experimental Mechanics. 1970;10:245-50.

[123] Wolfenden A. Dynamic elastic modulus measurements in materials: ASTM International; 1990.

[124] Thostenson ET, Ren Z, Chou T-W. Advances in the science and technology of carbon nanotubes and their composites: a review. Composites science and technology. 2001;61:1899-912.

[125] Oikawa H, Sato H, Maruyama K. Influence of temperature on the transition of deformation characteristics of Al‧1Mg alloy in the power law creep regime. Materials Science and Engineering. 1985;75:21-8.

[126] Gao X, Nie J. Characterization of strengthening precipitate phases in a Mg–Zn alloy. Scripta Materialia. 2007;56:645-8.

[127] Robson J, Stanford N, Barnett M. Effect of precipitate shape on slip and twinning in magnesium alloys. Acta materialia. 2011;59:1945-56.

[128] Wei L, Dunlop G, Westengen H. Precipitation hardening of Mg-Zn and Mg-Zn-RE alloys. Metallurgical and Materials Transactions A. 1995;26:1705-16.

[129] Bettles C, Gibson M, Venkatesan K. Enhanced age-hardening behaviour in Mg–4 wt.% Zn micro-alloyed with Ca. Scripta Materialia. 2004;51:193-7.

[130] Nie J. Effects of precipitate shape and orientation on dispersion strengthening in magnesium alloys. Scripta Materialia. 2003;48:1009-15.